SISSA
Scuola
Internazionale
Superiore di
Studi Avanzati

Neuroscience Area –

PhD course in Neurobiology

Reduction of α-tubulin acetylation through depletion of Atat1 using genomic, post-transcriptional and post-translational approaches

Candidate:
Joana Maria Monteiro Serrão

Advisor:
Professor Paul Heppenstall

Academic Year 2020-21

Table of Contents

Acknowledgements 6

1. Abstract 7

2. List of abbreviations 9

3. List of Figures 11

4. Introduction 13

4.1 The somatosensory system 13

4.1.1 Dorsal Root Ganglia (DRG) neurons 13

4.1.2 Spinal cord 15

4.1.3 Mechanosensory neurons of touch 17

4.1.3.1 Low-threshold mechanosensory neurons 17

4.1.3.2 High-threshold mechanosensory neurons 21

4.2 Mechanosensitive (MS) ion channels 22

4.2.1 Gating of mechanosensitive ion channels 25

4.3 The Cytoskeleton 29

4.3.1 Microtubules and α-tubulin acetylation 30

4.4 Gene Manipulation 34

4.4.1 Knock-out of gene expression - CRISPR gene editing 34

4.4.2 Knock-down of gene expression – RNAi 37

4.4.3 Delivery systems of genetic material 39

5. Methods 43

5.1 Cloning 43

5.1.1 Cloning mCherry-Atat1-CRISPR 43

5.1.2 Cloning Atat1-CRISPR 45
5.1.3 Cloning mini-CMV-tdTomato 46
5.1.4 Cloning Atat1-sh 47
5.2 N2a cell culture and transfection 48
5.3 TIDE analysis 48
5.4 Immunocytochemistry 49
5.5 Western-blot 49
5.6 Expression and purification of Frankenbody-mGFP 50
5.7 Virus production 51
5.8 Virus modification 52
5.9 Primary cell culture of DRG neurons 52
5.10 Organotypic cultures of spinal cord and DRG slices 53
5.11 Immunofluorescence on organotypic cultures 54
5.12 Intrathecal injections 54
5.13 Immunohistochemistry 54
5.14 Chemical Screening 55
5.15 Image analysis 55
5.16 Statistical analysis 56
5.17 Ethical statement 56
5.18 List of antibodies 57
6. Results 58
6.1 Targeting of Atat1 with CRISPR 58
6.1.2 Design and insertion of gRNA sequences for knock-out of Atat1 by SaCas9 58
6.1.2 rAAV in *ex-vivo* cultures of DRG neurons 66

6.1.3 HA-tag epitope detection systems 66

6.1.4 Mini-CMV vs CAG promoter 69

6.1.5 Organotypic cultures of spinal cord and DRG as an *ex-vivo* model to observe viral transduction 70

6.1.6 Atat1-CRISPR in *ex-vivo* cultures 72

6.1.7 Nocodazole on *ex-vivo* organotypic cultures of spinal cord and DRG neurons 74

6.1.8 Atat1-CRISPR *in-vivo* 75

6.2 shRNA knock-down 79

6.2.1 Cloning of RNAi sequences into rAAV vectors and *in-vitro* efficiency assessment 79

6.2.2 Atat1 *ex-vivo* knock-out 82

6.2.3 Atat1-sh *in-vivo* 85

6.3 Chemical inhibition of Atat1 88

7. Discussion 94

7.1 Targeting Atat1 through gene editing 95

7.2 Targeting Atat1 through RNAi 97

7.3 Targeting Atat1 *in-vivo* 98

7.4 Targeting Atat1 with protein inhibitors 99

7.5 Atat1 as a potential therapeutic target for different diseases 99

8. Conclusions 101

9. References 103

Report on Activities and Scientific Articles published during the PhD Course ..... **Error! Bookmark not defined.**

Acknowledgements

I would like to thank firstly my supervisor, Professor Paul Heppenstall, for hosting me in his laboratories in EMBL and in SISSA and for his mentorship throughout my doctoral studies.

I would also like to thank my Thesis Advisor Committee: Professor Laura Ballerini, Professor Cornelious Gross and Professor Robert Prevedel for the insightful comments and scientific discussions throughout my PhD course.

I like to thank Ciro Danubio, for choosing to do this Master studies with me and for his dedication and commitment for this project.

I would like to acknowledge Monika Lachner and the Graduate Offices from EMBL and SISSA, for the administrative support during the transition of the laboratory from Rome to Trieste.

I would like to thank the Scientists and Friends from EMBL and SISSA, in particular the Heppenstall Laboratory for the help and company in the last four years.

Finally, I would also like to thank the unconditional support of my Family.

1. Abstract

Microtubules are highly conserved structures, made of polymers of α and β tubulin organised in a polarised way (Hohmann and Dehghani, 2019). Their function can be fine regulated through post-translational modifications (Gadadhar et al., 2017), such as acetylation of α-tubulin. In mice, this post-translational modification is catalysed by α-tubulin acetyltransferase 1 (Atat1) (Kalebic et al., 2013a). Ablation of the expression of Atat1 and its orthologues in sensory neurons prevents acetylation of α-tubulin and has been associated with deficits in mechanosensation (Akella et al., 2010; Morley et al., 2016; Yan et al., 2018). Nonetheless, it is unknown if this phenotype is a consequence of an absence of Atat1 expression at embryonic stages or if it is possible to achieve this phenotype by ablation/inhibition of Atat1 in fully developed mice.

Here I explored the potential of Atat1 ablation in mouse cells, with a gene therapy strategy, using clustered regularly interspaced short-palindromic repeat (CRISPR) and RNA interference (RNAi) technologies delivered by modified versions of recombinant adeno-associated viruses (rAAVs).

In-vitro assays in neuroblastoma 2a (N2a) cells demonstrated that both CRISPR (Jinek et al., 2012) and RNAi technologies (Fire et al., 1998) were able to reduce the amount of acetylated α-tubulin, if delivered by lipid based methods. Therefore, in order to address if these constructs were able to reduce acetylated α-tubulin in *ex-vivo* preparations, I have produced rAAV viruses containing the best CRISPR and RNAi sequences targeting Atat1, identified in the initial screening. Immunofluorescence assays on *ex-vivo* organotypic cultures of spinal cord and dorsal root ganglia (DRG) neurons infected with the CRISPR virus demonstrated that it is possible to achieve a reduction in acetylated α-tubulin by targeting Atat1 at a genomic level. However, regarding the RNAi virus, *ex-vivo* organotypic cultures of spinal cord and DRG infected with this virus, did not show an effect in acetylated α-tubulin, comparing to control. Intrathecal administration of CRISPR and RNAi rAAV viruses in *in-vivo* mouse models failed to successfully achieve viral transduction.

In addition to the gene therapy strategies, I evaluated the potential of inhibition of Atat1 at the protein level, using putative chemical inhibitors in *in-vivo* assays in N2a cells and *ex-vivo* primary cultures of DRG neurons. The chemical screen did not provide consistent results, which lead to the conclusion that it might be possible to chemically inhibit Atat1, however there is still a need for optimization of putative inhibitors.

The overall results obtained provide an effective platform for studies targeting Atat1 in mouse cells. It is well-known that this protein is involved in many diseases and the experimental setting that I developed could be used not only in somatosensory research but also in other research areas, such as neurodegeneration or oncology (Castro-Castro et al., 2012; Dompierre et al., 2007; Govindarajan et al., 2013).

2. List of abbreviations

DRG	Dorsal root ganglia
AAV	Adeno-associated virus
Ago	Argonaute
ASIC	Acid sensing ion channels
Atat1	α -tubulin acetyltransferase 1
BDNF	Brain derived nerve factor
C. Elegans	*Caenorhabditis elegans*
Cas	CRISPR associated
CRISPR	Clustered regularly interspaced short-palindromic repeat
deg/ENaC	degenerin/epithelial sodium channel
DMSO	Dimethyl Sulfoxide
dPBS	Dulbecco's Phosphate Buffered Saline
FBS	Fetal bovine serum
GDNF	Glial cell derived neurotrophic factor
GFP	Green fluorescent protein
gRNA	Guide RNA
HDAC6	Histone deacetylase 6
HDR	Homology directed repair
HSPG	Heparan sulfate proteoglycans
HTMR	High threshold mechanoreceptors
IB4	Isolectin B4
K40	Lysine 40
LTMR	Low threshold mechanoreceptor
miRNA	MicroRNA
MS	Mechanosensitive
MscL	Mechanosensitive channels of large conductance
MscS	Mechanosensitive channels of small conductance
N2a	Neuroblastoma 2a
NGF	Nerve growth factor
NGS	Normal goat serum
NHEJ	Non-homologous end joining repair
NOMPC	No mechanoreceptor potential C
NT4/5	Neurotrophin 4/5
NUC	Nuclease lobe
PAM	Protospacer adjacent motif
PCR	Polymerase chain reaction
PFA	Paraformaldehyde
rAAV	Recombinant AAV
RA-LTMR	Rapidly adapting-LTMR
REC	Recognition domain

RFP	Red fluorescent protein
RISC	RNA-induced silencing complex
Sa	*Staphylococcus aureus*
SA-LTMR	Slowly adapting-LTMR
SD	Standard deviation
sdRNA	Double-strand RNA
shRNA	Short-hairpin RNA
siRNA	Small interfering RNA
SIRT2	Desacetyltansferase sirtuin type 2
SNP	Single nucleotide polymorphism
ssDNA	Single strand DNA
STOML3	Stomatin-like protein 3
TALEN	Transcription activator-like effector nucleases
tdTomato	Tandem dimer Tomato
Trk	Tropomyosin receptor kinase
TRP	Transient receptor potential
ZFN	Zinc finger nuclease

3. List of Figures

Figure	Page
Figure 1 – The dorsal horn of the spinal cord receives input of primary sensory neurons at specific laminae	12
Figure 2 – Organization of LTRM within the glabrous skin	14
Figure 3 – Organization of LTRM within the hairy skin	15
Figure 4 – Gating of mechanosensors ion channels – single-tether model	23
Figure 5 – α-tubulin acetylation on microtubules	26
Figure 6 – CRISPR-Cas9	31
Figure 7 – Adeno-associated viruses	35
Figure 8 – Strategy for Atat1 gene knock-out	53
Figure 9 – gRNA1 is the best sequence to knock-out Atat1	55
Figure 10 – Knock-down of Atat1 with Atat1-CRISPR leads to a decrease in the amount of acetylated α-tubulin	52
Figure 11 - Knock-down of Atat1 with pAAV-Atat1-CRISPR-HA leads to a decrease in the amount of acetylated α-tubulin.	56
Figure 12 – Anti-HA-Frankenbody-mGFP is a good reporter for immunocytochemistry in N2a	62
Figure 13 – *Ex-vivo* cultures of DRG neurons infected with CRISPR-Atat1 virus fixed at 8 DIV	63
Figure 14 – Mini-CMV promoter drives a low amount of protein expression	64
Figure 15 – Organotypic cultures infected with rAAV-eGFP and rAAV-tdTomato	66
Figure 16 – Atat1-CRISPR leads to a reduction in acetylated α-tubulin in *ex-vivo* cultures	68
Figure 17 – Nocodazole does not disrupt stable microtubules of neuronal axons.	66
Figure 18 – Atat1-CRISR *in-vivo*	70
Figure 19 – Design strategy for Atat1 knock-down	74
Figure 20 – Atat1-shRNA leads to a decrease in the ratio of acetylated α-tubulin over α-tubulin in N2a cells.	75
Figure 21 – *Ex-vivo* cultures of DRG neurons infected with AAV2-GFP and Atat1-sh fixed at 8 DIV	77
Figure 22 – Atat1-sh leads to a reduction in acetylated α-tubulin in ex-vivo cultures.	78

Figure 23 – Atat1-sh *in-vivo*	80
Figure 24 – Western-blot of N2a cells incubated with 50µM of the shortlisted chemical compounds and analysed at different time points	83
Figure 25 – Immunocytochemistry of N2a cells incubated with 50µM of the shortlisted chemical compounds and analysed at different time points	85
Figure 26 – Immunocytochemistry of DRG neurons incubated with 50µM of the shortlisted chemical compounds and analysed at different time points	87

4. Introduction

4.1 The somatosensory system

Animals interact with the external environment based on the perception from their sensory organs, which sets the way one interacts with the world.

The somatosensory system comprises all phenomena relevant to the integration of interoreceptive and exteroreceptive stimuli (internal and external, respectively) as well as proprioceptive stimuli (regarding the control of position and balance) (Abraira and Ginty, 2013). This system allows to decode and discriminate among different types of sensations (mechanical, chemical, thermal and itch), intensities (innocuous and noxious) and to precisely localize it within the body (Basbaum et al., 2009). Importantly, the somatosensory system signals the presence of an eminent or actual danger situation, forcing engagement of protective behaviours to avoid damage or to allow tissue recovery after physical damage (Collier, 2018).

Within the peripheral nervous system, the main components of the somatosensory system are the nerve fibres, whose cell bodies are aggregated in the dorsal root ganglia (DRG) and trigeminal ganglia, and the dorsal horn of the spinal cord (Todd, 2010). Somatosensory events initiate by the activation of receptors in specific populations of the nerve fibres within the skin, which codify this physical information into electrochemical signals. These signals propagate along nerve fibres of DRG neurons, which synapse in specific laminae of the dorsal horn of the spinal cord. The information is further propagated to the central nervous system, where the information is integrated (Todd, 2010).

4.1.1 Dorsal Root Ganglia (DRG) neurons

The first cell type from the somatosensory system that becomes activated upon somatosensory stimuli are the dorsal root ganglia neurons (DRG), also described in the literature as primary sensory neurons.

Dorsal root ganglia neurons are pseudo-unipolar neurons, made of a long peripheral axonal branch that enervates the skin and deeper tissues of the body, as well as a smaller centrally projecting axonal branch that synapses with specific laminae of the dorsal horn of the spinal cord horn and a cell body (Waxman and Zamponi, 2014). Cell bodies of DRG neurons are clustered in ganglia located inside the backbone and the rostrocaudal location of cell bodies of DRG neurons mirrors the enervation of the distal axonal branch (Story et al., 2003). These ganglia are located in pairs, on the left and right side of the spine, and are divided into in cervical, thoracic, lumbar, sacral and coccygeal ganglia (Krames, 2014). Therefore, based on the place where one experiences pain, it is possible to trace back which nerve and dorsal root ganglia are involved in that sensation.

Sensory neurons are classified into Aβ, Aδ or C fibres, accordingly to their cell body size, axonal diameter, myelin processes and axonal conduction velocity (Abraira and Ginty, 2013) Aβ fibres have the largest cell bodies and their axons are highly myelinated, which provides electrical isolation for axons, conferring a higher conduction velocity of electrical impulses (15-100ms^{-1}). Aδ fibres have cell bodies with an intermediate cell body size, are lightly myelinated and the conduction velocity is classified as intermediate among the sensory fibres (5-30ms^{-1}). Finally, C fibres have a small cell body and lack a myelin sheath, having therefore a slower conduction velocity of electrical impulses (0.2-2ms^{-1}) (Iggo, 1985).

Most Aβ fibres and some of Aδ and C-fibres become activated by low-threshold mechanical stimuli, relevant for detection of innocuous stimuli, while a small amount of Aβ fibres are activated by high-threshold mechanical stimuli and the majority of Aδ and C-fibres are activated by high-threshold mechanical and thermal stimuli, playing an important role in detection of noxious stimuli (Zimmerman, 2009).

DRG neurons sensory afferents are additionally classified into subpopulations according to the sensory stimuli detected (thermosensors, chemosensors, mechanosensors, nociceptors and proprioceptors) (Hjerling-Leffler et al., 2007). The recognition of different sensory modalities is possible due to a diversity of specialized cellular identities of sensory neurons (Sharma et al., 2020).

A further classification of DRG neurons is based on the expression of receptors for neurotrophins, such as tropomyosine receptor kinases (Trk) TrkA, TrkB and TrkC expressed in their membranes. Nerve growth factor (NGF) binds to TrkA receptors, while brain derived neurotrophic factor (BDNF) and neurotrophin 4/5 (NT4/5) binds to TrkB receptors, lastly, neurotrophin 3 (NT3) binds to TrkC receptors. The activation of Trk receptors leads to the activation of cascades of events within the somatosensory pathway (Pezet and McMahon, 2006). TrkA are nociceptors and TrkB and TrkC are low threshold mechanoreceptors and proprioceptors (Hjerling-Leffler et al., 2007). Nonetheless, each of these populations is further divided into subpopulations, according to their gene expression and currently there are more than twelve functional distinct subpopulations of DRG neurons (Sharma et al., 2020). Given the scope of the present work, I will discuss subpopulations of mechanosensors in more detail later.

Importantly, the discovery of specific receptors expressed in subpopulations of DRG neurons opened new possibilities in synthetic biology, particularly in targeting specific cell populations, with ligand-guided molecules, which is a valuable asset not only as a research tool, but also as a delivery platform for cell therapy as I will discuss later (Maffei et al., 2019).

Activation of sensory receptors of DRG neurons, initiates a cascade of events that ultimately leads to the conversion of sensory information into action potentials that travel from the extremities of the afferents, to the other extremity of the primary sensory neuron inside the dorsal horn of the spinal cord.

4.1.2 Spinal cord

The spinal cord is segmented into a system of ten layers, denominated as laminae of Rexed I to X, represented on Figure 1 (Abraira and Ginty, 2013). Primary sensory neurons terminate in the dorsal horn of the spinal cord in specific laminae, according to the sensory information conveyed. Low threshold mechanosensors (see below) innervate laminae III to V,

whereas nociceptors (pain sensing neurons) and thermoreceptors innervate lamina I and lamina II (Todd, 2010).

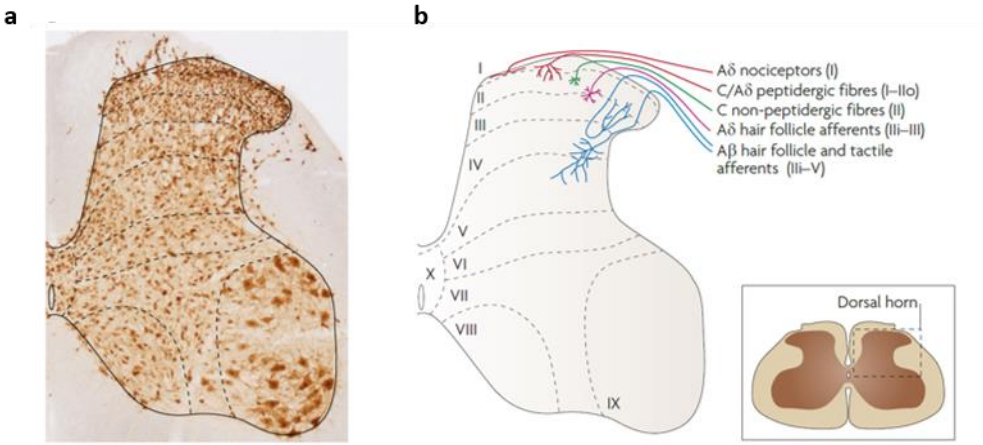


Figure 1 – The dorsal horn of the spinal cord receives input of primary sensory neurons at specific laminae. **(a)** Transverse section of rat spinal cord, labeled with the neuronal marker NeuN. Rexed laminae are represented with dashed lines. **(b)** Representation of the terminal regions of primary afferents in the spinal cord. Taken from (Todd, 2010)

The spinal cord constitutes the first stage of sensory stimuli processing, in which a complex circuit of both inhibitory and excitatory interneurons tightly regulated leads to nocifensive reflexes in order to protect the body towards a dangerous or potentially dangerous stimulus (Ren et al., 2021). The absence of a proper regulation of inhibitory and excitatory activity within the spinal cord can evolve to an abnormal pain perception, such as allodynia (an exaggerated pain sensation to non-painful stimuli) (Hughes and Todd, 2020).

Moreover, the spinal cord contains also projection neurons, expressed mostly in lamina I, whose axons cross the midline and terminate in the central nervous system, more particularly in the brainstem and thalamus. These neurons are particularly involved in the perception of noxious and thermal stimuli (Todd, 2010).

4.1.3 Mechanosensory neurons of touch

The process by which mechanical stimuli are transcribed into electrical signals is termed mechanotransduction (Chalfie, 2009). It serves not only as a way for us to discriminate our environment, but also to interact with others through affective touch (McGlone et al., 2014). Furthermore, mechanotransduction is also involved in other pivotal physiological processes, such as the sense of hearing and regulation of osmotic and blood pressure (Kefauver et al., 2020). Here I will focus on mechanosensory events within skin, involved in touch.

4.1.3.1 Low-threshold mechanosensory neurons

Innocuous touch stimuli in the skin are detected by low-threshold mechanoreceptors (LTMRs), which as mentioned previously are classified into Aβ, Aδ and C-LTMR. Furthermore, LTMR can be divided according to their adaptation to static indentation of the skin into slowly adapting (SA-LTRM) and rapidly adapting (RA-LTMR) (Abraira and Ginty, 2013). SA-LTMR exhibit maintained firing during application of static indentation, contrasting to RA-LTMR that fire at the initial and final moments of mechanical stimuli (Abraira and Ginty, 2013).

The skin is divided into three types, glabrous (non-hairy), hairy and mucocutaneous regions, which possess different enervation patterns that ultimately confer a distinct tactile sensitivity (Kefauver et al., 2020). Here I will focus on the enervation of glabrous and hairy skin types, represented on Figure 2 and 3.

In the glabrous (non-hairy) skin, primary afferents are associated with end organ structures: Merkel cell-neurite complex, Meissner corpuscles, Pacinian corpuscles and potentially with Ruffini corpuscles (Raoux et al., 2007). Specifically, Aβ slowly adapting type 1 (Aβ SAI-LTRM) associate with Merkel cell-neurite complex in the epidermal rete ridge and are activated by skin indentation. Aβ rapidly adapting type 1 (Aβ RAI-LTRM) associate with Meissner corpuscles in the dermal papillae and are activated by skin indentation and vibration. Finally the Aβ rapidly adapting type 2 (Aβ RAII-LTRM) associate with Pacinian corpuscle in the

deep dermis and periosteum of certain bones (Handler and Ginty, 2021) and are activated by skin indentation and high frequency vibration (Kefauver et al., 2020).

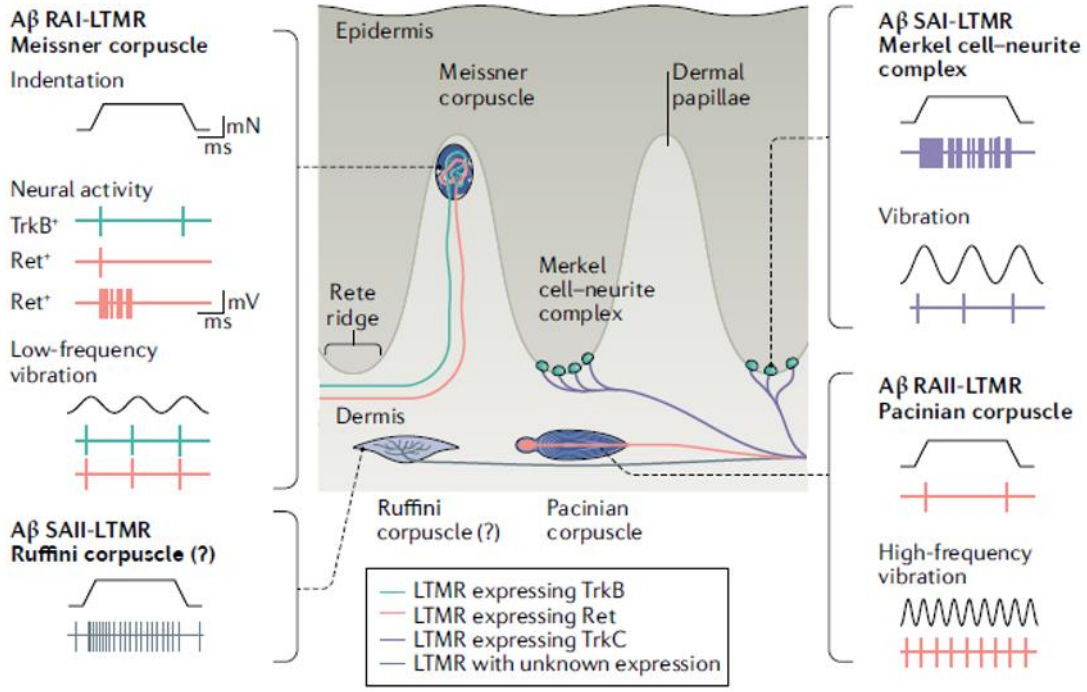


Figure 2 – Organization of primary afferent in the glabrous skin In the glabrous skin, primary afferent LTMRs associate with end organ structures: Merkel cell-neurite complexes, Ruffini endings, Meissner corpuscles and Pacinian corpuscles. These fibres express different proteins and have distinct electrical properties that culminate in different sensory sensitivity. Taken from (Kefauver et al., 2020).

In hairy skin (Figure 3), the three main hair follicles (guard hairs, awl/auchene hairs and zigzag hairs) are enervated by a unique combination of LTRMs, that renders a specific physiological function to these hairs (Li et al., 2011). Additionally, hairy skin contains clusters of Merkel cells, forming a touch dome in the epidermis of the skin near guard hairs and Pacinian corpuscles in the deep dermis, that provides higher sensitivity to skin indentation and vibration (Handler and Ginty, 2021).

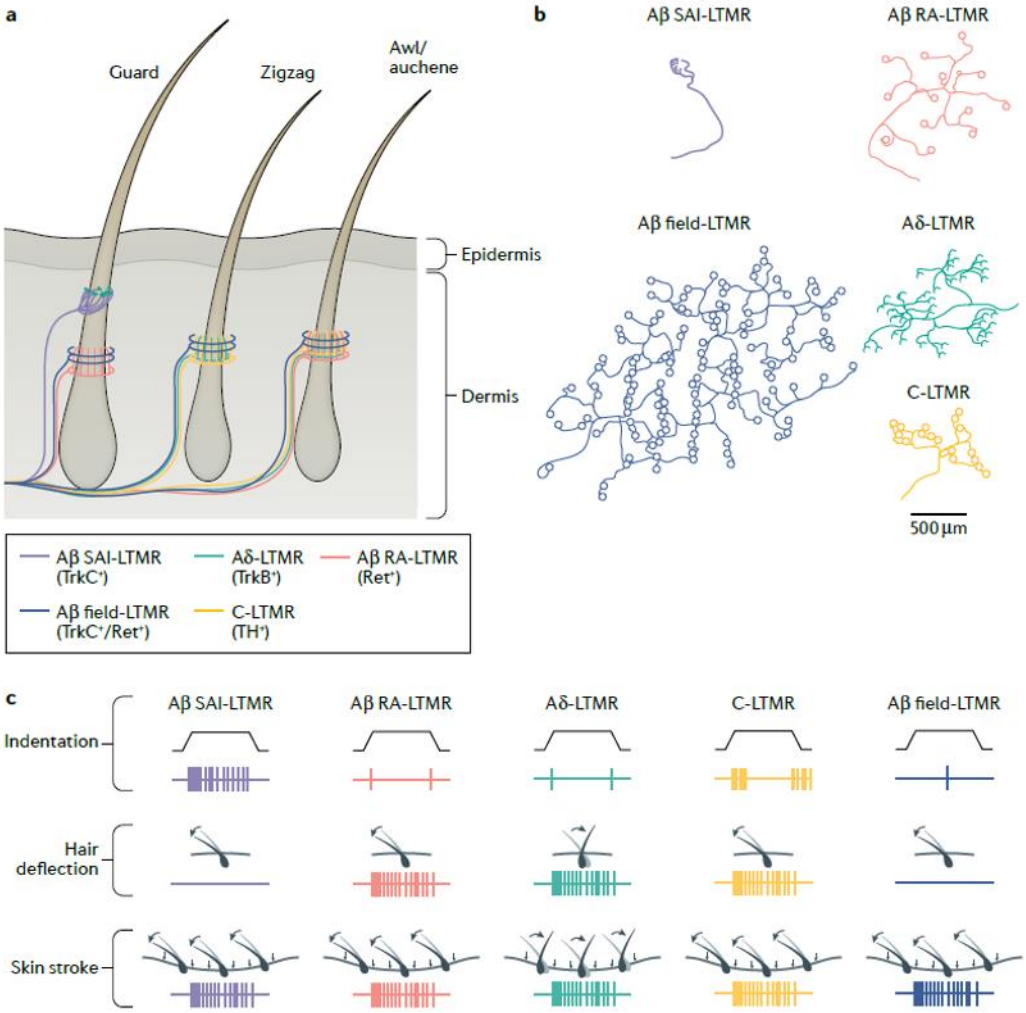


Figure 3 – Organization of primary afferent in the hairy skin. LTMR enervating the hairy skin present different activation profiles in response to indentation, hair deflection and skin stoke, which provides a more accurate description of the sensory stimuli. Primary afferents are mostly associated with hair follicles: guard, zigzag and awl/auchene. Additionally, in hairy skin Aβ SAI-LTRM are associated with a cluster of Merkel cells, forming a touch dome in the epidermis of the skin near guard hairs and Pacinian corpuscles in the deep dermis (not represented). Taken from (Kefauver et al., 2020)

Primary afferents enervate hair follicles as either longitudinal lanceolate endings, that run parallel to the hair shaft or as circumferential endings, surrounding hair follicles distal to lanceolate endings (Lechner and Lewin, 2013). Nonetheless, primary afferents follow a similar classification to nerve fibres found in the glabrous skin, based on size and adaptation to sustained stimuli.

Aβ slowly adapting type 1 low threshold mechanoreceptors (Aβ SAI-LTMR) are associated with clusters of Merkel cells (Li et al., 2011), providing sensitivity to skin indentation (Kefauver et al., 2020).

Aβ RA-LTRMs form lanceolate endings in awl/auchene hairs (78%) and guard hairs (22%) (Li et al., 2011). These fibres are activated by hair deflection, skin stroke and indentation (Kefauver et al., 2020).

The hairy skin is also enervated by a slowly adaptive Aβ-LTRM, denominated by Aβ field-LTRM that terminate in circumferential endings, surrounding guard and awl/auchene hairs (Li et al., 2011). These fibres are activated by gentle stroke in the skin (Handler and Ginty, 2021).

Moreover, hairy skin also contains the rapidly adapting Aδ-LTRM (also called D-hairs) that are associated with zigzag hairs (77%) and awl/auchene hairs (23%) (Li et al., 2011). D-hairs are the most sensitive mechanosensor fibres in the hairy skin (Lechner and Lewin, 2013). The polarised conformation of the lanceolate endings of D-hairs allows the distinction of hair deflection direction (Lechner and Lewin, 2013).

Moreover, hairy skin contains a high density of C-LTRMs, these terminate as longitudinal lanceolate endings and are associated with zigzag hairs (80%) and awl/auchene hairs (20%) (Li et al., 2011). These fibres are particularly sensitive to skin stroke and are associated with affective touch (McGlone et al., 2014).

Finally, Aβ SAII-LTRM are present in both glabrous and hairy skin, it has been proposed that these fibres form the Ruffini corpuscle, nonetheless the actual presence of these structures and their physiological properties still needs to be further elucidated (Abraira and Ginty, 2013).

4.1.3.2 High-threshold mechanosensory neurons

Mechanical stimuli of higher intensities are detected by high-threshold mechanoreceptors (HTMRs). Most HTMRs are Aδ and C-HTMRs, whilst a small proportion are Aβ-HTMRs (Basbaum et al., 2009). Both Aδ and C-HTMR fibres may be polymodal, which means that they can be activated by different sensory stimuli (Lewin and Moshourab, 2004).

Aδ-HTMR, also described as A-fibre mechanonociceptors (AM), have a thin myelin layer and an intermediate conducting velocity of electrical impulses. C-HTMR fibres, that account for the majority of nociceptive neurons, do not have a myelin sheet and their conduction of electrical stimuli is slower than Aδ and Aβ-HTMRs (Woolf and Ma, 2007).

Furthermore, nociceptive C-fibres may fall into two additional classes: peptidergic and non-peptidergic. C-fibres are considered as peptidergic if they produce the neuropeptides substance P and calcitonin gene related peptide and if they express the tropomyosin receptor kinase (Trk) A receptor for NGF (Lechner and Lewin, 2013). However, C-fibres are considered as non-peptidergic if they do not express neither these neuropeptides nor TrKA and if they bind to isolectin B4 (IB4) and express the glial cell derived neurotrophic factor (GDNF) receptor C-ret (Zylka et al., 2005).

As mentioned previously, DRG neurons possess a peripheral and a central axonal branch (Fu and Shi, 2017). The peripheral branch of peptidergic neurons enervate the deeper epidermis whilst the peripheral branch of non-peptidergic fibres enervate the regions of the epidermis closer to the skin surface. In terms of the central branch (Figure 1), peptidergic nerve fibres terminate at lamina I and outer lamina II in the dorsal horn of the spinal cord; whilst non-peptidergic fibres terminate in lamina II (Todd, 2010). From the structural differences between peptidergic and non-peptidergic C-fibres it is not surprising that these fibres convey different sensory stimuli. Indeed, ablation of peptidergic neurons led to deficits in thermal sensation, while ablation of non-peptidergic neurons let to the loss of nociception (Cavanaugh et al., 2009).

4.2 Mechanosensitive (MS) ion channels

Mechanotransduction initiate with the conversion of mechanical stimuli into electrical signals. This process is performed by mechanically activated ion channels and it is essential for many physiological processes such as mechanosensation, hearing or body fluid regulation (Ranade et al., 2015).

Opening of mechanically activated ion channels leads to an influx of cations and a consequent depolarization of the membrane potential, which may elicit the generation of action potentials (Waxman and Zamponi, 2014). The frequency of action potentials codifies the sensory stimuli into electrical signals that the brain can interpret (Waxman and Zamponi, 2014).

For an ion channel be considered as a "mechanosensitive ion channel", it must follow certain general rules. Firstly, it should be expressed in the membrane of mechanotransducers and ablation of such expression must cause deficits in mechanosensation. Moreover, expression of the MS ion channel in heterologous systems must provide mechanosensitivity to it (Beaulieu-Laroche et al., 2020). Furthermore, the channel must have an ion conducting pore and should have a rapid ion conduction following gate opening (Beaulieu-Laroche et al., 2020). Finally, if the ion channel does not require any auxiliary proteins to function, it should confer mechanosensitivity when purified and added into reduced systems, such as liposomes.

Mechanosensitive ion channels are divided in different families and subfamilies and may be evolutionary conserved.

Prokaryotic mechanosensitive channels of small and large conductance (MscS and MscL, respectively) were the first mechanosensitive ion channels identified. In bacteria, the membrane tension variates accordingly to the osmotic pressure inside the cell. An increase in membrane tension of bacteria leads to the opening of MscL and MscS channels, which allows the efflux of solutes, preventing cell lysis (Cox et al., 2018). Up to now, there are no orthologues for these channels found in mammals (Kefauver et al., 2020).

In *Caenorhabditis elegans (C.elegans)*, two proteins of the degenerin/epithelial sodium channel (deg/ENaC) family, MEC-4 and MEC-10, can form a protein complex that acts as a mechanosensitive ion channel (Basbaum et al., 2009). The activity of this ion channel is modulated by another protein, MEC-2, that is essential for channel opening. Ablation of the expression of both genes of MEC-4 and MEC-10 renders *C.elegans* insensitive to touch (Goodman et al., 2002). Orthologues of MEC-4 and MEC-10 in drosophila and mammals do not seem to be involved in mechanosensation, nonetheless, the mammalian orthologue of MEC-2, stomatin-like protein 3 (STOML3), has been shown to be essential for the activity of piezo mechanosensitive ion channels, as I will elaborate later on (Herget et al., 2014).

Acid sensing ion channels (ASIC) belong to a subfamily of the deg/ENaC channel family; three ASIC channels are expressed in DRG neurons. However, these channels do not contribute to mechanical sensation in mammals (Ranade et al., 2015).

The transient receptor potential (TRP) is a large family of ion channels, evolutionarily conserved, which play an essential role in a wide range of sensory modalities. TRP channels are subclassified into subfamilies, TRPA, TRPC, TRPM, TRPML, TRPN, TRPP and TRPV, based on their sequence homology (Ranade et al., 2015). Furthermore, some TRP ion channels are polymodal and may be activated by both chemical and thermal stimuli (Julius, 2013).

The subfamily of TRPN ion channels have been associated with mechanosensation. Interestingly, in drosophila larvae, the No mechanoreceptor potential C (NOMPC or TRPN1) mediates touch sensation and hearing (Zhang et al., 2015). In *C. elegans,* the TRPN orthologue TRP-4 expressed in the cilium of the Cephalic neuron is essential for light touch sensation (Ranade et al., 2015). In zebrafish larvae, ablation of the expression of NOMPC orthologue (TRPN1) sensory hair cells of the inner ear causes deafness and imbalance (Sidi et al., 2003). Interestingly, in lower vertebrates TRPN1 coexists with TRPA1 ion channels, however in higher vertebrates expression of TRPN1 is lost and TRPA1 is expressed (Shin et al., 2005). In mammals, some studies reported that TRPA1 is activated by cold, heat and mechanical stimuli (Talavera et al., 2020). Moreover, stretch activated TRPC1 was demonstrated to contribute to

mechanically evoked action potentials in Aβ-fibres and D-hairs (Garrison et al., 2012; Maroto et al., 2005).

The piezo family of mechanosensitive ion channels is evolutionarily conserved among plants and mammals (Ranade et al., 2015), comprising the channels piezo 1 and piezo 2. Piezo 2 channels are expressed in many cell types, namely Merkel cells, outer hair cells and in neurons of the somatosensory ganglia (Anderson et al., 2017). Selective ablation of piezo 2 channels in the peripheral nervous system led to loss of mechanical sensibility in slowly adaptive and rapidly adaptive low-threshold mechanoreceptors, and to deficits in locomotion without influencing nociception (Anderson et al., 2017; Ranade et al., 2014).

Contrary to most ion channels involved in mechanosensation, ion channels from the two pore potassium channel family, TREK-1, TREK-2 and TRAAK, play a fundamental role in preventing misfiring of neurons (Ranade et al., 2015). Activation of these channels causes an outward current of potassium ions which causes a hyperpolarization of the cell membrane, preventing generation of action potentials. Previous studies in which the expression of these three channels was ablated in mice lead to hypersensitivity to mechanical stimuli (Brohawn, 2015).

The ion channel TACAN (Tmem120A) has been shown to be essential for nociception in mice, without influencing touch or thermal sensation (Beaulieu-Laroche et al., 2020). However, a recent study focused on electrophysiology and structural biology assays have failed to show mechanosensitive features in TACAN (Niu et al., 2021). Therefore there is a need to clarify exactly how TACAN influences nociception, if it is directly implicated or whether it interacts with other proteins essential for nociception (Hill and Bautista, 2020).

4.2.1 Gating of mechanosensitive ion channels

Ion channels facilitate the flow of ions across the cellular membrane, the activation of mechanosensitive ion channels leads to a cascade of intracellular signalling events and physiological responses. Nonetheless, how exactly do mechanical forces promote the opening of mechanosensitive ion channels remains an open question. There are three main models proposing the gating of mechanosensitive ion channels, “force-from-lipids”, “dual tether model” and “single tether models”.

All ion channels embedded in the cellular membrane experience molecular and physical forces exerted by the lipid bilayer (Thompson and Baenziger, 2020).The force-from-lipids model postulates that changes in lipid membrane tension promotes opening of the gates of mechanosensitive ion channels, without the need of auxiliary proteins or involvement of the cytoskeleton (Kefauver et al., 2020). According to this model, changes in the physical forces of the membrane, such as membrane tension and curvature, influence gating of ion channels (Ranade et al., 2015). This model was first demonstrated in 1994 by Lett et al., by showing that MscL ion channels reconstructed in a lipid bilayer kept their physiological activity in response to mechanical stimuli applied in the reduced lipid system (Lett et al., 1994).

In bacteria, an increase in the osmotic pressure inside cells causes an increase in membrane tension, which pulls the N-terminal helix of MscL away from the central pore. This conformational alteration of the channel’s structure promotes an outward flow of solutes, preventing the disruption of the cell (Thompson and Baenziger, 2020). The paradigm of the force-from-lipids model is a model that suits some ion channels from bacteria and their orthologues in Archaea, fungi and plants (Cox et al., 2019), as well as mechanosensitive channels TRAAK, TRK1 and Piezo 1 (Kefauver et al., 2020).

As mentioned previously, the activation of mechanosensitive ion channels can be modulated by proteins, such as MEC-2 in *C. elegans* and the STOML3 in mice (Wetzel et al., 2007). Particularly, STOML3 recruits cholesterol to the cellular membrane, which makes it stiffer and with more tension, in comparison to STOML3 mutant mice (Qi et al., 2015). Importantly, ablation of STOML3 in mice leads to a complete loss of mechanical activated currents in 35% of mechanoreceptors (Wetzel et al., 2007). Similarly, cholesterol depletion also has led to a reduction in mechanically activated sensory neurons in wild-type mice, while it did not affect STOML3 mutant mice (Qi et al., 2015). DRG neurons lacking STOML3, have an higher activation threshold (Handler and Ginty, 2021). These findings suggest that tension in the lipid bilayer influences activation of piezo channels.

The dual tether model of gating of MS speculates that, the channel is connected to the actin cytoskeleton and to adjacent stereocilia by means of intra and extracellular tethers, respectively (Chalfie, 2009). These tethers, also known as “tip-links”, maintain the ion channel in a closed conformation and are pulled out upon stretching stimuli, which turns MS ion channels in an open conformation (Chalfie, 2009). This model is supported for hear cells, where it was shown that loss of “tip links” leads to a loss in transduction (Assad et al., 1991).

In the single tether model, both lipids and tethers influence the opening of MS. Here, the membrane is connected to the cytoskeleton by means of tethers. Changes in the position (upward or downward) of those tethers leads to conformational changes in the ion channel structure (Chalfie, 2009).

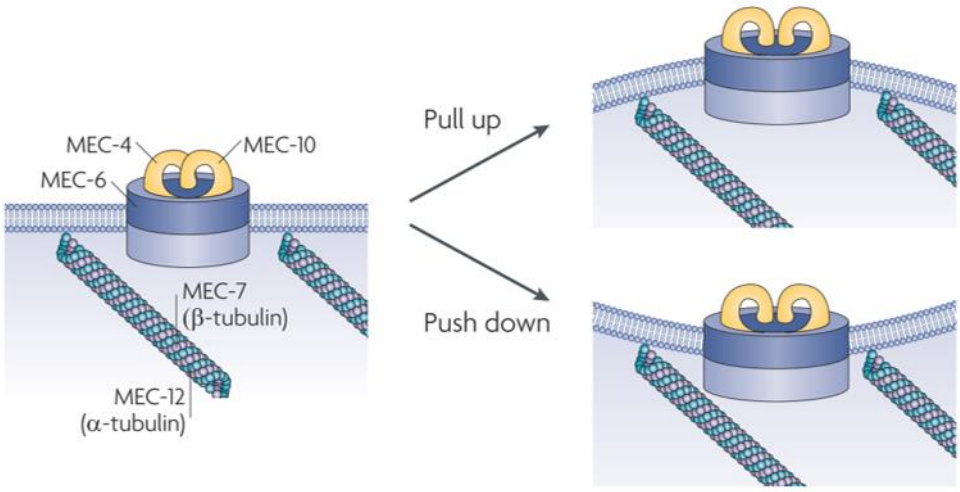


Figure 4 – Gating of mechanosensor ion channels – single-tether model In *C. elegans*, the complex made of the pore forming proteins MEC-4 and MEC-10 together with MEC-6 forms an ion channel. Following cell deformation, microtubule tethers made of MEC-12 and MEC-7 move in the up or downward direction, which causes the opening of the MS ion channel. Taken from (Chalfie, 2009).

In drosophila, NOMPC ion channels contain 29 spring-like ankyrin repeat domains, also known as membrane-microtubule connectors, that tether the cellular membrane to the microtubule cytoskeletal network, pulling them together (Zhang et al., 2015). Upon microtubule deformation, these ankyrin repeats transmit the mechanical stimuli to NOMPC, leading to the opening of the pore channel (Jin et al., 2017). The link between NOMPC ion channels and microtubules became more evident with the demonstration that infusion of nocodazole, a microtubule depolymerizing drug, reduced NOMPC mechanically gated ion currents (Zhang et al., 2015).

Another evidence favouring the force-from-filament paradigm arose from experiments carried out in primary cultures of DRG neurons. In this study, Hu et al., identified extracellular protein tethers, that link the membrane of the mechanosensor to the extracellular matrix (Hu et al., 2010). Moreover, the authors have shown that treatment with non-specific

endopeptidases destroyed those tethers and abolished rapidly-adapting mechanosensitive currents (Hu et al., 2010).

Both, the lipid bilayer and the cytoskeleton are affected by mechanical stimuli, therefore it seems reasonable that these two models of gating of mechanosensitive ion channels may not be mutual exclusive (Cox et al., 2019). Indeed, piezo 1 function can be perturbed from the perspective of both of the gating models. As mentioned previously, STOML3 modulates the activation threshold of piezo channels by increasing membrane stiffness. However, there are also findings supporting tethering models. Indeed, the disruption of cell interactions with the extracellular matrix increases the activation threshold of piezo 1 channels, while increasing cell adhesions with extracellular proteins sensitizes it (Gaub and Müller, 2017).

Before diving into more detail on how the cytoskeleton may influence mechanosensation and how it can be a useful target to modulate, I will introduce some basic concepts regarding it.

4.3 The Cytoskeleton

The cytoskeleton is a dynamic three-dimensional network of filaments, made of protein polymers and regulatory factor (Fletcher and Mullins, 2010). It is involved in many physiological processes, such as providing structural support, maintaining cell's integrity in response to internal and external physical forces during for instance muscle contraction or cell division. Moreover, it is also important for cell signalling events, intracellular transport and cell motility (Fletcher and Mullins, 2010).

The main protein polymers that compose the cytoskeleton are: microtubules, actin filaments and intermediate filaments (Pegoraro et al., 2017).

Microtubules are evolutionary conserved dynamic tubular structures, expressed from prokaryotes to humans, involved in many cellular processes, such as maintenance of the cellular structure, cell division, cell motility among others (Gadadhar et al., 2017). These filaments are present not only in the cytoskeleton, but also in the mitotic spindle, centrioles, cilia and flagella (Janke and Magiera, 2020). Microtubules are the largest and stiffest filaments of the cytoskeleton. These filaments are composed of heterodimers of α and β-tubulin, organized in a dynamic and polarized way, forming a hollow tube (Fletcher and Mullins, 2010).

Actin filaments, as microtubules, are polarized filaments made of linear polymers of β-actin. Actin filaments have an intermediary stiffness and are pointed out as key players in pushing (protrusive) and pulling (contractile) forces, therefore involved in whole cell migration, phagocytosis, intracellular motility, cell adhesion with extracellular matrixes of neighbouring cells, among other functions (Svitkina, 2018).

Given the polarized structure of both microtubules and actin filaments, these structures can function as tracks for motor proteins (Fletcher and Mullins, 2010). Motor proteins from the kinesin and dynein families associate with microtubules to promote anterograde and retrograde transport of intracellular cargos, respectively (Hirokawa et al., 2009). Moreover, these are also involved in the assembly of the microtubule array during cell division (Fletcher and Mullins, 2010). Motor proteins of the myosin family associate with actin filaments and

impose contractile forces, causing for example, muscle contraction (Svitkina, 2018). In addition, myosin also enable cells to sense their external environment (Fletcher and Mullins, 2010).

Intermediate filaments are the least stiff polymers of the cytoskeleton, these filaments can be divided into five different categories, which are cell-type dependent (Fletcher and Mullins, 2010). Additionally, intermediary filaments also interact with microtubules and actin filaments, rendering cells resistant to tensile and compressive forces and therefore, facilitating physiological processes (Bott and Winckler, 2020).

Now I will describe in more detail how microtubules and specifically how post-translational modifications of α-tubulin are implicated in mechanosensory events.

4.3.1 Microtubules and α-tubulin acetylation

As mentioned above, microtubules are highly conserved structures, essential for many cellular processes (Janke and Bulinski, 2011). Microtubules reorganize their spatial distribution by undergoing cycles of polymerization and depolymerisation (Mitchison and Kirschner, 1984). Moreover, the physiological function of microtubules is regulated by several post-translational modifications, which are also described in the literature as the tubulin code (Janke and Magiera, 2020). In my work, I am particularly interested in manipulating α-tubulin acetylation and its involvement in mechanosensation.

Microtubules undergo acetylation and deacetylation on the ε-amino group of the lysine residue 40 (K40), located on the inner side of the lumen of microtubules, as shown in Figure 5 (Janke and Magiera, 2020; L'Hernaul and Rosenbaum, 1985; LeDizet and Piperno, 1987). K40 acetylation is catalysed by α -tubulin acetyltransferase 1 (Atat1) in mammals (Akella et al., 2010; Shida et al., 2010) and can be reversed mainly by histone deacetylase 6 (HDAC6) (Hubbert et al., 2002) and less by the deacetylase sirtuin type 2 (SIRT2) (North et al., 2003).

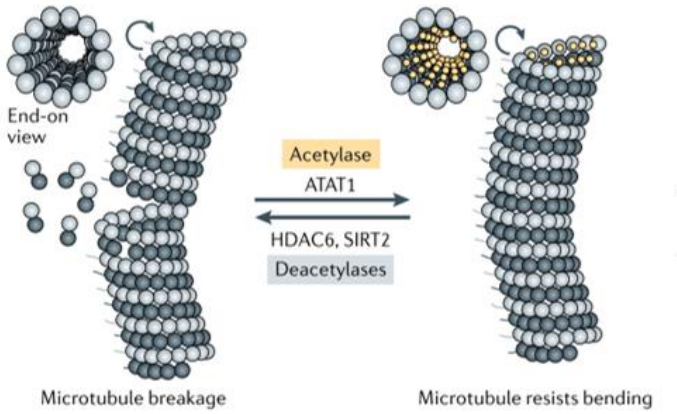


Figure 5 – α-tubulin acetylation on microtubules. α-tubulin acetylation is catalysed by Atat1, and reversed by the deacetylases HDAC6 and SIRT2. α-tubulin acetylation renders microtubules more resistant to mechanical stress. Adapted from (Janke and Magiera, 2020)

Lysine acetylation is a highly conserved post-translational modification, occurring from prokaryotes to humans (Choudhary et al., 2009). K40 acetylation on microtubules is observed throughout different species by orthologues of Atat1. In *C. Elegans* the α-tubulin orthologue, MEC-12, is acetylated by the Atat1 orthologue MEC-17, whilst in drosophila the reaction is catalysed by dTAT and in zebrafish by zgc.65893 (Akella et al., 2010; Yan et al., 2018).

Atat1 presents a preference for α-tubulin in its polymerized state and acetylation of microtubules is seen as a hallmark of stable long-lived microtubules (Szyk et al., 2014). Indeed, even though α-tubulin acetylation occurs in a less accessible region of microtubules (Soppina et al., 2012), Atat1 has a preference for microtubules over free tubulin (Shida et al., 2010). Friedmann et al., hypothesized that this observation could be due to the fact that the recognition site of Atat1 requires lateral contact between α-tubulin and neighbouring β-tubulins (Friedmann et al., 2012). Indeed, experiments using Atat1 tagged with the green fluorescent protein (GFP) demonstrated that Atat1 enters the lumen of microtubules through lateral cracks or bends in microtubules or through their opening extremities (Coombes et al., 2016). Once inside the microtubule structure, Atat1 browses the length of microtubules and randomly acetylates K40 along the way (Ly et al., 2016; Szyk et al., 2014).

Tubulin acetylation can have different roles in different tissues. Nevertheless, at a resolution of 8 to 9 Å, acetylation of K40 on α-tubulin does not seem to influence microtubule assembly and architecture. (Howes et al., 2014) Therefore, microtubule acetylation must influence cells' physiology by interaction with other cellular structures.

In *C.elegans*, the orthologue of Atat1, MEC-17 is the main α-tubulin acetyltransferase (Akella et al., 2010). Atat1 influences microtubule length in *C. elegans* and its ablation is related to morphological defects and loss of mechanosensitivity in touch receptor neurons (Akella et al., 2010; Shida et al., 2010; Topalidou et al., 2012)

In drosophila, d-TAT, the orthologue of MEC-17 has also proven to have a pivotal role in response to gentle touch (Yan et al., 2018). Yan et al. showed that flies expressing a mutated d-TAT unable to acetylate α-tubulin present a reduced response to mechanical stimuli, but not to noxious thermal stimuli (Yan et al., 2018). Moreover, in another experiment, the team observed that hyperacetylation of microtubules or taxol-induced microtubule stabilization render fly larvae sensitized to gentle touch (Yan et al., 2018).

In zebrafish, acetylated microtubules are enriched in neurons and cilia (Wilson 1991). When the expression of the orthologue of Atat1, zgc:65893 (mec17), is reduced in zebrafish embryos, animals show developmental and neuronal defects, such as a reduced or absent response to sensory stimuli. Nonetheless, depletion of zgc:65893 (mec17) did not lead to a reduced expression of acetylated microtubules on zebrafish cilia, which indicates the presence of another acetyltransferase in these structures (Akella et al., 2010).

In mammalians, tubulin acetylation occurs in stable microtubules, usually present in neuronal axons and cilia (Kalebic et al., 2013b). This post-translational modification is involved in many cellular processes such as intracellular transport (Reed et al., 2006) or neuronal development (Li et al., 2019). Ablation of Atat1 in mice abolishes tubulin acetylation in microtubules, (Kalebic et al., 2013a) and causes defects on spermatozoa morphology and motility, nonetheless, these animals remain viable (Kim et al., 2013). Specific ablation of Atat1 in the peripheral nervous system reduces mechanical sensitivity in mice, possibly due to changes in the stiffness of primary sensory neurons (Morley et al., 2016).

Neurons are polarized cells with specific subcellular components and intense neuronal trafficking (Even et al., 2019). For these cells, the cytoskeleton and particularly microtubules have fundamental roles for neuronal communication (Janke and Bulinski, 2011). Motor proteins, from the kinesin or dynein superfamily of proteins, are responsible for facilitating antero and retrograde intracellular transport, respectively. These proteins bind to their cargos (protein complexes, mRNA, vesicles) and transport them along microtubule tracks (Hirokawa et al., 2009). In order to reach the microtubules at a long distance from the cell body of neurons, Atat1 binds to the external surface of motile vesicles and travels through the cells, acetylating microtubules (Even et al., 2019). Previous experiments on hippocampal neurons demonstrated that interactions between motor proteins and post-translational modifications on microtubules, such as acetylation of microtubule tracks could guide intracellular transport to specific locations within cells (Reed et al., 2006).

Defects in microtubule structure and post-translational modifications have been associated with many diseases. Particularly, in Huntington's, Alzheimer's and Parkinson's disease, acetylation of α-tubulin is reduced, while in some cancer models, hyperacetylation of α-tubulin is associated with increased capacity for cell invasion (Boggs et al., 2015; Castro-Castro et al., 2012; Dompierre et al., 2007; Govindarajan et al., 2013; Outeiro et al., 2007; Yoshimoto et al., 2021)

Importantly, the findings of Morley and colleagues demonstrated that mice lacking Atat1 in the peripheral nervous system have a reduced mechanosensitivity and suggest that Atat1 could be a target for the treatment of mechanical pain. In my thesis, I aimed to deplete Atat1 expression using gene therapy approaches that I discuss in the next sections.

4.4 Gene Manipulation

Before the discovery of the structure of DNA, there has been a great effort on finding ways of manipulating gene expression. Advances in molecular biology has shined light to many genomic phenomena. Nonetheless, there is still much to unravel in terms of gene function and the potential in their manipulation.

The concept of gene therapy was firstly introduced in 1972, , when Friedmann and Roblin suggested that “genes can be medicine” (Friedmann and Roblin, 1972). Sequencing of the human genome has led to the discovery of a countless number of monogenic diseases that could be treated by delivering a corrected version of the mutated gene or by silencing its expression (Dunbar et al., 2018). Moreover, the use of gene therapy is not limited to genetic diseases, it could also be used to fight cancer and viral infections (Andrews et al., 2017).

Current ongoing clinical trials using gene therapy in which nucleic acids (DNA or RNA) are used as a treatment have given encouraging results that are paving the way toward new therapies against diseases currently without a treatment (van Haasteren et al., 2020).

4.4.1 Knock-out of gene expression - CRISPR gene editing

Genome editing was firstly described with the discovery of zinc-finger nucleases (ZFNs) and transcription activator-like effector nucleases (TALENs), both techniques require sequence specific nucleases to induce DNA mutations (Hirakawa et al., 2020). In the early 2000s, Jennifer Doudna and Emmanuelle Charpentier discovered clustered regularly interspaced short-palindromic repeat (CRISPR) technologies. Gene editing with CRISPR has provided a more simplified and accessible method to manipulate gene expression. Doudna and Charpentier received later on in 2020 the Nobel Prize in chemistry for developing the precise genome-editing technology.

CRISPR associated (Cas) enzymes were firstly identified in bacteria and archaea, these enzymes played a role of adaptive immune response against virus and plasmids (Moineau et al., 2007). CRISPR-Cas systems are organized in two classes based on its nuclease effector and

are further divided in six types and 27 subtypes (Barman et al., 2020). The most well-studied CRISPR system is the type II CRISPR-Cas9 system.

The CRISPR-Cas9 system is made of the programmable endonuclease Cas9, a CRISPR RNA (crRNA) and a trans-activating crRNA (tracrRNA). Both crRNA and tracrRNA are necessary to guide Cas9 to a specific DNA sequence close to a protospacer-adjacent motif (PAM) (Jinek et al., 2012). crRNA is a short ~20 nucleotide complementary sequence to the target DNA, while tracrRNA is recognized by Cas9 (Wiedenheft et al., 2012). Fusion of the 3' end of crRNA to the 5' end of tracrRNA results into a chimeric single guide RNA (gRNA). Manipulation of gRNA's sequence enables to programme Cas9 to cleave specific sites within the genome (Jinek et al., 2012).

Currently six orthologues of Cas9 enzymes have been identified in different organisms. Despite the resemblance of function, Cas9 enzymes may diverge in terms of size and sequence similarity (Fonfara et al., 2014). Nevertheless, structurally, all Cas9 enzymes share a bi-lobed structure, made of a nuclease lobe (NUC) and a recognition domain (REC) (Wilkinson et al., 2019). The NUC lobe comprises the nuclease domain HNH that cleaves the DNA target strand (complementary to the gRNA sequence) and the nuclease domain RuvC that mediates DNA cleavage in the non-target strand (Jinek et al., 2014). Different Cas9 orthologues have different PAM sequences (Anders et al., 2014; Mojica et al., 2009), which means that not all gRNA sequences will work for all Cas9 enzymes.

Figure 6 portraits the mechanism of gene knock-out through CRISPR-Cas9. The nuclease Cas9 browses the DNA regions adjacent to the PAM motifs, whenever there is a sequence complementarity between DNA and crRNA, the gRNA unwinds a portion of the double helix DNA and Cas9 exerts its nuclease function, causing a double strand break in the DNA (Wang et al., 2016)

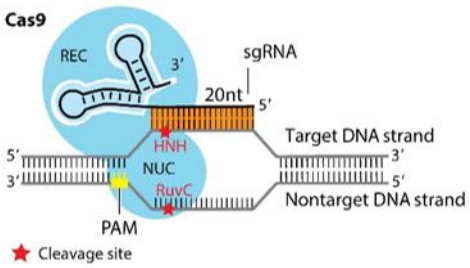


Figure 6 – CRISPR-Cas9 Cas9 nuclease is an RNA guided nuclease. It recognizes the site for inducing a double strand break in DNA molecules in the presence of base pairing between target DNA and gRNA and if this site is located adjacent to a PAM motif. Adapted from (Wang et al., 2016).

Following DNA cleavage by Cas9, the target locus may undergo one of two main pathways for DNA repair, called homology directed repair (HDR) pathway or non-homologous end joining repair (NHEJ) (Wang et al., 2016). The HDR pathway is less frequent and requires a template for DNA repair, which allows the correction of DNA sequences (Wilkinson et al., 2019). In the absence of a repair template, the most frequent situation, the double strand DNA breaks are re-ligated through NHEJ, causing insertion/deletions (indel) mutations, which may materialize in frameshift mutations or premature stop codons (Ran et al., 2013).

Delivery of Cas9 together with the gRNA sequence allows for precise and efficient modifications in the genome of mammalian cells, including human cell lines (Mali et al., 2013). The versatility of CRISPR-Cas9 and the easiness of designing gRNA sequences provide scientists with an effective and accessible gene editing toolbox, compared to previous systems, in which the bottleneck for gene editing resided in the design of specific nucleases for each targeted DNA sequence (Hirakawa et al., 2020).

In addition to the potential of CRISPR-Cas9 as a tool for scientists, it can also be a tool for treating diseases. With the advances in sequencing techniques, it has been possible to identify single nucleotide polymorphisms (SNPs) for which CRISPR-Cas9 can be useful to silent or correct the expression. Moreover, in the case of diseases caused by gain-of-function

mutations, it is not possible to treat the disease by simply delivering a functional gene, it is also necessary to knock-out the non-functional gene, what CRISPR-Cas9 can do (Dunbar et al., 2018).

Regardless the potential and accessibility of CRISPR technologies, there are still serious concerns about its safety, namely potential off-targets, long term effects, environmental effects and ethical implications (Doudna, 2020). There is therefore a great need for finding effective regulations that allow the progress of scientific development but also protects the world (Doudna, 2020).

4.4.2 Knock-down of gene expression – RNAi

Small interfering RNA (siRNA) are non-coding RNAs of 20 to 30 nucleotides in length, involved in post-transcriptional gene silencing in a sequence specific manner. This natural process, called RNA interference (RNAi), was firstly described in *C. elegans,* in which delivery of a double stranded (ds)RNA targeted par-1 mRNA for degradation (Fire et al., 1998). These findings honoured Andrew Fire and Craig Mello with the Nobel Prize in physiology and medicine in 2006. RNAi is an intrinsic system found also in plants, fungi and animal cells and it can be described as a way of allowing cells to fine tune the regulation of gene expression (Crooke et al., 2018).

Different types of RNA molecules are described in the literature as gene regulators through RNAi: micro RNA (miRNA), small interfering RNA (siRNAs) and shRNA (short-hairpin RNA) (Crooke et al., 2018; Siolas et al., 2005). miRNAs are usually genome-encoded and are able of targeting different genes through incomplete complementarity. siRNAs are dsRNAs that can be chemically synthetized. When delivered to cells, they can cause transient sequence-specific gene repression (Elbashir et al., 2001). Finally, shRNAs are encoded by DNA sequences that after transcription are processed into siRNAs (Siolas et al., 2005).

Delivery of siRNAs into cells can be transient or stable. In the former case, one can ectopically deliver dsRNAs through lipid-based transfection reagents, nanoparticles, chemical

modification of oligonucleotides (Dowdy, 2017). In the latter case, one can achieve a stable delivery of siRNAs using plasmids or viral vectors with shRNAs sequences associated with promoters for constitutive expression, such as U6 promoter (Brummelkamp et al., 2002). Constitutive expression of shRNAs may lead to knock-down of gene expression and consequent protein depletion (Echeverri and Perrimon, 2006).

The precursor shRNA transcript is made of a sequence of approximately 21 nucleotides siRNA, separated from its reverse complement by a short spacer (Siolas et al., 2005). After transcription, by means of intramolecular complementarity, the shRNA single strands acquire a secondary structure resembling an hairpin and it is exported to the cytoplasm by exportin-5 (Yi et al., 2003), to be further processed. Dicer, a RNAse III-family nuclease, converts the hairpin structure of the shRNA into a siRNA (Gu et al., 2012; Siolas et al., 2005), which is then integrated into an argonaute 2-contaning RNA-induced silencing complex (RISC) and the proteins from the argonaute (ago) family from RISC unwind the dsRNA into passive and active single strand RNAs (Hutvagner and Simard, 2008). The endonuclease RISC eliminates the passive, while the active strand will guide RISC to the target mRNA.

Importantly, in 2001, Elbashir et al, showed for the first time, that delivery of exogenous siRNA can silence gene expression in mammalian cells (Elbashir et al., 2001). Ever since, more evidences of gene silencing through RNAi have been published and that paved the way for transitioning RNAi from basic research to potential therapies for diseases with unmet clinical needs. In 2010, the first RNAi-mediated therapy targeted the VEGF receptor-1 and ever since, many more genes were demonstrated to be targeted by RNA therapies (Bumcrot et al., 2006).

In my thesis, I explore the potential of RNAi therapies for the treatment of chronic pain, combined with a delivery through recombinant adeno-associated viral (AAV) vectors.

4.4.3 Delivery systems of genetic material

Delivery of exogenous genetic material to cells has shown great potential in altering cell fate. In modern medicine, the concept of gene therapy has become a more tangible therapeutic approach given the critical discoveries made in the last decades (Dunbar et al., 2018). With gene therapy, it would be possible to prevent or delay the onset of a disease, hinder or cure it. The cure for a disease may arise from the delivery of a gene, when the monogenic disease is due to the lack of a gene, or by silencing the expression of a defective gene. Despite its potential, how to successfully deliver genes *ex-vivo* and *in-vivo*, remains one of the many hurdles for gene therapy (Li and Samulski, 2020).

Current gene delivery methods rely mostly on lipid-based methods, nanoparticles, non-replicating viral vectors, such as lentivirus, adenovirus and adeno-associated virus (AAVs) (van Haasteren et al., 2020). In the last years, viral vectors have become the most promising method for gene therapy, due to its high efficiency of delivery and lower genotoxicity (Dunbar et al., 2018).

Wild-type AAVs are unable to self-replicate, for that, they require a helpervirus (an adenovirus or a herpesvirus) to replicate (Riyad and Weber, 2021). AAV viruses belong to the *Parvoviridae* family of viruses and have an icosahedral capsid that hosts a single-stranded DNA AAV genome (Srivastava, 2016).

As shown in Figure 7, the wild type AAV genome comprises two genes, *rep* and *cap*, flanked by inverted terminal repeats (ITRs). The *rep* gene supports genome replication and virion assembly and because it can be transcribed from different promoters, p5, p19 and undergo alternative splicing, the *rep* gene renders the codification of four *rep* transcripts (*rep78, rep68, rep52* and *rep40*) (Riyad and Weber, 2021). The *cap* gene encodes three overlapping proteins VP1, VP2 and VP3 that constitute the viral capsid. VP proteins share the same C-terminal, however since they have different starting codons within the same *cap* gene, they differ in their N-terminal sequence. Indeed, the sequence of VP3 is contained integrally in the VP1 and VP2 proteins (Sonntag et al., 2010). Finally. the capsid of AAV viruses is assembled by approximately 60 VP monomers at a ratio of VP1: VP2:VP3 of 1:1:10 (Büning

and Srivastava, 2019). In some AAV serotypes (see further) there is an assembly activating protein (APP) codified in the *cap* gene, through an alternative open reading frame in *cap.*

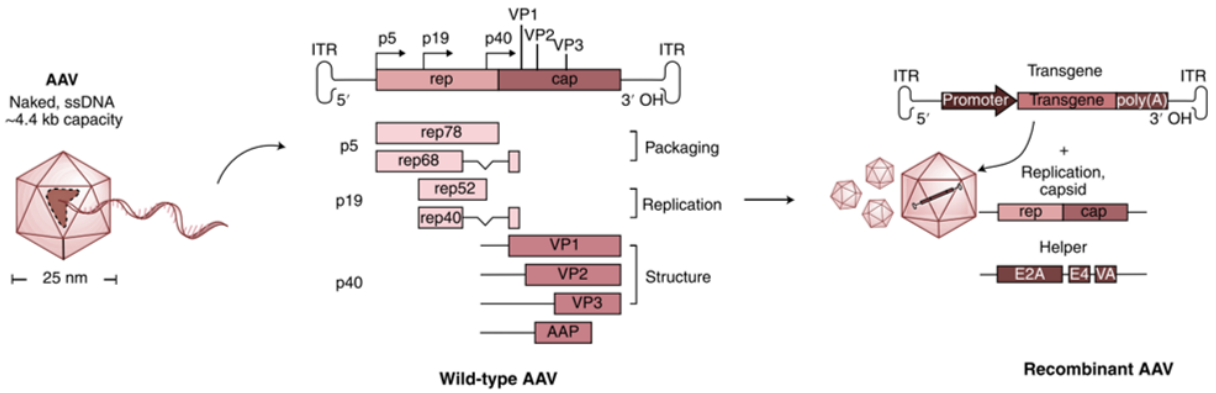


Figure 7 – Adeno-associated viruses AAV vectors carry a ss-DNA inside, containing cap and rep genes essential for viral replication and capsid assembly. By removing these two genes from AAVs and replacing them with a transgene and promoter of interest, it is possible to produce recombinant AAVs, capable of delivering genetic material to cells. Taken from (van Haasteren et al., 2020).

AAV vectors can be modified to induce expression of a transgene of interest. Recombinant AAV (rAAV) are AAV vectors in which the portion comprising rep and cap genes is replaced by a promoter and a transgene of interest and other sequences of interest. The inverted terminal repeats (ITR) of AAV are essential for transgene expression and vector production and therefore cannot be replaced. A drawback of using rAAVs viruses is associated to its maximum of 4.5kb of packaging limit between ITRs (Li and Samulski, 2020). Given that rAAV do not possess the sequences for the proteins of the capsid, these viruses are no longer able to replicate.

Up to date there are identified 13 natural variants of AAV viruses and more than 100 different variants (Mietzsch et al., 2014). Naturally occurring AAV serotypes can be a valuable platform of gene delivery to distinct tissues, by recognition of different types of glycans as cell receptors. However, despite the variety of AAV serotypes available, there are still challenges

in targeting specific cell populations, such as DRG neurons whose location hinders AAV efficiency (Challis et al., 2019). A great effort has been made in engineering rAAV capsids in order to increase cell tropism, viral efficiency and reduce immunogenic response from the host organism (Wang et al., 2019). Most promising strategies of AAV capsid engineering fall into genetic mutation of capsids, chimeras of capsids from different AAV serotypes and chemical modification of capsids (Lee et al., 2018).

The serotype 2 (AAV2) is currently the serotype that has been most studied for gene therapy applications, given its broad tropism and high transduction efficiency (Zincarelli et al., 2008). AAV2 has a natural tropism towards the liver and the spleen, where the capsid interacts with heparin sulfate proteoglycans (HSPG) on the cell surface before being internalized. Mutation of the capsid region that interacts with HSPG, generates a detarget AAV2, which is unable to be internalized by liver and spleen cells. Further modification of the detarget capsid delta-HSPG AAV2, through introduction of ligand binding sites allows the retargeting of delta-HSPG AAV2 to other cell populations that were previously resistant to viral infection. This ligand-guided delivery of molecules with therapeutic potential has been previously described for cells traditionally challenging to reach (Dhandapani et al., 2018; Maffei et al., 2019).

The efficiency of viral transduction depends on the virus, ie, on its interaction with the host cell or depends on the transgene regulation. Great efforts have been made for the last 20 years to improve the viral capsid not only to increase viral transduction, but also for increasing safety.

The aim of this work was to understand if it is possible to manipulate the acetylation of α-tubulin by depletion of Atat1. To do this, I divided this work in three different approaches targeting Atat1 at a genomic, post-translational and post-transcriptional level. I have tested these approaches in an increasing complexity of preparations, starting from *in-vitro,* followed by *ex-vivo* and *in-vivo* models. I aimed to develop a platform of manipulation of Atat1 expression that could be used to understand how manipulation of acetylated α-tubulin could be used in different disease models in mouse cells. Ultimately, I aimed to explore the use of gene editing techniques associated with a viral delivery for manipulating mechanosensation

in fully developed mice and understand if these strategies could be translated into a new therapy for the treatment of diseases of the somatosensory system.

5. Methods

5.1 Cloning

5.1.1 Cloning mCherry-Atat1-CRISPR

To knock-out the expression of Atat1 in mice using CRISPR-Cas9, sequences for gRNAs were chosen using the *GPP sgRNA Designer* tool from the Broad Institute (https://portals.broadinstitute.org/gpp/public/analysis-tools/sgrna-design accessed in July 2019). The five best scoring non-overlapping gRNAs targeting the coding sequence of Atat1 were selected (Kim et al., 2018). Possible off-target genes were tested by running a BLAST of gRNAs sequences against the mouse genome (GRCm38) in ENSEMBLE (Cunningham et al., 2019).

Table 1 – Selected gRNA sequences for targeting Atat1 gene

gRNA	Sequence 5'-3'	Location in gene bp	Primers for PCR amplification
1	GAAGGACACCTCAGCCCGACC	5797-5817	FW:5'- GACTATTGTAGATGAGCTGGG-3'
			RV:5'- GAAACAACCCGAGGTAGAAC-3'
2	GACTTTTACATCCACGAGTCG	6155-6175	Same as gRNA1
3	TGAGAGCAACTCGACACTCTC	10918-10938	FW:5'- CTTACCTTGTGTCAGCCTAG-3'
			RV:5'- TACACATTTTGAGCATTCGC-3'
4	TGCACCCATCACCAGCGCTTT	5740-5760	Same as gRNA1
5	CTGGCCATTGACCGACCATCG	6436-6456	Same as gRNA1

The pairs of oligonucleotides of each gRNA were synthetized with the 5'-CACC and 3'-AAAC BsaI overhangs by Sigma Aldrich. 10µL of complementary oligos (100µM) were annealed in 1.2x annealing buffer (10mM Tris, 60mM NaCl and 1mM EDTA). To insert the gRNA sequences into pX601-mCherry plasmid (Addgene #84039) (Ye et al., 2016), firstly the vector was digested with the restriction enzyme BsaI (New England Biolab, NEB #R0535S), the digestion products were separated in a 1% agarose gel and visualised by Mirodi green advance (Genetics #MG04). The band corresponding to the backbone of the vector (8kb) was excised from the gel and DNA was purified with the kit QIAquick Gel Extraction (Qiagen #28704). The

annealed product of gRNAs was ligated into the purified vector using T4 Ligase enzyme (NEB #M0202S) following manufacturer's instructions. Chemically competent Stbl3 *E.Coli* (Invitrogen LSC737303) were transformed with the ligation product. Single colonies were picked for mini-prep inoculation and DNA purification with the kit QIAprep Spin Miniprep Kit (Qiagen #27104). The purified DNA was sequenced by Eurofins Genomics, at the region downstream of the U6 promoter, to confirm a correct gRNA insertion.

Table 2 – Features of pX601-mCherry plasmid

Feature	Name	Function
ITR	Inverted terminal repeat	Sequence that flanks the DNA sequence that gets packaged into AAV viruses (Lee et al., 2018)
CMV enhancer	human cytomegalovirus immediate early enhancer	DNA regulatory element that increases gene transcription (Stinski and Isomura, 2008)
CMV	cytomegalovirus immediate-early promoter	Strong mammalian expression promoter from the human cytomegalovirus (Qin et al., 2010)
SV40 poly(A) signal	simian virus 40 polyadenylation signal	Helps the nuclear export of RNA and RNA translation. Promotes RNA transcript longevity
T2A	thosea asigna virus 2A	2A self-cleaving peptide, allows co-expression of separate proteins under the same promoter (Liu et al., 2017)
mCherry	mCherry	monomeric red fluorescent protein, acts as a reporter for the transfection (Kleeman et al., 2018)
U6	U6 promoter	From the human U6 small nuclear promoter – small RNA expression (Paule and White, 2000)
gRNA	Guide RNA	Sequence brings Cas9 to DNA (Jinek et al., 2012)

5.1.2 Cloning Atat1-CRISPR

In order to insert gRNA1 into pX601 miniCMV-SaCas9-SpA-sgRNA scaffold (Addgene #107055, here described as Ctrl-CRISPR), a new set of oligonucleotides of gRNA1 were synthesized with 5'-ACC and 3'-AAC BspQI overhangs (gRNA1 fw: 5' accGAAGGACACCTCAGCCCGACC, gRNA rw: 5' aacGGTCGGGCTGAGGTGTCCTTC). Oligos were annealed and inserted into BspQI (NEB #R0712S) digested and purified Ctrl-CRISPR vector, as previously described. Stbl3 *E.Coli* were transformed with the ligation product and DNA of isolated colonies were purified. To confirm the success of gRNA insertion, the purified DNA was sent to be sequenced at the region downstream of the U6 promoter using the primer 5'-CTATTTCCCATGATTCCTTC, by Eurofins Genomics.

Table 3 – Features of pX601 miniCMV-SaCas9-SpA-sgRNA (Ctrl-CRISPR)

Feature	Name	Function
ITR	Inverted terminal repeat	Sequence that flanks the DNA sequence that gets packaged into AAV viruses (Lee et al., 2018)
minimal-CMV	minimal-CMV promoter	Promoter fragment derived from the CMV immediate early promoter (Johari et al., 2021)
Kozak sequence	Kozak sequence	Functions as the protein translation initiation site (Hernández et al., 2019)
SV40 NLS	simian virus 40 nuclear localization sequence	Signal fragment that targets proteins to be imported to the nucleus (Lu et al., 2021)
SaCas9	Staphylococcus aureus Cas9 nuclease	Protein sequence (Kleinstiver et al., 2015)
HA	haemagglutinin (HA)-tag	Genetically encoded tag (Xiang et al., 2019)
U6	U6 promoter	From the human U6 small nuclear promoter – small RNA expression (Paule and White, 2000)
gRNA	Guide RNA	Sequence brings Cas9 to DNA (Jinek et al., 2012)

5.1.3 Cloning mini-CMV-tdTomato

Ctrl-CRISPR was digested with the restrictions enzymes KpnI (NEB #R3142) and EcoRI (NEB #R3101) to excise the SaCas9 sequence from the vector. The restriction enzyme HindIII (NEB #R0104) was added to the digestion mixture to enable clear visualization of the DNA fragment of interest in an agarose gel. The insert tdTomato was obtained by digestion of the plasmid pAAV-CAG-tdTomato (Addgene #59462) with KpnI and EcoRI. Both digestion products were run in a 1% agarose gel and the bands of interest were purified as previously described. The vector and insert were ligated using T4 ligase, following manufacturer's instructions. Stbl3 *E.Coli* were transformed with the ligation product and DNA of isolated colonies was purified. To confirm the success of the insertion of tdTomato in the vector Ctrl-CRISPR, N2a cells were transfected with the purified DNA, to check for expression of tdTomato.

Table 4 – Features of pAAV-CAG-tdTomato

Feature	Name	Function
ITR	Inverted terminal repeat	Sequence that flanks the DNA sequence that gets packaged into AAV viruses (Lee et al., 2018)
CAG	CMV major immediate-early enhancer combined with the chicken beta-actin promoter	Strong hybrid mammalian promoter (Qin et al., 2010)
Kozak sequence	Kozak sequence	Functions as the protein translation initiation site (Hernández et al., 2019)
tdTomato	Tandem dimer Tomato	red fluorescent protein, acts as a reporter for the transfection (Kleeman et al., 2018)
WPRE	Woodchuck Hepatitis Virus (WHP) Posttranscriptional Regulatory Element	Aids the nuclear export of mRNA and the expression of AAV transgene (Loeb et al., 1999)
SV40 poly(A) signal	simian virus 40 polyadenylation signal	Helps the nuclear export of RNA and RNA translation. Promotes RNA transcript longevity

5.1.4 Cloning Atat1-sh

The starting point of knock-down experiments were two siRNA sequences previously studied in the laboratory (Atat1-sh: 5'-UUUGCAUUCUGGACUUUUAUU, Atat1-sh2: 5'-UUUGCAUUCUGGACUUUUAUU) and a third one already published in experiments using rat animal models (Atat1-sh3: 5'-GCAGCAAATCATGACTATTGT) (Even et al., 2019). Oligos enconding shRNAs were synthesized by Sigma Aldrich, with overhangs for BamHI and XbaI. siRNA and complementary siRNA sequences were tested for off-target effects by running a BLAST of sequences against the mouse genome (GRCm38) in ENSEMBLE (Cunningham et al., 2019).

shRNA sequences were cloned into AAV-shRNA_tet3 (Addgene #85740) pAAV vector (Yu et al., 2015) as previously described, using BamHI (NEB #3136) and XbaI (NEB #R0145) restriction enzymes to digest AAV-shRNA_tet3.

Table 5 – Features of AAV-shRNA_tet3

Feature	Name	Function
ITR	Inverted terminal repeat	Sequence that flanks the DNA sequence that gets packaged into AAV viruses (Lee et al., 2018)
U6	U6 promoter	From the human U6 small nuclear promoter – small RNA expression (Paule and White, 2000)
shRNA	Short-hairpin RNA	Sequence that is processed into siRNA in cells (Siolas et al., 2005)
EF1α	elongation factor 1 α	Strong constitutive mammalian expression promoter (Qin et al., 2010)
eYFP	Enhanced Yellow Fluorescent Protein	Yellow fluorescent protein, acts as a reporter for the transfection (Kleeman et al., 2018)
WPRE	Woodchuck Hepatitis Virus (WHP) Posttranscriptional Regulatory Element	Aids the nuclear export of mRNA and the expression of AAV transgene (Loeb et al., 1999)
hGH polyA signal	Human growth hormone polyadenylation signal	Important for stability and protection from degradation of mRNA transcripts. Involved in nuclear export and translation processes. (https://doulix.com/biomodules/Q4NCNL4/)

5.2 N2a cell culture and transfection

Neuro-2a (N2a) cells were cultured in Dulbecco's Modified Eagles Medium (DMEM), high glucose, Glutamax, pyruvate, supplemented with 10% Fetal Bovine Serum (FBS, Euroclone #ECS0180L) and 1% Penicillin-Streptomycin (Euroclone #ECB3001D). Cells were maintained at 37 °C and 5% CO_2 in a humidified incubator.

For imaging experiments, 96-well plates were seeded with 0.04e6 cells per well. 100ng of DNA were delivered to each well with Lipofectamine 3000 (ThermoFisher), accordingly to manufacturer's instructions. Cells were grown 48h after transfection before being plated into 35mm glass-bottom (MatTek) dish coated with poly-L-lysine (100µg/mL) and laminin (20µg/mL). 72h after transfection, cells were analysed through immunocytochemistry.

For Western-blot experiments, 6-well plates were seeded with 1.2e6 cells per well. 2.5µg of DNA were delivered to each well with Lipofectamine 3000. 72 hours after transfection cells were collected to be processed.

5.3 TIDE analysis

96-well plates were seeded with 0.04e6 N2a cells per well and transfected as previously described with pX601mCherry and pX601mCherry-Atat1-CRISPR. At 72 hours after transfection cells were pelleted and genomic DNA was extracted using the PCRBIO Rapid Extract PCR Kit (PCR Biosystems #PB10.24), accordingly to manufacturer's instructions. The genomic region targeted by each gRNA was amplified through polymerase chain reaction (PCR), using the primers described in Table 1. PCR amplicons of on-target sites were purified using QIAquick PCR Purification Kit (Qiagen #28104) and sequenced by Eurofins Genomics. Sanger traces were submitted for TIDE analysis on http://shinyapps.datacurators.nl/tide/ (Brinkman et al., 2014).

5.4 Immunocytochemistry

Cells were fixed with 4% paraformaldehyde (PFA) for 10 minutes at room temperature, permeabilized with 0.05% Triton-X-100 in PBS for 10 minutes at room temperature and blocked in 3% normal goat serum (NGS) in 0.01% Tween-20 in PBS for 30 minutes at room temperature. Cells were incubated with a mix of primary antibodies in blocking solution in a moist chamber, overnight at 4°C. Cells were carefully washed with PBS and incubated with a mixture of secondary antibodies, diluted in blocking solution for 2 hours at room temperature in the dark. Samples were extensively washed with and imaged in PBS.

5.5 Western-blot

Cells were collected in ice cold phosphate-buffered saline (PBS) and pelleted by centrifugation (4 min, 1000rpm). Total soluble protein content was obtained by incubating samples in cold lysis RIPA buffer (300mM NaCl, 1mM EDTA, 0.5% DOC, 0.5% Triton-X 100, 0.1% SDS, 50mM Tris, pH 7.4), supplemented with a cocktail of protease inhibitors (Roche #11697498001) and 1µM of DTT. Samples were kept on ice for 30 minutes and genomic DNA was sheared at halftime by passing the lysate through a 25G needle for three times. Soluble proteins were isolated by centrifugation at 4° C for 10 minutes at 13000 rpm and the supernatant was collected.

Total protein content was quantified using the Micro BCA™ Protein Assay Kit (ThermoFisher #23235). Protein (20 µg) was separated through SDS-PAGE in precast 4–20% gradient polyacrylamide gels (BioRad #4561094) and transferred to a polyvinylidene difluoride membrane (PVDF) immunoblot membrane (made in duplicate). After transfer, membranes were incubated in blocking solution (5% non-fat milk powder in PBS-0.1% Triton-X-100 for 1 hour. One membrane was incubated with the primary mouse antibody anti-acetylated α-tubulin (1:1000, Sigma-Aldrich #T7451) and the other with the rabbit primary antibody anti-α-tubulin (1:1000, Abcam #ab52866), both in blocking solution, overnight at 4°C. Blots were washed three times in PBS-0.1% Triton-X, followed by incubation for 1 hour at room temperature with the secondary antibodies. The membrane incubated with the mouse

antibody was incubated with the secondary antibody goat anti-mouse conjugated to horseradish peroxidase (HRP) at a 1:2500 dilution (GE Healthcare #NA931V), while the membrane incubated with the rabbit antibody was incubated with the secondary antibody goat anti-rabbit at 1:2500 dilution (Dako #P0449). After incubation, blots were extensively washed in PBS-0.1% Triton-X. Detection of proteins were made using ECL plus western blotting detection system (GE Healthcare #RPN2232) in FUJI machine.

Signals from Western-blots membranes were quantified by densitometry in Image J and the relative expression of acetylated α-tubulin was normalized to the densitometry of α-tubulin.

5.6 Expression and purification of Frankenbody-mEGFP

The protocol for expression and purification of frankenbody-mEGFP was adapted from Zhao et al. (Zhao et al., 2019). *E.coli* BL21 (DE3) were transformed with the plasmid pET23b-15F11-HA-mEGFP-6xHis (Addgene #129593) for expression of frankenbody-mEGFP (FB-mEGFP). One colony was selected to grow in 25mL of LB media containing ampicillin (100mg/L), overnight at 37°C with shaking. In the next morning, the culture was expanded for 1L and cells were left growing at 37°C until OD600=0.6. Protein expression was induced with 0.4mM Isopropyl-β-D-thiogalactoside (IPTG) and the temperature was lowered to 18°C. Cells were harvested 16 hours later by centrifugation at 3500g and resuspended in 300mM NaCl, 10mM imidazole, 0.2mM 4-(2-Aminoethyl) benzenesulfonyl fluoride hydrochloride (AEBSF) in PBS. Cells were lysed by sonication. The lysate was clarified by ultracentrifugation (40000rpm, 45 minutes at 4°C) and the supernatant was collected. The protein solution was loaded into 1mL of Ni^{2+} column and left incubating for 1 hour at room temperature with rotation. FB-mGFP was eluted with 250mM and 500mM of imidazole in 300mM NaCl, 0.2mM AEBSF in PBS. Buffer exchange was performed in a PD-10 desalting column, following manufacturer's instructions. FB-mGFP was eluted in 3mL of HEPES-based buffer (25 mM HEPES pH 7.9, 12.5 mM MgCl2, 100 mM KCl, 0.1 mM EDTA, 0.01% NP40, 10% glycerol, and 1 mM DTT) and stored at -80°C

after flash freezing in liquid nitrogen. Different dilutions of the purified FB-mEGFP were tested in cells and optimized dilution for using it was at 1:50.

5.7 Virus production

Each individual preparation of Δ-HSPG rAAV2 viruses was produced with the following protocol. Human embryonic 293T cells were cultured in DMEM, high glucose, Glutamax, pyruvate, supplemented with 10% FBS and 1% Penicillin-Streptomycin. Cells were maintained at 37°C and 5% CO_2 in a humidified incubator.

Each virus was produced in ten 15cm cell culture dishes at 70% confluency, transfected with the 600µg of DNA of Δ-HSPG rAAV2, helper plasmid pFdelta6 (Addgene #112867) and cargo vector at a ratio of 1:2:1 (capsid:pHelper:cargo), using linear polyethylenimine (PEI; 0.33mg/mL linear PEI diluted in water for injection pH 2-3, using HCl). Transfections were performed at a ratio of 1µg of DNA to 11µL of Linear PEI (0.33mg/mL). The volume of DNA and linear PEI needed were separately diluted in Dulbecco's Phosphate Buffered Saline (DPBS) at a final volume of 10mL. The linear PEI solution was added to the DNA solution and incubated for 15 minutes at room temperature. 2mL of the DNA-linear PEI mixture was added dropwise to each cell culture dish and media was replaced six hours after transfection. At 72 hours after transfection, cultures were removed from the incubator and Triton-X 100 and RNase were added at a final concentration of 0.05% and 25mg/mL, respectively. Cells were kept at 37°C for 1 hour, shaking. Residual cells and media were pooled down together, concentrated by tangential flow and purified through isopycnic ultracentrifugation (Dias Florencio et al., 2015). Purified viral particles were cleaned with 0.0001% of Pluronic (ThermoFisher Scientific F68), 200mM NaCl in PBS and concentrated using 100kDa filters (Amicon) to a final volume of approximately 150µL (Grieger et al., 2006). Viral titration was performed through q-PCR using primers targeting the AAV2 ITR regions (fwd ITR primer, 5'-GGAACCCCTAGTGATGGAGTT; rev ITR primer, 5'-CGGCCTCAGTGAGCGA) and as standard curve, the plasmid pAAV-CAG-tdTomato (Addgene #59462) (Aurnhammer et al., 2012)

Table 6 – Features of the rAAV viruses used

Virus	Function
Atat1-CRISPR	Ablate Atat1 gene
Mini-CMV-tdTomato	Negative control of Atat1-CRISPR
CAG-tdTomato	Reporter
CAG-eGFP	Reporter
Atat1-sh	Ablate Atat1 mRNA
Ctrl-sh	Negative control of Atat1-sh
AAV2-GFP	Reporter, Positive control for ΔHSPG-rAAV2

5.8 Virus modification

The protocol for the virus modification was developed by the Start-up company Borea Therapeutics. For confidentiality reasons, the exact details of the protocol cannot be described in detail in the present thesis.

5.9 Primary cell culture of DRG neurons

DRG neurons from adult C57/Bl6 mice were prepared as previously described (Hu and Lewin, 2006). Adult mice were euthanized in a CO_2 chamber. DRGs were collected in cold phosphate-buffered saline (PBS). DRG neurons were enzymatically digested in Collagenase type IV (10ng/µL, Sigma-Aldrich C5138) for 30 minutes at 37°C, followed by incubation with 0.05% Trypsin EDTA (Gibco 25300-054), for 22 minutes at 37°C and mechanically isolated by repeated pipetting. Cell debris was removed by passing cell suspension through a 100µm filter. The cell suspension was pelleted and resuspended in DMEM, high glucose, Glutamax, pyruvate, supplemented with 10% FBS and 1% Penicillin-Streptomycin and plated in 35mm glass-bottom (MatTek) dish coated with poly-L-lysine (100µg/mL) and laminin (20µg/mL). Cells were maintained at 37 °C and 5% CO_2 in a humidified incubator.

Viruses were applied at 2 days *in-vitro* (DIV) and the cultures were analysed through immunofluorescence assays at 7 DIV.

5.10 Organotypic cultures of spinal cord and DRG slices

Organotypic cultures of spinal cord and DRG slices from E12-13 C57/Bl6 mice were prepared as previously described (Giacco et al., 2019). Pregnant female mice were euthanized in a CO_2 chamber. Embryos were delivered through a caesarean section and placed on cold Gey's Balanced Salt Solution (GBSS, in mM: 149 NaCL, 5.37 KCl, 0.44 KH_2PO4, 0.49 $MgCl_27H20$, 0.41 $MgSO_47H_2O$, 1.25 $CaCl_22H_2O$, 5.55 glucose, pH 7.4, 296 mOsm). The backs from each embryo from low thoracic and high lumbar region were isolated and transversely sliced (257µM) in a tissue chopper. The tissue surrounding the spinal cord and DRG slices was cleaned with a scalpel. Cleaned slices were embedded into a matrix made of chicken plasma (Sigma P3266) and thrombin (Sigma T4648) in a glass coverslip mounted in a flat bottom plastic tube. From 1 to 7 DIV, slices were cultured in DMEM supplemented with 25% FBS, 2% B27, mouse nerve growth factor (mNGF) (0.02µg/mL), 8% H2O, 1% Penicillin-Streptomycin. After 7 DIV, the cultured media was changed to DMEM supplemented with 25% FBS, 1% B27, mNGF (0.05µg/mL), 8% H2O, 1% Penicillin-Streptomycin and the anti-mitotics uridine (10µM), 5-Fluoro-2-deoxymidine (10µM) and cytosine β-D-arabinofuranoside (10µM). From 8 DIV, cells were maintained in DMEM supplemented with 25% FBS, 2% B27, mNGF (0.05µg/mL), 8% H2O, 1% Penicillin-Streptomycin. The tubes were kept with 1mL of media in a roller drum rotating at 120 rotations per hour at 37 °C and 5% CO_2 incubator.

Viruses were added to the media at 3 DIV and cultures were collected for immunofluorescence assays 21 DIV after virus application.

5.11 Immunofluorescence on organotypic cultures

The protocol for immunofluorescence in organotypic slices is described in Giacco et al. (Giacco et al., 2019). Briefly, cultures were fixed in 4% PFA for 1 hour at room temperature, followed by quenching of free aldehyde groups with 0.1M glycine for 10 minutes at room temperature. Cultures were permeabilized and blocked simultaneously with 10% FBS, 5% bovine serum albumin (BSA) and 0.3% Triton-X for 1 hour at room temperature. After that, cultures were incubated overnight at 4°C with the primary antibody mixture diluted in blocking solution. Slices were extensively washed with PBS and incubated with a mixture of secondary antibodies diluted in blocking solution for 2 hours at room temperature in the dark. Samples were mounted with Prolong gold (Invitrogen #P36930) on glass slides.

5.12 Intrathecal injections

Young adult (8 weeks old) C57/Bl6 female mice were housed with food and water *ad libitum*, under a 12h light/dark cycle and kept at a maximum of 6 animals per cage.

Anaesthesia was induced with 4% isoflurane delivered with 2% O2 and room air in a closed chamber, until loss of reflexes. During the procedure, isoflurane was lowered for 2%. The lower back of mice was disinfected with 70% ethanol and a small incision was made to expose the lumbar region of the backbone. Mice were intrathecally (IT) injected using a Hamilton syringe and 30G needle between L4 and L5 with 15µL of chemically modified *Δ*-HSPG-rAAV2. Following injections, mice were left recovering under a heating pad until full motor activity was resumed.

5.13 Immunohistochemistry

Following 7 to 10 weeks after intrathecal injections of chemically modified viruses, animals were euthanized for organ collection and histology analysis. Lumbar DRG were collected in ice cold PBS and fixed with 4% PFA for 2 hours at room temperature. After extensive washing, DRGs were embedded in 2% agarose in PBS and sectioned at 50µm with a

vibrotome. Sections were treated with 50% ethanol for 30 minutes and later incubated with blocking solution: 5% serum (goat or donkey) in 0.3% Triton-X in PBS for 1 hour at room temperature. Samples were incubated with primary antibodies diluted in blocking solution, overnight at 4°C. Secondary antibodies were added in blocking solution and samples were incubated overnight at 4°C. Slices were mounted with Prolong gold on glass slides.

5.14 Chemical Screening

Cells to be tested with the chemical compounds were seeded one day before compound addition. Shortlisted compounds were diluted in Dimethyl Sulfoxide (DMSO), and further diluted to a 2.5M stock solution and stored at -80°C. The compounds were fresh diluted at 50µM (0.5% DMSO) in full media, before adding to cells.

5.15 Image analysis

Immunofluorescence images were obtained as z-stacks using a Nikon Eclipse Ti2 confocal microscope. For *in-vitro* experiments in N2a cells, images were acquired in a 40x 0.95 NA air objective. For *ex-vivo* experiments in primary cultures of DRG neurons were acquired in a 40x 0.95 NA objective and in organotypic cultures of DRG and spinal cord were acquired in a 60x 1.4 NA oil objective for acquisition of axonal regions and at a 10x 0.45NA air objective for whole slice acquisition. Finally, image acquisition of DRG slices were made using a 10x 0.45 NA air objective.

Image analysis was performed using ImageJ. Quantification of fluorescence intensity was performed in maximum intensity projections of z-stacks. Regions for fluorescence intensity quantifications were selected by first adjusting the threshold of the images, so that it could select the relevant area. Neighbouring cells were separated with the command Watershed, followed by the command Analyse Particles. The fluorescence intensity was finally measured in the channel for the immunostaining for α-tubulin and acetylated α-tubulin. Ratios of acetylated α-tubulin over aα-tubulin were calculated in Microsoft Excel.

5.16 Statistical analysis

For imaging analysis, outliers were removed with the ROUT method, using a Q value of 10% (Motulsky and Brown, 2006), with Graphpad (version 9.2.0). Differences between two groups of samples without a normal distribution were analysed by non-parametric Mann-Whitney test, while samples having a normal distribution were analysed through t-test, unless stated otherwise. Values are presented as average ± standard deviation (SD), error bars in graphs represent SD. All statistical analysis was performed in GraphPad Prism (version 9.2.0).

5.17 Ethical statement

All animal procedures were performed in accordance with European Union (EU) guidelines (2010/63/UE) and Italian law (decree 26/14) and the ethical committee from SISSA. Animal use was approved by the Italian Ministry of Health, in agreement with the EU Recommendation 2007/526/CE.

5.18 List of antibodies

Antibody	**Dilution**	**Reference Supplier**
Mouse monoclonal anti-Acetylated α-tubulin	1:5000	T7451 Sigma-Aldrich
Rabbit anti- α-tubulin antibody	1:500	Ab52866 Abcam
Mouse Monoclonal anti-α-tubulin	1:500	T6199 Sigma-Aldrich
Chicken anti-GFP	1:500	GFP-1020 Aves labs
Goat anti-GFP antibody	1:200	ab6673 Abcam
HA Tag Monoclonal Antibody (16B12), Alexa Fluor 488	1:500	A-21287 ThermoFisher
Chicken anti-beta III Tubulin antibodyt	1:500	ab41489 Abcam
Rabbit RFP Antibody Pre-adsorbed	1:500	600-401-379 Rockland
Goat anti-Mouse IgG2b Cross-Adsorbed Secondary Antibody, Alexa Fluor 647	1:1000	A-21242 ThermoFisher
Goat anti-Mouse IgG1 Cross-Adsorbed Secondary Antibody, Alexa Fluor 488	1:1000	A-21121 ThermoFisher
Goat anti-Mouse IgG (H+L) Cross-Adsorbed Secondary Antibody, Alexa Fluor 647	1:1000	A-21235 ThermoFisher
Goat anti-Rabbit IgG (H+L) Cross-Adsorbed Secondary Antibody, Alexa Fluor 546	1:1000	A-11010 ThermoFisher
Goat anti-Chicken IgY (H+L) Secondary Antibody, Alexa Fluor 488	1:1000	A-11039 ThermoFisher
Donkey anti-Rabbit IgG (H+L) ReadyProbes™ Secondary Antibody, Alexa Fluor 594	1:1000	R37119 ThermoFisher
Donkey anti-Goat IgG (H+L) Cross-Adsorbed Secondary Antibody, Alexa Fluor 488	1:1000	A11055 ThermoFisher
Donkey anti-Mouse IgG (H+L) Highly Cross-Adsorbed Secondary Antibody, Alexa Fluor 647	1:1000	A-31571 ThermoFisher
Goat Anti-Mouse Immunoglobulins/HRP	1:2500	Na931V GEHealthcare
Goat Anti-Rabbit Immunoglobulins/HRP	1:2500	P0448 DAKO

6. Results

6.1 Targeting of Atat1 with CRISPR

6.1.2 Design and insertion of gRNA sequences for knock-out of Atat1 by SaCas9

With the goal of knocking-out expression of Atat1 in mice (NCBI gene ID: 73242), I opted to deliver Cas9 nuclease from *Staphylococcus aureus* (SaCas9) and one gRNA using recombinant adeno-associated viral (rAAV) vectors. I started by identifying 5 potential gRNA sequences targeting the coding sequence of Atat1, using the genetic perturbation platform (GPP) sgRNA Designer from the Broad Institute (Najm et al., 2018). Among all possibilities of gRNA sequences provided by the GPP sgRNA Designer, I selected the 5 ones (gRNA 1-5; table 1), that scored the best and that were not located in overlapping regions of the Atat1 coding sequence (Figure 8). *In silico* screening for potential off-targets for gRNA was performed through BLAST analysis using the reference mouse genome (GRCm38) deposited in ENSEMBLE (Cunningham et al., 2019). All gRNA sequences had 100% homology to Atat1 gene and no off-targets were identified.

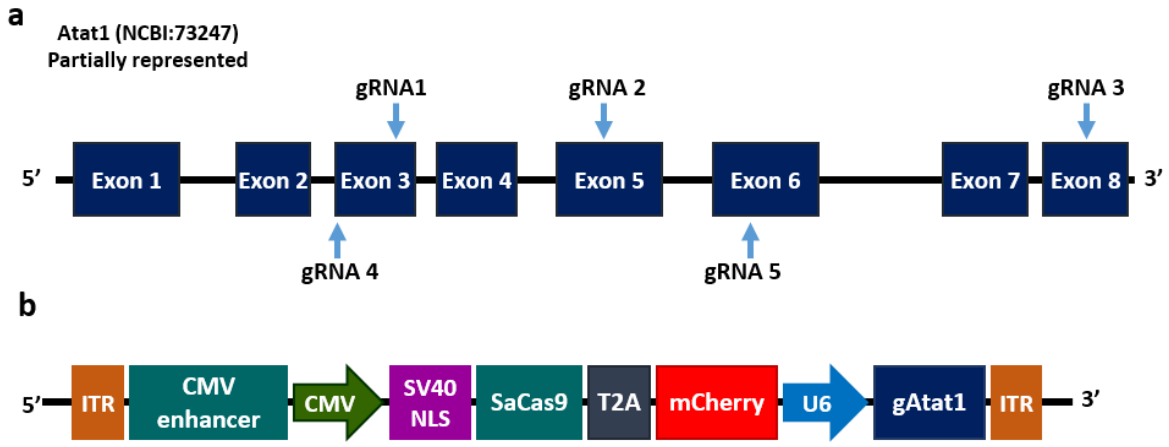


Figure 8 – Strategy for Atat1 gene knock-out (a) Relative distribution of the five gRNA sequences within Atat1 gene **(b)** Schematic representation of pAAV vector pX601-mCherry, expression of SaCas9 and the fluorescent reporter mCherry are driven by the human cytomegalovirus (CMV) enhancer and promoter and gRNA nucleotide expression driven by the U6 promoter.

When preparing rAAV vectors, the first step is to construct the viral cargo as a plasmid in *E.Coli*. I used the pAAV vector pX601-mCherry (Addgene #84039, (Ye et al., 2016)), depicted in Figure 8b, to deliver the constructs of interest. This vector contains the sequence of SaCas9 and the fluorescent protein mCherry under the same CMV enhancer and promoter. Additionally, it contains a site for insertion of one gRNA sequence driven by the U6 promoter. In order to include the selected sequences for targeting Atat1, I designed gRNAs with overhangs compatible with insertion at BsaI restriction sites of pX601-mCherry, and used the original pX601-mCherry as negative control.

In order to understand if any of the gRNAs were able to guide Cas9 to knock-out a specific Atat1 locus, I transfected N2a cells with different pX601-mCherry plasmids containing gRNA1 to 5 inserted (gRNA1-gRNA5). 72 hours after transfection, I extracted the genomic DNA of the cells and amplified through PCR the target genomic locus of Atat1. Sequencing of PCR amplicons demonstrated that from the initial 5 gRNAs tested, only gRNA1 (pX601mCherry-Atat1-CRISPR) knocked-out Atat1 (fig 9b-f). To further understand with accuracy the spectrum and frequency of mutations caused by gRNA1, Sanger traces were analysed by tracking of indels by decomposition (TIDE) (Brinkman et al., 2014). Figure 9f shows that indel events occurred in 59.1% of amplicons when cells were transfected with pX601mCherry-Atat1-CRISPR, comparing to pX601mCherry and that one base pair was the mutation most frequent.

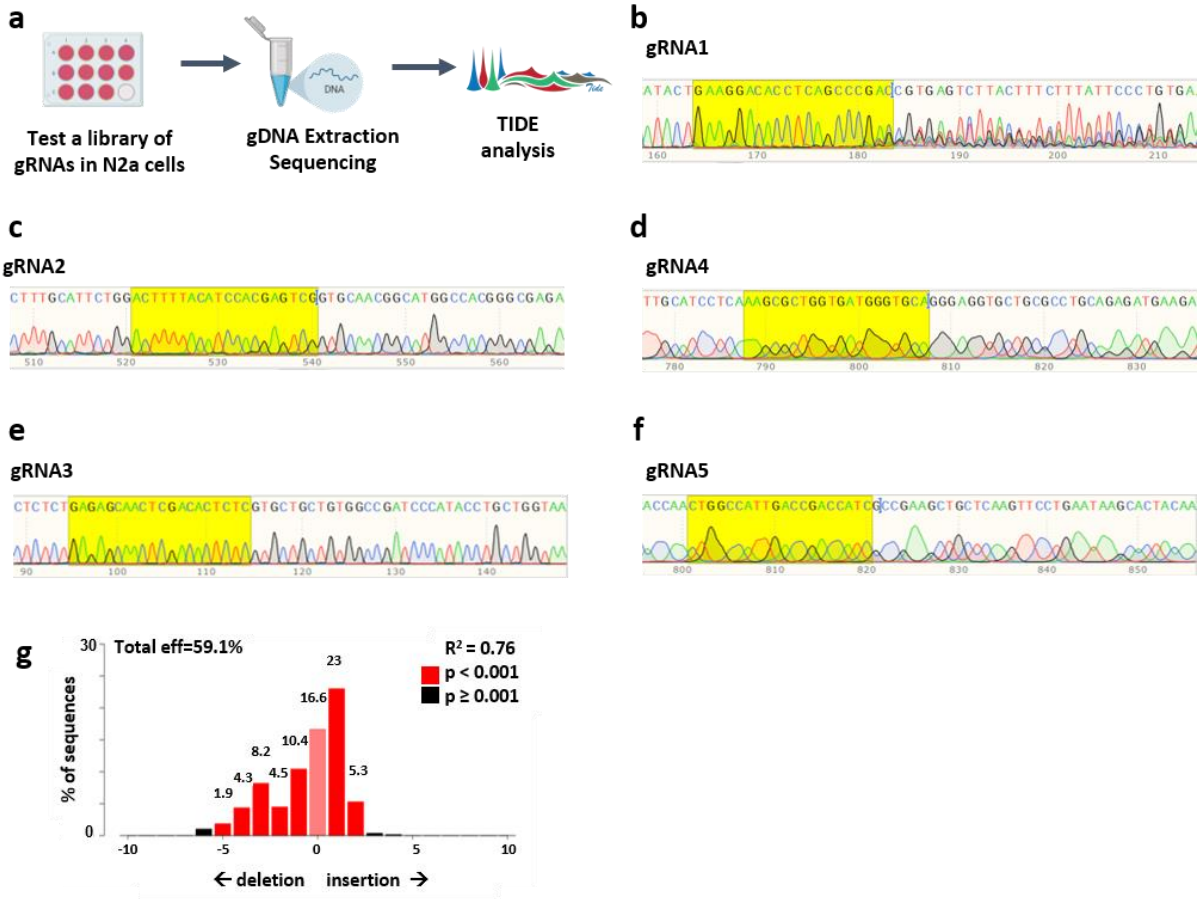


Figure 9 – gRNA1 is the best sequence to knock-out Atat1 (a) Workflow for assessment of Atat1 knock-out in N2a cells. **(b-f)** Sequencing results from genomic locus targeted by gRNAs show that only gRNA1 in b, was able to knock-out Atat1. **(g)** TIDE analysis of genomic DNA from N2a cells transfected with pX601mCherry-Atat1-CRISPR shows 59.1% of indels mutations, compared with control pX601mCherry. Experiment not replicated.

Having established that gRNA1 can effectively knock-out Atat1 in N2a cells, the next step for validation involved understanding whether Atat1 knock-out could indeed reduce acetylated α-tubulin. To achieve that, I transfected N2a cells with pX601mCherry-Atat1-CRISPR and pX601mCherry, and quantified through immunocytochemistry the ratio of acetylated-α-tubulin over α-tubulin.

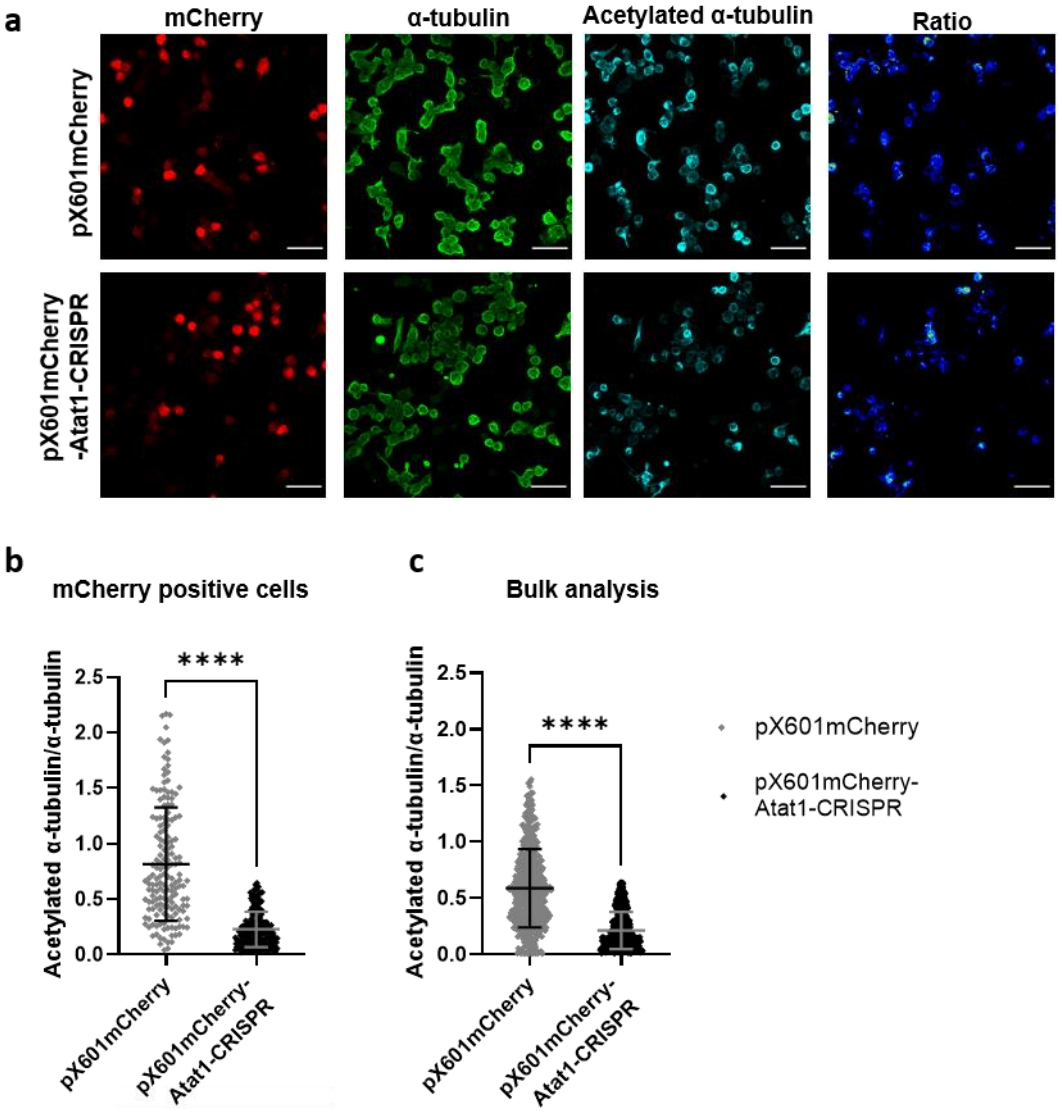


Figure 10 – Knock-out of Atat1 with pX601mCherry-Atat1-CRISPR leads to a decrease in the amount of acetylated α-tubulin. (a) N2a cells analysed 72 hours after transfection with pX601mCherry-Atat1-CRISPR and pX601mCherry immunostained for α-tubulin (green) acetylated α-tubulin (cyan), positively transfected cells are shown in red and ratios of acetylated α-tubulin over α-tubulin images are shown on the right. Scale bar 50µm **(b)** Quantification of the ratio of fluorescence intensity of acetylated α-tubulin over α-tubulin in positively transfected cells. pX601mCherry n= 161, pX601mCherry-Atat1-CRISPR n=192 **(c)** Bulk analysis of the ratio of acetylated α-tubulin over α-tubulin. pX601mCherry n= 653, pX601mCherry-Atat1-CRISPR n=680, **** $p<0.0001$, Mann-Whitney test. Experiment performed in triplicate (technical replicate), each dot represents an individual cell.

Since pX601mCherry contains a fluorescent reporter, in a first analysis, I measured the intensity fluorescence ratios in mCherry positive cells. The average ratios of acetylated-α-tubulin over α-tubulin of pX601mCherry-Atat1-CRISPR (0.23±0.01, n=192) was significantly lower than pX601mCherry (0.81±0.04, n=161), which indicates that Atat1 knock-out leads to a decrease in acetylated-α-tubulin in N2a cells.

Knowing that pX601-mCherry contains 2A self-cleaving peptides (T2A) that allows a separate expression of SaCas9 and mCherry under the same promoter, we can assume that mCherry is always co-expressed with SaCas9. However, this assumption is not valid for the protein quantity/intensity of mCherry fluorescence. The translation of SaCas9 and mCherry can be regulated at a post-transcriptional level and therefore, there might be cells whose mCherry fluorescence is below the detectable level using the imaging settings that I defined, but have a sufficient expression of Cas9 to cause Atat1 knock-out. It is important to note that the amount of gRNA available is a more limiting factor than the amount of SaCas9 to have CRISPR events. For these reasons, in a second analysis, instead of selecting only mCherry positive cells, I performed a bulk analysis and measured the ratios in all cells. The results demonstrated a statistically significant difference between pX601mCherry-Atat1-CRISPR (0.21±0.16, n=680) and pX601mCherry (0.59±0.01, n=653). It is important to mention that the bulk analysis comprised negatively transfected cells and as expected, the difference between the ratios is smaller than when I threshold the analysis to only mCherry positive cells.

Both results from TIDE and imaging analysis gave me confidence to pursue the experiments to produce a rAAV virus with the construct I designed. However, production of rAAV is restricted by a packaging capacity of 4.5kb between inverted terminal repeats (ITRs) (Li and Samulski, 2020). For this reason, since the construct of pX601-mCherry exceeds the packaging limit of rAAV (>5kb), I cloned the gRNA sequence into another pAAV vector.

The new vector of choice to deliver CRISPR-Cas9 was the pX601 miniCMV-SaCas9-SpA-sgRNA scaffold (Addgene #107055) from Hewitt lab (Fig11a). The main differences between the new rAAV vector and the one previously used lie in the exchange of the CMV enhancer and promoter by a mini-CMV promoter that is remarkably smaller (>40bp) than CMV (508bp), the addition of the human influenza hemagglutinin (HA-tag) epitope to SaCas9 and the removal of the fluorescent reporter mCherry. I cloned gRNA into the plasmid pX601 miniCMV-SaCas9-SpA-sgRNA scaffold (from now on referred to as pAAV-Atat1-CRISPR), and compared its efficiency on decreasing acetylated α-tubulin through protein expression analysis with the original pX601 mini-CMV-SaCas9-SpA-sgRNA scaffold plasmid (from now on referred to as pAAV-Ctrl-CRISPR).

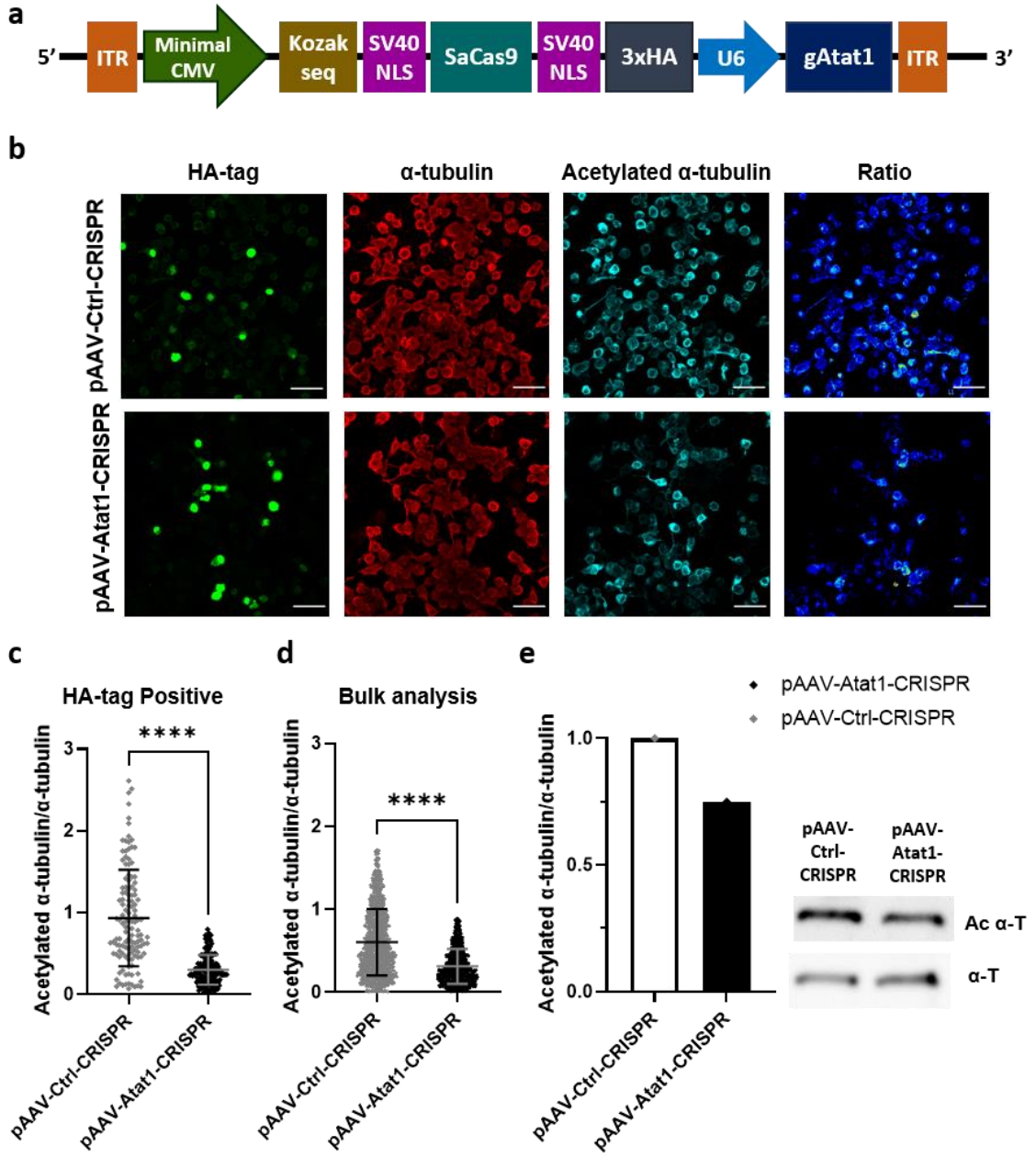


Figure 11 – Knock-out of Atat1 with pAAV-Atat1-CRISPR leads to a decrease in acetylated α-tubulin. (a) Schematic representation of pAAV-Atat1-CRISPR. Expression of SaCas9-HA-tag is driven by the mini-CMV promoter and expression of gRNA nucleotide is driven by the U6 promoter. **(b)** N2a cells analysed 72 hours after transfection with pAAV-Ctrl-CRISPR and pAAV-Atat1-CRISPR immunostained for HA-tag (green), α-tubulin (red) and acetylated α-tubulin (cyan). Ratios of acetylated α-tubulin over α-tubulin images are shown on the right. Scale bar 50µm. Experiment performed in triplicate (technical replicates) each dot represents individual cells **(c)** Quantification of the ratio of the fluorescence intensities of acetylated α-tubulin over

α-tubulin in HA-tag positive cells. pAAV-Ctrl-CRISPR n=125, pAAV-Atat1-CRISPR n=152. **** p<0.0001, Mann-Whitney test. **(d)** Bulk analysis of the ratio of fluorescence intensity of acetylated α-tubulin over α-tubulin. pAAV-Ctrl-CRISPR n= 1613, pAAV-Atat1-CRISPR n=1094. **** p<0.0001, Mann-Whitney test. **(e)** 20µg of soluble proteins from cells transfected with with pAAV-Ctrl-CRISPR and with pAAV-Atat1-CRISPR, analysed through western blot for expression of acetylated α-tubulin (Ac-α-T) and α-tubulin (α-T). Densitometry of western-blot bands. Experiment not replicated

In the first analysis, I performed immunocytochemistry as previously described. However, in this case, I selected positively transfected cells using an antibody against HA-tag (Figure 11b). The average ratios of the fluorescence intensity of acetylated-α-tubulin over α-tubulin of pAAV-Atat1-CRISPR (0.30±0.18, n=152) was significantly lower than pAAV-Ctrl-CRISPR (0.93±0.05, n=125), which indicates that Atat1 knock-out with the new construct leads to a decrease in acetylated-α-tubulin in N2a cells (Figure 11c). Bulk analysis of the cells corroborated previous findings, in which the average ratio of pAAV-Atat1-CRISPR (0.31±0.00, n=1094) was significantly lower than the average ratio of pAAV-Ctrl-CRISPR (0.60±0.05, n=1613).

Additionally, I performed western-blot analysis on N2a cells 72 hours post-transfection with pAAV-Atat1-CRISPR and pAAV-Ctrl-CRISPR. Given that the plasmids do not encode a selection marker for transfected cells, I performed a bulk analysis of a mixed population of negatively and positively transfected cells. I extracted soluble proteins of cells and evaluated the amount of acetylated α-tubulin and α-tubulin in 20µg of total protein. The result shows that cells transfected with pAAV-Atat1-CRISPR have 25% less of acetylated α-tubulin, compared to control (Figure 11e). The result obtained with western-blot analysis was consistent with the immunofluorescence assays, showing a decrease in acetylated α-tubulin in cells transfected with pAAV-Atat1-CRISPR, however in much smaller proportion.

6.1.2 rAAV in *ex-vivo* cultures of DRG neurons

Following identification of a suitable pAAV vector to deliver SaCas9 and an efficient gRNA sequence targeting Atat1, I could finally produce a recombinant adeno-associated virus (rAAV) carrying my cargo of interest. For that, I have selected a modified version of AAV2 capsid without infectivity capacity. This capsid contained a mutation on the binding site of heparan sulfate proteoglycans (HSPG) that is essential for viral internalization. This capsid, ΔHSPG-rAAV2, can be redirected to specific cells populations using a technology developed by Borea Therapeutics, in which a modification is introduced in the capsid of ΔHSPG-rAAV2, enabling a new cell tropism to the virus. Targeting of specific cell populations is possible to achieve through different modifications.

In a first analysis, I modified the capsid of the virus ΔHSPG-rAAV2-Atat1-CRISPR (Atat1 CRISPR) to direct it to most primary sensory neurons. I applied 1µL (1.5E12 vg/mL) of Atat1 CRISPR virus in a primary culture of DRG neurons at 1 DIV. At 15 days past the inoculation with the virus, I fixed the culture and performed an immunofluorescence using antibodies anti-acetylated α-tubulin and α-tubulin. At this moment, I was not able to visualise the HA-tag epitope. This could be due a poor transgene expression of the virus or to an inefficient labelling of the HA-tag, using antibodies. Adding to that, at 15 DIV, the primary culture of DRG developed a dense axonal network, which did not allow the visualization of any individual nerve fibre, making it impossible to quantify fluorescence intensities in a rigorous way (data not shown, experiment performed in duplicate).

6.1.3 HA-tag epitope detection systems

In order to circumvent the issue related to the immunodetection of HA-tag, I have tested two genetically encoded probes, called anti-HA frankenbodies (Zhao et al., 2019). These probes are proteins made of hybrid single chain variable fragments (scFvs) fused to a fluorescent protein (Zhao et al., 2019). Firstly, I tested the anti-HA frankenbody mCherry (Addgene #129591), that was encoded in a vector for mammalian expression systems. It is claimed the anti-HA frankenbody mCherry binds to mature and nascent HA tagged proteins. I

co-transfected N2a cells with Atat1 CRISPR and anti-HA frankenbody mCherry and compared with N2a cells exclusively transfected with anti-HA frankenbody mCherry. Visually, I could not establish a distinct pattern of both groups of cells (data not shown, experiment performed in duplicate), which means that the anti-HA frankenbody mCherry was not an efficient reporter of cells delivered with Atat1-CRISPR.

The second genetically encoded probe that I tested was anti-HA tag frankenbody-mEGFP, which is the frankenbody fused with the monomeric enhanced GFP (mEGFP) (Zhao et al., 2019). The new frankenbody is encoded in a vector suitable for protein expression in *E. Coli* and is compatible with immunofluorescent assays on fixed samples. I expressed and purified anti-HA frankenbody-mEGFP from bacteria, tested it in N2a cells transfected with pAAV-Atat1-CRISPR-HA and compared the quality of the staining with the anti-HA-tag antibody previously used (Figure12). Indeed, both detection methods could successfully identify cells expressing the HA-tag, which gave me confidence to pursue the experiments, using the frankenbody in DRG neurons.

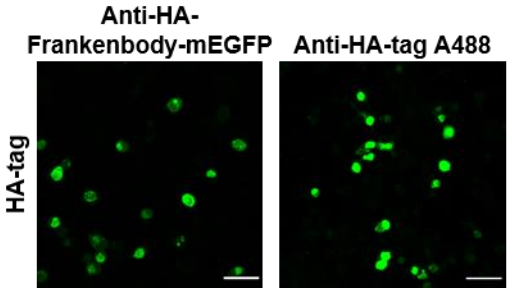


Figure 12 – Anti-HA-Frankenbody-mEGFP is a good reporter for immunocytochemistry in N2a cells. N2a cells were transfected with pAAV-Atat1-CRISPR in duplicate. One of the cultures was immunostained with anti-HA-Frankenbody-mEGFP, while the other was immunostained using the antibody anti-HA tag, conjugated with Alexa 488. Sale bar 50µm. Experiment performed in duplicate (technical replicate).

Taking into account that testing the modified Atat1-CRISPR virus in primary cultures of DRG neurons for 15 days did not allow a clear visualisation of virus transduction, in my second trial I did some adaptations to my experimental design. I modified Atat1-CRISPR virus to target

non-peptidergic nociceptors and analysed the culture at 8 DIV. By reducing the number of targeted cells and the length of the experiment, I expected to be able to improve the quality of my analysis. I performed an immunofluorescence assay as before, using antibodies against acetylated α-tubulin and α-tubulin and added the purified anti-HA-tag frankenbody-mEGFP (Figure 13). The quality of the staining against acetylated α-tubulin and α-tubulin improved, given that I could distinguish single axons. However, similarly to what I observed previously, I could not visualise the HA-tag.

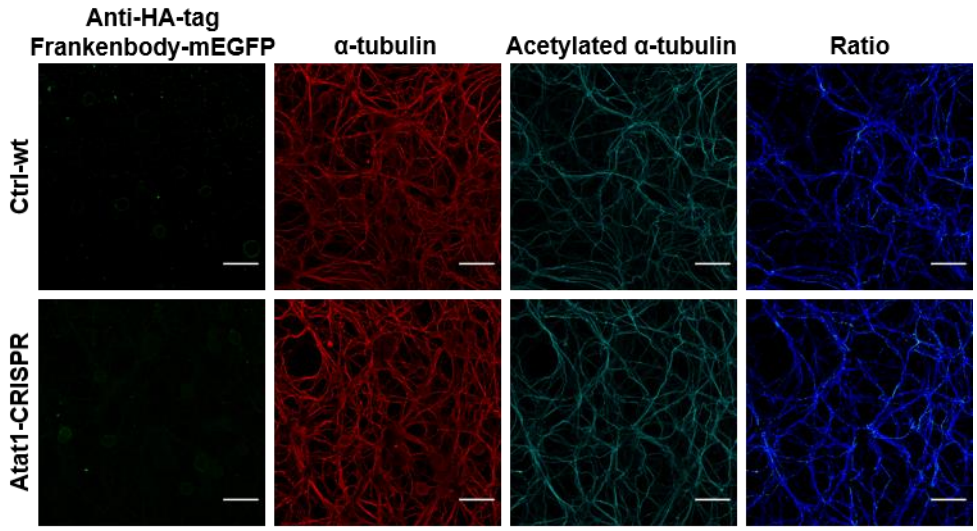


Figure 13 – *Ex-vivo* cultures of DRG neurons infected with CRISPR-Atat1 virus fixed at 8 DIV. Cultures were immunostained α-tubulin (red) acetylated α-tubulin (cyan), HA-tag positive cells were expected to be seen in green, ratios of acetylated α-tubulin over α-tubulin images are shown on the right. Scale bar 50µm. Experiment not replicated.

The absence of signal for the HA-tag could be due to an issue related to the transduction efficiency or with the experimental setup itself therefore, I decided to tackle these questions with two strategies. Firstly, given that there are not much information published using the promoter mini-CMV associated with CRISPR, I compared its strength with the well-known promoter CAG. Secondly, I experimented the virus in organotypic cultures, which are another type of *ex-vivo* cultures, as I will elaborate later.

6.1.4 Mini-CMV vs CAG promoter

The plasmid pAAV-Atat1-CRISPR contains SaCas9-HA under the expression of the minimal-CMV promoter. In order to understand the strength of the promoter in driving protein expression, I decided to compare with the well known CAG promoter (Jun-ichi et al., 1989). To do that, I used the plasmid pAAV-CAG-tdTomato (Addgene #59462), that contains the sequence of fluorescent reporter tdTomato driven by the CAG promoter. To better compare the two promoters, it is necessary to have expression of the same fluorescent protein (tdTomato) driven by the minimal-CMV promoter (pAAV-mini-CMV-tdTomato). In order to clone this new pAAV vector, I removed the portion of pAAV-Atat1-CRISPR containing SaCas9-HA-tag and replaced it with the tdTomato sequence from pAAV-CAG-tdTomato.

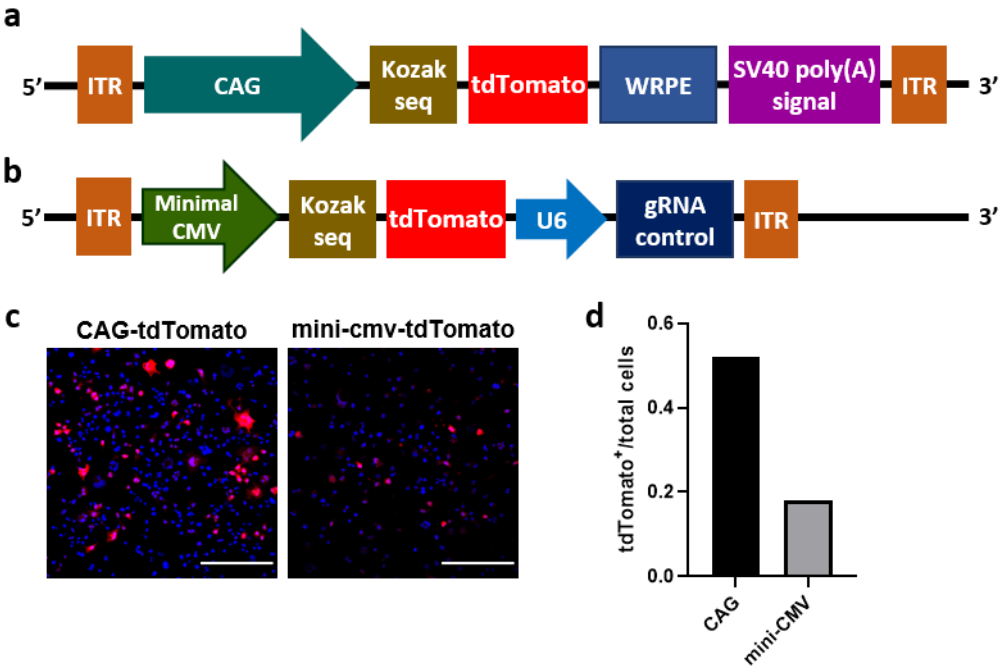


Figure 14 – The mini-CMV promoter has a lower strength for driving protein expression, comparing to the CAG promoter. (a) Schematic representation of pAAV-CAG-tdTomato. **(b)** Schematic representation of pAAV-mini-CMV-tdTomato **(c)** N2a cells transfected with pAAV-CAG-tdTomato and pAAV-mini-CMV-tdTomato. Scale bar 50µm. **(d)** Normalized amount of tdTomato expressing cells in pAAV-CAG-tdTomato (0.52) and pAAV-mini-CMV-tdTomato (0.18). Experiment performed in duplicate (technical replicate).

I transfected N2a cells with pAAV-CAG-tdTomato and pAAV-mini-CMV-tdTomato (Figure 14). At 72 hours after transfection, the amount of tdTomato positive cells normalised to the total amount of cells seeded in the pAAV-CAG-tdTomato condition was of 0.52, while in pAAV-mini-CMV-tdTomato, the ratio was of 0.18. The results demonstrate therefore, that in comparison to the CAG promoter, the mini-cmv promoter has a weaker strength promoting protein expression.

6.1.5 Organotypic cultures of spinal cord and DRG as an *ex-vivo* model to observe viral transduction

As mentioned earlier, viruses might need more than 7 days to have a stable expression of its cargo in *ex-vivo* cultures, which can limit primary cultures of DRG neurons as an adequate platform for testing viruses. Organotypic cultures of the spinal cord and DRG neurons on the other hand, could be a more suitable model to test viruses.

Organotypic cultures are *ex-vivo* models for simulating *in-vivo*-like situations and have been used in pre-clinical studies (Salas et al., 2020). Organotypic cultures of tissue slices preserve cell diversity, genetic background and synaptic properties of neurons. Importantly, under proper care, they can be maintained alive up to two months.

With the goal of understanding first the viral infection efficiency of modified rAAV in organotypic cultures of spinal cord and DRG neurons, I produced a *Δ*HSPG-rAAV2-CAG-tdTomato virus. To target most neurons of the culture, I modified the virus and applied 1µL (1.5E12 vg/mL) of modified virus per slice and kept the slices alive for 3 weeks. At 21 DIV I fixed the slices and imaged at a confocal microscope, (Figure 15, middle panel). The strong expression of the reporter tdTomato demonstrate that the modified capsid *Δ*HSPG-rAAV2 can effectively deliver genetic material to *ex-vivo* neurons.

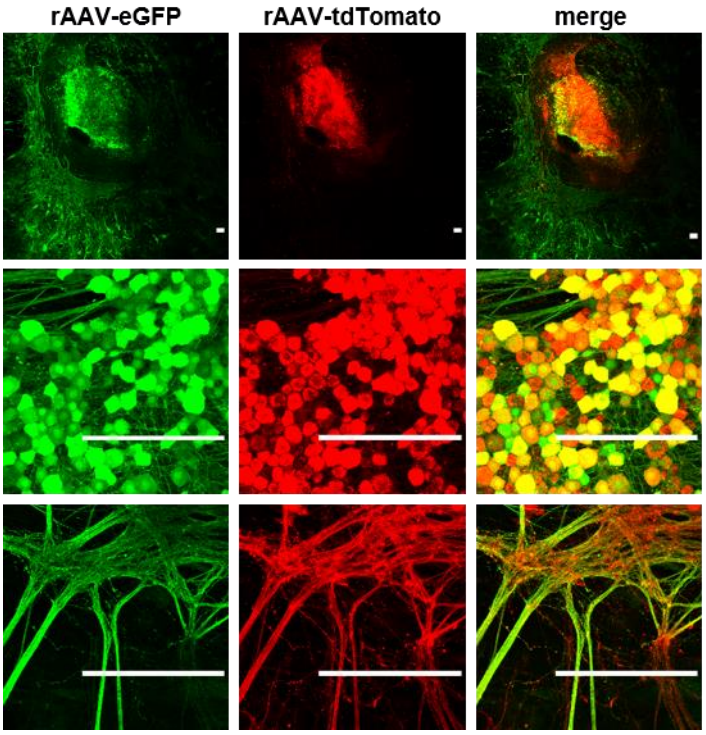


Figure 15 – Organotypic cultures infected with rAAV-eGFP and rAAV-tdTomato. Images acquired 20x and 60x magnifications. Left panel – transduction of rAAV-eGFP virus (green), middle panel – transduction of rAAV-tdTomato (red) and right panel – merged images of transduction of both viruses, co-transduction represented in yellow. Scale bar 1000 µm. Experiment performed in triplicate (technical replicate).

Given the issues with the immunofluorescence assays targeting HA-tag epitopes, I tested whether a co-infection of equal amounts of chemically modified virus infected the same populations of neurons. To do that, I used a new *Δ*HSPG-rAAV2-CAG-eGFP virus and modified it as I did with the CAG-tdTomato virus. A factor that one needs to take into account when performing these type of experiments is that tdTomato is a much brighter reporter than other fluorescent proteins. In order to amplify signal of eGFP, I used a primary antibody anti-GFP and a secondary antibody conjugated with Alexa 488, representative images are shown in Figure 15. My analysis demonstrated that both viruses are highly efficient on driving gene

expression in organotypic cultures and that when modified the same way, the viruses target roughly the same cells.

6.1.6 Atat1-CRISPR in *ex-vivo* cultures

The results obtained with co-infection of rAAV-eGFP and rAAV-tdTomato in organotypic cultures gave me confidence to use another virus to act as a reporter for the CRISPR experiments, instead of continuing trying to optimize the staining of HA-tag. Even though rAAV-tdTomato is highly efficient in targeting cells in organotypic cultures, seeing the accentuated differences in strength between CAG and minimal-CMV promoters (Figure 14), I produced a *Δ*HSPG-rAAV2-mini-CMV-tdTomato (mini-CMV-tdTomato). This new virus will be a better reporter of the expression of SaCas9 and its viral transduction when co-infected with Atat1-CRISPR and will be used as a negative control.

In Figure 16, we can observe images acquired at the confocal microscope of organotypic cultures infected with these viruses, at 3 weeks after infection. In order to amplify the signal of tdTomato expressed under the minimal CMV-promoter, I have used an antibody, raised in rabbit, against-red fluorescent protein (RFP) and a secondary antibody goat anti-rabbit conjugated with Alexa 546.

One limitation of immunofluorescence assays is that when testing for three different epitopes, one can only use primary antibodies of the same class and subclass if they were raised in different host species. For the assays in N2a cells, I used a polyclonal antibody against α-tubulin raised in rabbit and a monoclonal antibody raised in mouse. Having both polyclonal antibodies anti-RFP and anti-α-tubulin raised in rabbit, makes it impossible to use them simultaneously on the same sample. In order to surpass this limitation, I replaced the antibody anti-α-tubulin with an antibody anti-βIII-tubulin raised in chicken. As mentioned in the Introduction, microtubules are made of polymers of α and β-tubulin at equal parts, βIII-tubulin is expressed exclusively in neuronal cells and is used routinely as a marker for these cells (Giacco et al., 2019). For these reasons, I assumed that the total amount of α and β- tubulin

are the same within the same cell. By replacing the staining of α-tubulin with the staining of βIII-tubulin makes it specific for neuronal cells, which is what I am targeting.

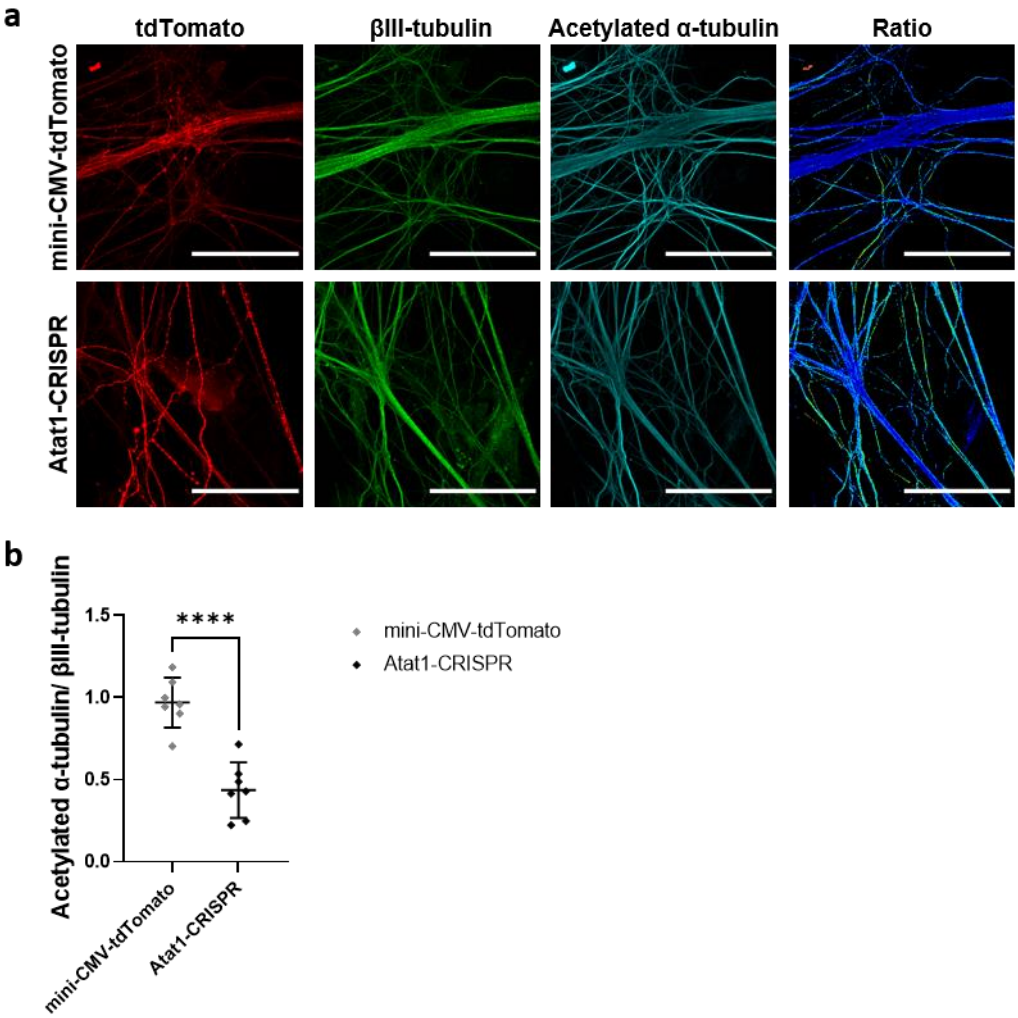


Figure 16 – Atat1-CRISPR leads to a reduction in acetylated α-tubulin in *ex-vivo* cultures. (a) Immunofluorescence of organotypic cultures infected with Atat1-CRISPR together with mini-CMV-tdTomato and with mini-CMV-tdTomato alone. Cultures were stained for tdTomato (red), βIII-tubulin (green) and acetylated α-tubulin (cyan). Ratio of the images of acetylated α-tubulin over βIII-tubulin shown on the right. Scale bar 100µm **(b)** Ratios of the fluorescence intensity of acetylated α-tubulin (n=7) over βIII-tubulin (n=7) in tdTomato positive regions of the cultures. ****p<0.001, t-test. Experiment performed in duplicate (biological and technical replicate), each data point represents different axonal bundles.

Having sorted out a better way of analysing the *ex-vivo* efficiency of Atat1-CRISPR virus, I could finally start the experiment. I prepared organotypic cultures of spinal cord and DRG neurons and at 3 DIV, I applied in each slice, 1µL (1.5e12 vg/mL) of Atat1-CRISPR and mini-CMV-tdTomato modified viruses. As a negative control, I applied 1µL (1.5E12 vg/mL) of modified mini-CMV-tdTomato virus. At 21 days after viral infection, I fixed the slices, performed an immunofluorescence assay and quantified the fluorescence intensities of acetylated α-tubulin and βIII-tubulin on tdTomato positive axons. Unexpectedly, it was not possible to identify any tdTomato positive cell body in the core of the organotypic culture, possibly because the antibody did not penetrate well into that area. Nonetheless, axons were well immunostained and in Figure 16, we can observe representative images acquired at the confocal microscope for acetylated α-tubulin and βIII-tubulin. Quantification of fluorescence intensities of the staining of these two proteins in tdTomato positive axons demonstrated that the average ratio of acetylated α-tubulin over βIII-tubulin in cultures receiving Atat1-CRISPR (0.44±0.17, n=7) was significantly lower than cultures receiving only mini-CMV-tdTomato (0.97±0.06, n=7).

6.1.7 Nocodazole on *ex-vivo* organotypic cultures of spinal cord and DRG neurons

Acetylation of α-tubulin is a post-translational modification that occurs preferentially in stable microtubules, indeed this post-translational modification is seen as a marker for long-lived microtubules (Portran et al., 2017). In this next experiment, I have tried to understand if I could disrupt completely the axonal microtubule network of microtubules and if the treatment with the virus Atat1-CRISPR could prevent the acetylation of newly formed microtubules.

To do that, I have incubated organotypic cultures of spinal cord and DRG neurons with 10µM of nocodazole for 16 hours. Nocodazole is a depolymerising agent of dynamic microtubules (Xu et al., 2017), usually used at lower concentrations and smaller incubation times. By increasing the concentration and the time of incubation of nocodazole, I expected

to observe a reduction of microtubules in the cultures. After incubation with nocodazole, I fixed the cultures and performed an immunofluorescence assay, using antibodies against acetylated α-tubulin, α-tubulin and βIII-tubulin. As it is represented in Figure 17, incubation with nocodazole did not disrupt the microtubule network in axons. For this reason, I decided not to pursue the experiments using this drug and to proceed with the *in-vivo* experiments.

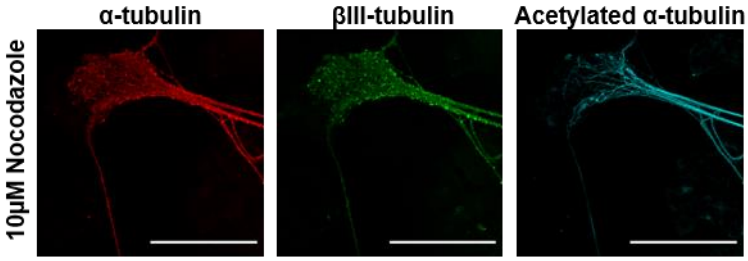


Figure 17 – Nocodazole does not disrupt stable microtubules of neuronal axons. Immunofluorescence on organotypic cultures of spinal cord and DRG neurons were incubated with 10μM of nocodazole for 16 hours. Cultures were stained for α-tubulin (red) βIII-tubulin (green) microtubules and acetylated α-tubulin (cyan). Scale bar 300μm. Experiment made in duplicate (technical replicate).

6.1.8 Atat1-CRISPR *in-vivo*

In order to understand if chemically modified viruses are efficient vectors to deliver genetic material and if Atat1-CRISPR can induce a decrease in the ratio of acetylated-α-tubulin in fully developed animals, I targeted populations of DRG neurons involved in mechanosensation and nociception. I modified the capsid of *Δ*HSPG-rAAV2-mini-CMV-Atat1-CRISPR and *Δ*HSPG-rAAV2-mini-CMV-tdTomato to give them broad specificity to sensory neurons.

DRG neurons are particularly difficult to target, due to their location within the body, both in terms of delivery of drugs and viruses. Previous research demonstrated that intrathecal delivery of rAAV is an efficient method to drive local expression within cell body of

DRG neurons (Vulchanova et al., 2010). I modified a total of 21µL of ΔHSPG-rAAV2-mini-CMV-Atat1-CRISPR (1.5E12 vg/mL) and 21µL of ΔHSPG-rAAV2-mini-CMV-tdTomato (1.5E12 vg/mL). Since the volume of the mixture to inject exceeded the limit fitting inside the intrathecal space, I concentrated it into 15µL using a 100K centrifugal filter. I have followed the same procedure for the control animals injected with mini-CMV-tdTomato. The efficiency of viral transduction was analysed through immunohistochemistry 7 to 10 weeks after viral administration.

In my initial plans for the histology analysis, I was expecting to be able to use the same antibodies I used for the *ex-vivo* analysis in organotypic cultures. However, when I tested the antibodies in DRG sections of wild-type mice, the secondary antibody anti-chicken conjugated with Alexa 488 did not pass my negative control tests, since it binds to the sample in the absence of a chicken primary antibody. For that reason, I had to use an alternative antibody for the primary anti-βIII-tubulin previously used, that would be compatible with the anti-acetylated-α-tubulin and anti-RFP antibodies. Once again, having in consideration the limitations of immunofluorescence assays, I decided to keep the antibody anti-acetylated-α-tubulin raised in mouse that I have been using throughout the whole project and the antibody anti-RFP raised in rabbit and introduce a new antibody anti-α-tubulin raised in mouse. Since the antibody anti-acetylated-α-tubulin was from the subclass IgG2 and the antibody anti-α-tubulin was from the subclass IgG1, by using a specific secondary antibody anti-mouse IgG2 conjugated with Alexa 647 and a secondary antibody anti-mouse IgG1 conjugated with Alexa 488, I could proceed with the analysis.

Histological analysis of DRG neurons of animals injected with mini-CMV-tdTomato (Atat1-CRISPR and control animals) revealed that only a few cells per DRG were positive for tdTomato, which indicates an insufficient viral transduction in these cells (Figure 18). Histology analysis of slices from DRG of the animals revealed a great variability in the quality of staining, which makes the quantitative analysis particularly challenging. Notwithstanding, fluorescence quantification of the intensity of acetylated α-tubulin and α-tubulin in tdTomato positive cells,

did not reveal any difference between the two groups. Before ruling out the efficiency of the virus Atat1-CRISPR *in-vivo*, there is a great need for improving the delivery efficiency of the viruses and the immunohistochemistry protocol.

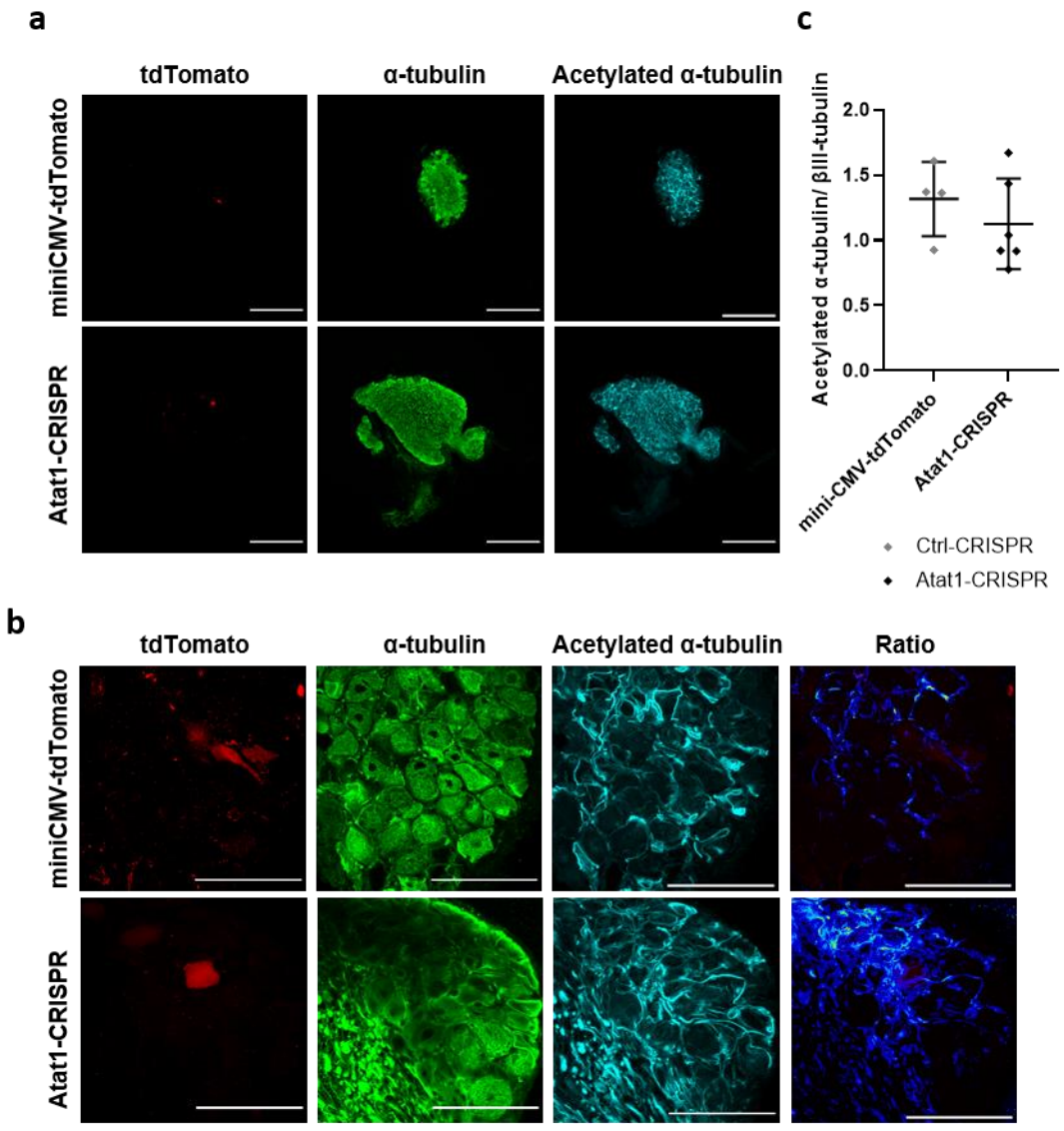


Figure 18 – Atat1-CRISR *in-vivo.* (a) Immunofluorescence assays on DRG slices of animals injected with Atat1-CRISPR (n=6) and mini-CMV-tdTomato (n=6) viruses. Slices were stained for expression of tdTomato (red), α-tubulin (green) and acetylated α-tubulin (cyan). Scale bar 300µm. **(b)** Confocal images of DRG slices acquired at higher magnification (60x). Ratio of

acetylated α-tubulin over α-tubulin images shown on the right. Scale bar 300μm. **(c)** Quantification of the ratio of fluorescence intensity of acetylated α-tubulin over α-tubulin fluorescence intensity in tdTomato positive cells from Atat1-CRISPR (n=6) and mini-CMV-tdTomato (n=4). Experiment performed in duplicate (technical replicate).

6.2 shRNA knock-down

RNAi-based therapeutics are a promising approach to treat many diseases, specifically monogenic diseases. A valuable asset of RNAi-based therapies is its potential of specifically downregulating protein expression before translation takes place. Nonetheless, delivery of RNAi to cell populations is still a great challenge, as well as the design of suitable RNAi sequences. I investigated the potential of using a stable RNAi delivery system through chemical modified rAAV vectors and its potential to reduce acetylated α-tubulin in DRG neurons.

6.2.1 Cloning of RNAi sequences into rAAV vectors and *in-vitro* efficiency assessment

With the goal of knocking-down expression of Atat1 in mice (NCBI gene ID: 73242), I started with three RNAi sequences, targeting exon 2, 5 and 6 of Atat1 gene (Atat1-sh1, Atat1-sh2, Atat1-sh3), shown in Figure 19a. The first two sequences were already tested in the laboratory when delivered as siRNA and the third one was already published in the literature as a good suppressor of Atat1 expression in mice (Even et al., 2019). *In silico s*creening for potential off-targets for RNAi and complementary sequences was performed through BLAST analysis using the reference mouse genome (GRCm38) deposited in ENSEMBLE (Cunningham et al., 2019). All RNAi sequences had 100% homology to Atat1 gene and no off-targets were identified.

I selected the vector AAV-shRNA_Tet3 (Addgene #85740) (Yu et al., 2015) to deliver RNAi sequences separately. As depicted on Figure 19b, the chosen vector contains a U6 promoter that allows expression of nucleotide sequences and an enhanced yellow fluorescent protein (eYFP) under the expression of the eukaryotic translation elongation factor 1 α (EF1α) promoter.

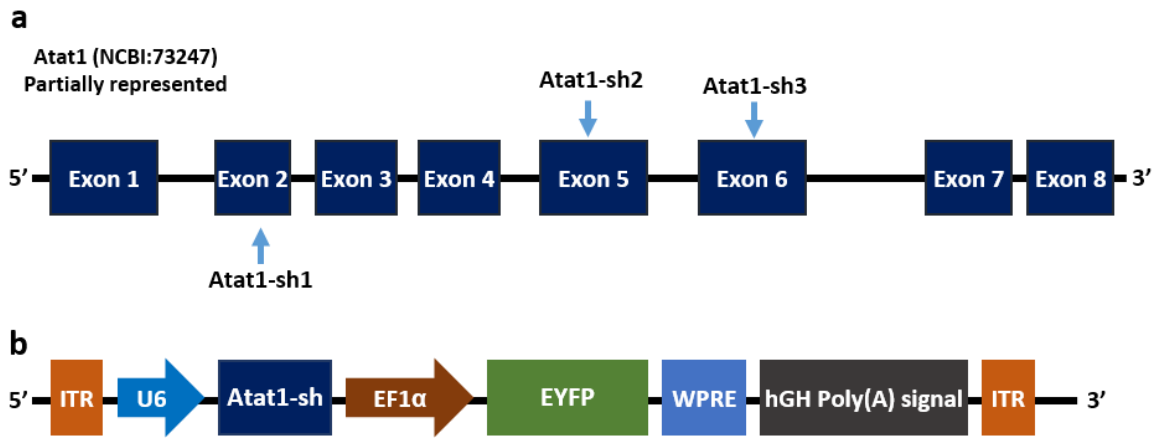


Figure 19 – Design strategy for Atat1 knock-down (a) Relative distribution of the three RNAi sequences within Atat1 gene **(b)** Schematic representation of pAAV-Atat1-sh (AAV-shRNA_Tet3), containing the shRNA sequence expression by the U6 promoter and the fluorescent eYFP driven by the promoter EF1α.

In order to identify which was the best RNAi sequence targeting Atat1 mRNA, I have transfected N2a cells separately with plasmids containing each RNAi sequence (pAAV-Atat1-sh1, pAAV-Atat1-sh2, pAAV-Atat1-sh3), as a negative control, I have used the plasmid AAV-shRNA_Tet3, that from now on, I will refer to as pAAV-Ctrl-sh. At 72 hours after transfection, I fixed the cells and performed an immunocytochemistry assay, using antibodies anti-acetylated α-tubulin and α-tubulin, and quantified ratios of fluorescence intensities for eYFP positive cells. Representative images are shown in Figure 20, the quantification of the average ratios of fluorescence intensity demonstrate that all Atat-sh sequences lead to a significant decrease of acetylated α-tubulin in comparison to Ctrl-sh (pAAV-Ctrl-sh 1.442±0.73, pAAV-Atat1-sh1 0.36±0.19, pAAV-Atat1-sh2 0.33±0.17, pAAV-Atat1-sh3 0.20±0.11, Kruskal–Wallis one-way analysis of variance $p<0.001$).

Additionally, I have also performed western-blot analysis of N2a cells transfected with the pAAV-Ctrl-sh, pAAV-Atat1-sh1, pAAV-Atat1-sh2 and pAAV-Atat1-sh3. Densitometry analysis of western-blot signals (Figure 20c) demonstrate that all Atat1-sh sequences led to a decrease in acetylated α-tubulin, with both pAAV-Atat1-sh2 (0.31) and pAAV-Atat-sh3 (0.31) being the most efficient sequences, while pAAV-Atat1-sh1 (0.67) was the least effective Atat1-sh.

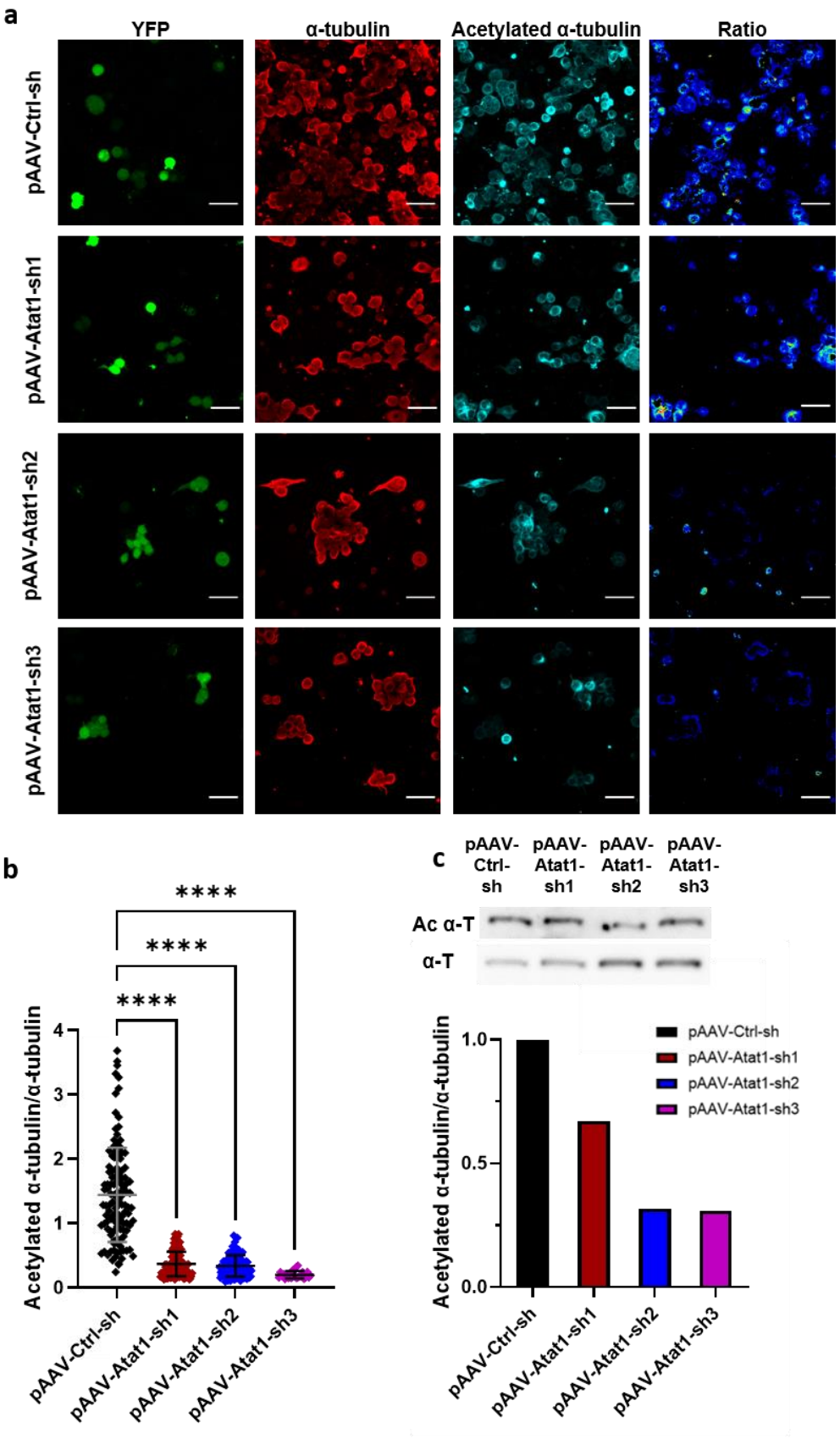

a
YFP
α-tubulin
Acetylated α-tubulin
Ratio
pAAV-Ctrl-sh
pAAV-Atat1-sh1
pAAV-Atat1-sh2
pAAV-Atat1-sh3
b
****
****
****
Acetylated α-tubulin/α-tubulin
0
1
2
3
4
pAAV-Ctrl-sh
pAAV-Atat1-sh1
pAAV-Atat1-sh2
pAAV-Atat1-sh3
c
pAAV-Ctrl-sh
pAAV-Atat1-sh1
pAAV-Atat1-sh2
pAAV-Atat1-sh3
Ac α-T
α-T
Acetylated α-tubulin/α-tubulin
0.0
0.5
1.0
pAAV-Ctrl-sh
pAAV-Atat1-sh1
pAAV-Atat1-sh2
pAAV-Atat1-sh3

Figure 20 – Atat1-shRNA leads to a decrease in the ratio of acetylated α-tubulin over α-tubulin in N2a cells. (a) N2a cells analysed 72 hours after transfection with pAAV-Atat1-sh1 -3 and pAAV-Ctrl-sh immunostained for α-tubulin (red) acetylated α-tubulin (cyan), positively transfected are shown in green and ratios of acetylated α-tubulin over α-tubulin images are shown on the right. Scale bar 50µm. Experiment performed in triplicate, each dot represents an individual cell (technical replicate). **(b)** Quantification of the fluorescence intensity ratio of acetylated α-tubulin over α-tubulin in positively transfected cells. pAAV-Atat1-sh n=121, pAAV-Atat1-sh1 n=105, pAAV-Atat1-sh2 n=93, pAAV-Atat1-sh3 n=26, Kruskal–Wallis one-way analysis of variance, **** $p<0.001$ **(c)** Western-blot analysis of expression of acetylated α-tubulin over α-tubulin (Ac αT and α-T, respetively) in N2a cells transfected with pAAV-Atat1-sh1 -3 and pAAV-Ctrl-sh. Densitometry analysis of the expression of acetylated α-tubulin normalised to the expression of α-tubulin. Experiment not replicated.

Combining the results of immunocytochemistry and western-blot analysis, it appears that pAAV-Atat1-sh2 was the sequence that presented a more consistent effect on acetylated α-tubulin. For that reason, I have pursued with this sequence for my subsequent analysis using rAAV vectors.

6.2.2 Atat1 *ex-vivo* knock-out

Having found the suitable RNAi sequence for targeting Atat1, I produced a recombinant adeno-associated virus with the capsid *Δ*HSPG-rAAV2, carrying Atat1-sh2 (Atat1-sh). With the intention of understanding if indeed primary cultures of DRG neurons are not a good method to test *Δ*HSPG-rAAV2 virus transduction, I repeated the experiments that I performed with Atat1-CRISPR, using Atat1-sh and as positive control AAV2-GFP. I modified 1µL 1.5E12 vg/mL of Atat1-sh. Both wild type AAV2-GFP and Atat1-sh were added to the cultures at 1 DIV. Cultures were kept alive during one week, to allow transgene expression. Figure 21 shows representative images of the cultures, in which it is possible to observe cell bodies expressing the fluorescent reporters of the viruses. Nonetheless, 7 days is not enough time to achieve transduction levels that allow for observation of the effect of knocking-out Atat1. These results indicate that primary cultures of DRG neurons are a good method to observe transduction of viruses expressing fluorescent reporters, but not satisfactory enough to perform complex analysis of protein expression. For this type of analysis, organotypic cultures are a better method.

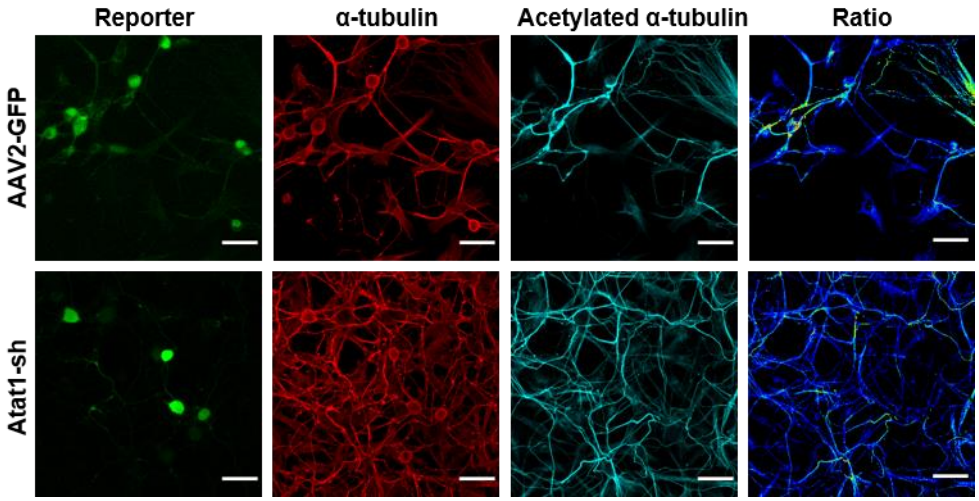


Figure 21 – *Ex-vivo* cultures of DRG neurons infected with AAV2-GFP and Atat1-sh fixed at 8 DIV. Cultures were immunostained for α-tubulin (red) acetylated α-tubulin (cyan), GFP and eYFP positive cells are shown in green, ratios of acetylated α-tubulin over α-tubulin images are shown on the right. Scale bar 50µm. Experiment not replicated.

For these experiments, I have produced a new virus, *Δ*HSPG-rAAV2-Ctrl-sh (Ctrl-sh) that is made of the same capsid as Atat1-sh and contains as cargo the sequences between the two ITRs from pAAV-Ctrl-sh. I used this virus as a negative control for my subsequent experiments using Atat1-sh. In order to test the viruses in *ex-vivo* preparations, I have modified 1µL of 1.5E12 vg/mL Atat1-sh and Ctrl-sh viruses and applied it into organotypic cultures of spinal cord and DRG at 3 DIV and allowed transgene expression for three weeks, before fixing cultures and initiate the immunofluorescence analysis. For a better identification of cells expressing eYFP, I have used an antibody anti-GFP raised in chicken, which also recognises eYFP. Since the antibodies previously used in *in-vitro* analysis in N2a cells were compatible with the antibody anti-GFP, I could keep them for the analysis of organotypic cultures.

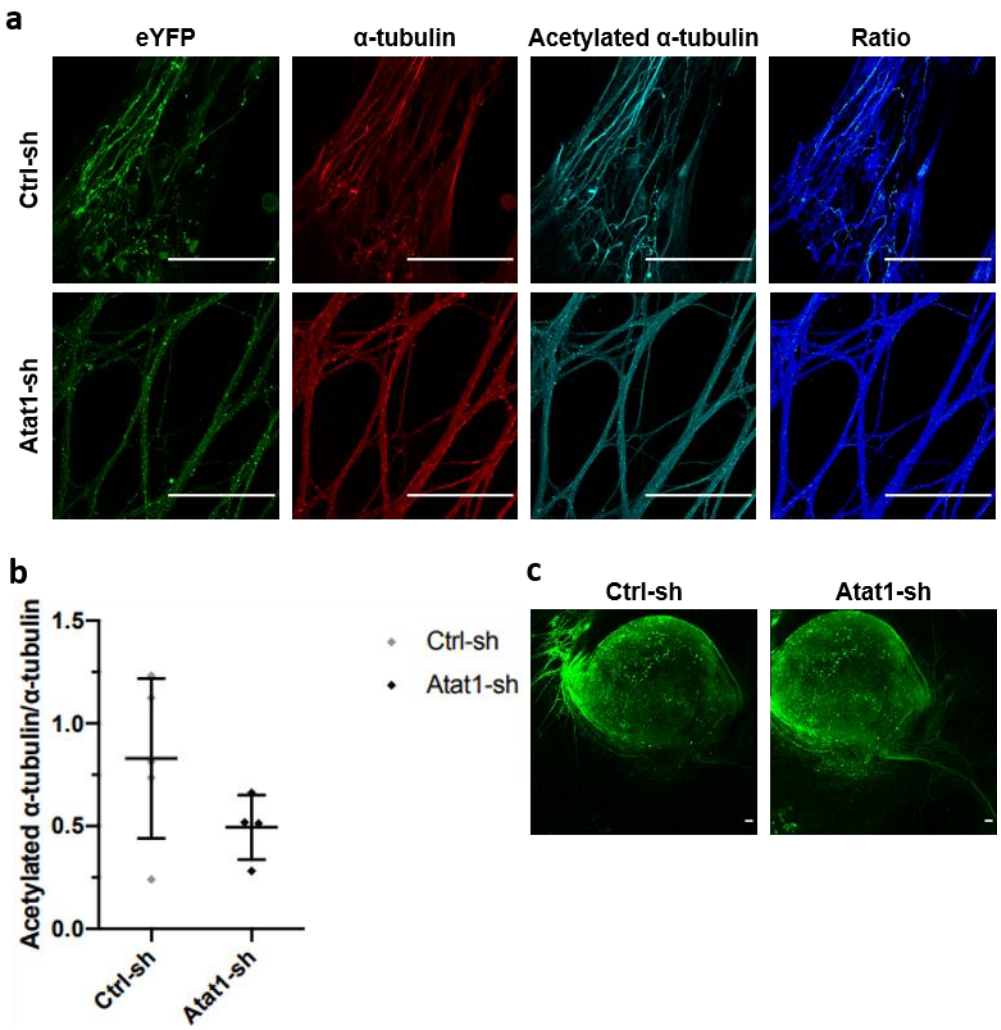


Figure 22 – Atat1-sh does not cause a significate decrease in acetylated α-tubulin in *ex-vivo* cultures. (a) Immunofluorescence of organotypic cultures infected with Atat1-sh and with Ctrl-sh. Cultures were stained for eFYP (green), α-tubulin (red) and acetylated α-tubulin (cyan). Ratio of the images of acetylated α-tubulin over α -tubulin shown on the right. Scale bar 100µm. **(b)** Ratios of fluorescence intensity of acetylated α-tubulin over α -tubulin in eYFP positive regions of Ctrl-sh (n=5) and Atat1-sh (n=4). Each dot represents the average of the ratios obtained for each slice **(c)** Representative images of eYPF expression in slices infected with Atat1-sh and Ctrl-sh at 24 DIV. Scale bar 100µm. Experiment performed in duplicate (technical replicate).

Representative images of slices analysed are shown in Figure 22. In Figure 22c, we can observe the expression of eYFP throughout the whole slice. In order to perform an analysis consistent with the experiments of Atat1-CRISPR, I concentrated my analysis of acetylated α-tubulin in the axons. I performed an immunofluorescence assay to observe the expression of acetylated α-tubulin and α-tubulin in axons expressing eYFP. The ratio of the fluorescence intensities of acetylated α-tubulin over α-tubulin is similar in the slices that received Atat1-sh (0.49±0.15, n=4) in comparison to slices that received Ctrl-sh (0.83±0.39, n=5). Taking into account that in my project I aimed to use RNAi targeting Atat1 in *in-vivo* models, I decided to nonetheless, administrate the virus in fully developed mice.

6.2.3 Atat1-sh *in-vivo*

In order to understand if the modified Atat1-sh virus could drive a decrease in acetylated α-tubulin through knock-down of Atat1 protein expression, I followed the same strategy as I did with Atat1-CRISPR. I modified the capsid of the viruses Atat1-sh and concentrated it in 15µL. Animals were divided into two groups, experimental receiving Atat1-sh or Ctrl-sh viruses. After injections, animals were kept for 7 to 10 weeks to allow transgene expression, before performing histology analysis in lumbar DRGs.

Since histology control experiments for Atat1-CRISPR demonstrated that the secondary antibody goat anti-chicken conjugated with Alexa 488 was not suitable for histology experiments, I needed to replace the antibody anti-GFP raised in chicken that I used previously in the organotypic slices. I tested a different antibody anti-GFP raised in goat in DRG slices of animals injected with AAV2-GFP intrathecally and in DRG slices from wild type animals and found out that both primary and secondary antibodies were suitable for the experiments.

Since I had to use a secondary antibody anti-goat to label eYFP, I could not use the secondary antibodies anti-mouse and anti-rabbit raised in goat that I have been using so far. Therefore, I used secondary antibodies produced in donkey: anti-mouse conjugated with Alexa 647 to label the primary antibody anti-acetylated α-tubulin and anti-rabbit conjugated with Alexa 546, to label the primary antibody anti α-tubulin.

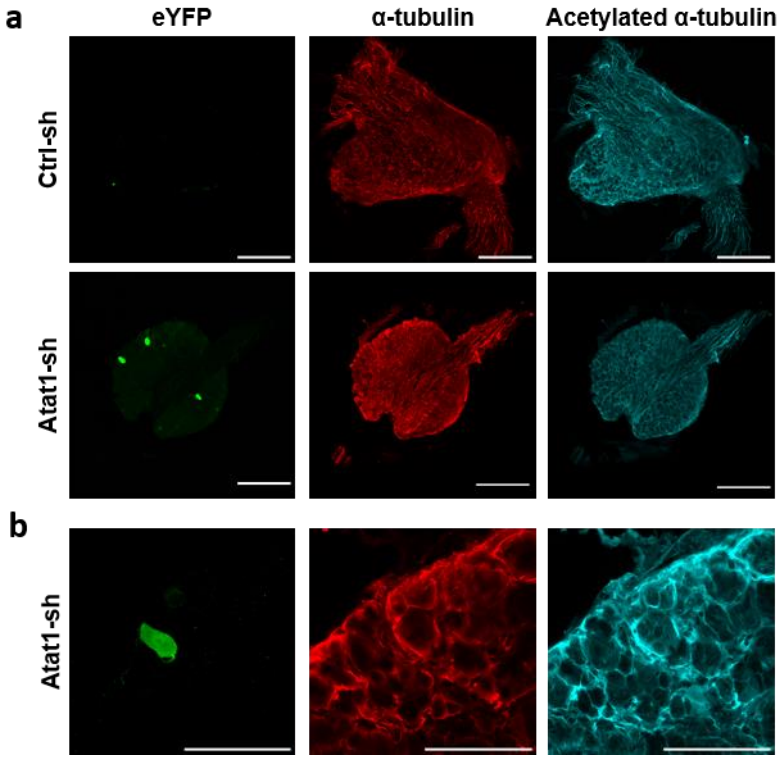


Figure 23 – Atat1-sh *in-vivo.* (a) Immunofluorescence assays on DRG slices of animals injected with Atat1-sh and Ctrl-sh viruses. Slices were stained for expression of eYFP (green), α-tubulin (red) and acetylated α-tubulin (cyan). Scale bar 300µm. **(b)** DRG slices confocal images acquired at higher magnification (60x). Scale bar 300µm.

Following antibody validation, I collected lumbar DRG from animals injected with Atat1-sh and with Ctrl-sh and performed immunohistochemistry experiments. Figure 23 shows representative images of DRG slices from those animals and once again, we can observe that only a few cells express eYFP. The results indicate that unfortunately, the modified capsids of *Δ*HSPG-rAAV2 viruses did not deliver efficiently the transgene. These defects in virus transduction were more evident in Ctrl-sh animals, since I could not find any eYFP positive cell.

Since the slices infected with Atat1-sh and slices infected with the virus mini-CMV-tdTomato were not immunostained with the same primary antibodies, it was not possible to make a comparison between these two groups.

6.3 Chemical inhibition of Atat1

In addition to the genetic approaches in targeting α-tubulin acetylation, I have also investigated whether it is possible to inhibit Atat1 with chemical compounds. To my best knowledge, there are no synthetic inhibitors of Atat1 and the discovery of new ones would open new possibilities for research and translational purposes. This part of my work was a collaboration with EMBL Chemical Biology Core facility and the technology transfer office EMBLEM from EMBL.

We started with a pool of 111 chemical compounds, which the Chemical Biology Core facility has screened for cytotoxicity, solubility and potential of reducing acetylated α-tubulin. They evaluated cell proliferation and compound cytotoxicity in mouse embryonic fibroblasts, using the ATPlipe 1 Step Luminiescence assay. In this assay, they started with 3000 cells that were incubated with different concentrations of chemical compounds and monitored them for 48 hours. A decrease in the amount of adenosine triphosphate (ATP) in cells was an indicator of cell death. Most of the chemicals studied were proven cytotoxic and therefore excluded from the initial screen.

In order to understand if the shortlisted compounds 700269, 718031 and 705638 were indeed able to ablate acetylation of α-tubulin, I have tested them firstly in N2a cells. Cells were incubated with the compounds at 50μM (0.5% DMSO) in cell media, at different time points, I extracted soluble proteins and analysed through western-blot for the expression of acetylated α-tubulin and α-tubulin (Figure 24).

Microtubules are dynamic structures that undergo cycles of polymerisation and depolymerisation, therefore post-translational modifications of microtubules also undergo oscillations in time. Indeed, that is what we observe in control cells (N2a cells incubated with 0.5% DMSO in full media). Incubation of N2a cells with any of the three chemical compounds has lead to a decrease in the amount of acetylated α-tubulin at 6, 24 and 48h. Compounds 718031 and 705638 were the most efficient Atat1 putative inhibitors.

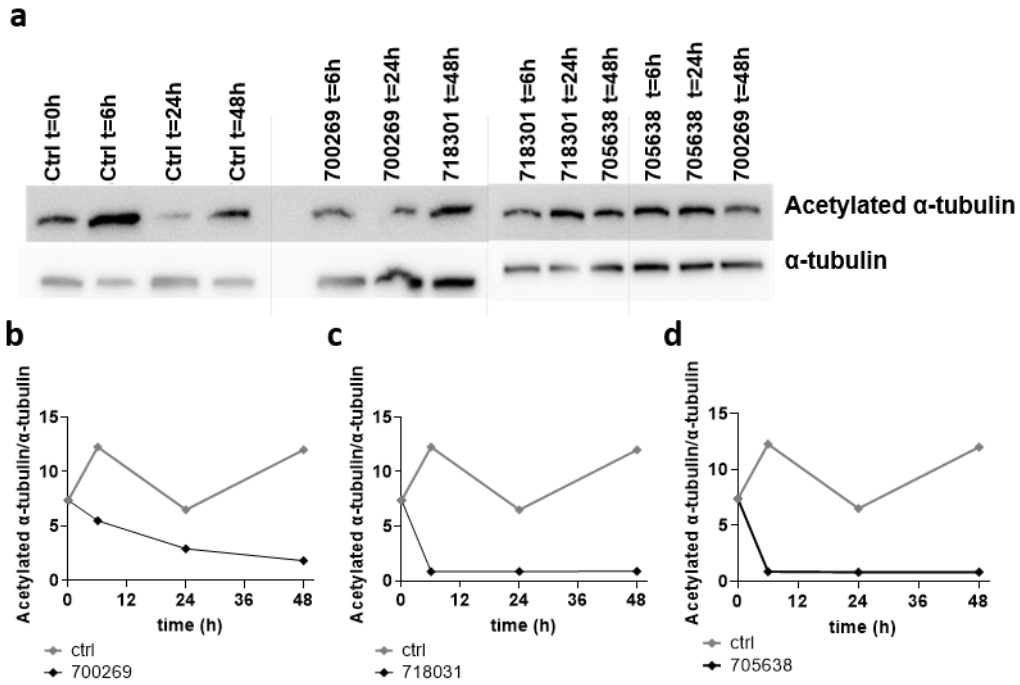
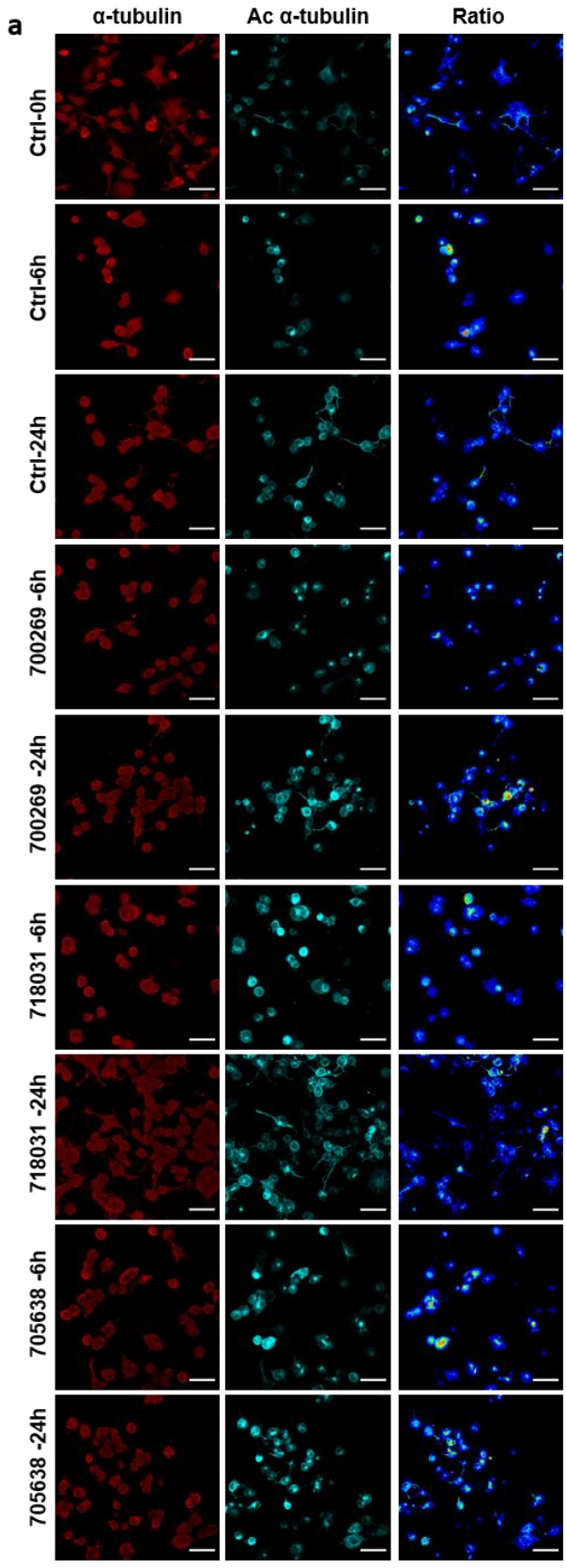
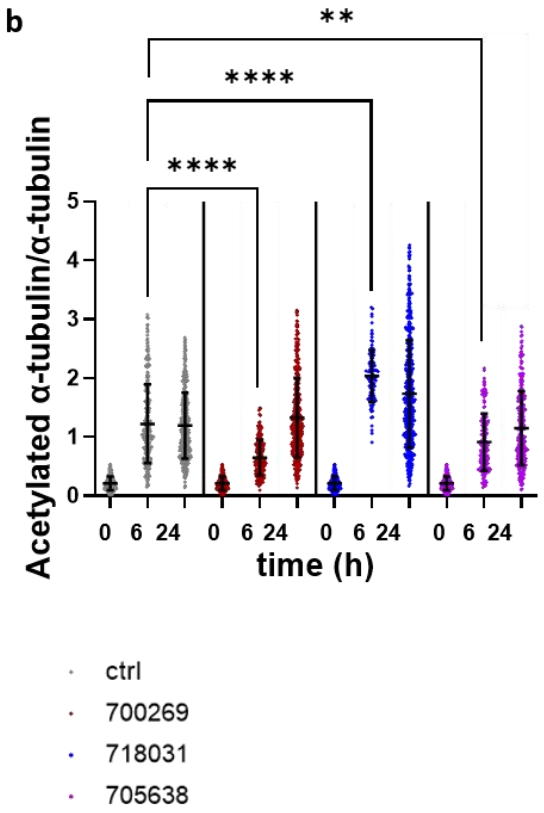


Figure 24 – Western-blot of N2a cells incubated with 50µM of the shortlisted chemical compounds and analysed at different time points (a) N2a cells were incubated with 50µM of the shortlisted compounds for 0, 6, 24 and 48 hours. Soluble proteins of those cells were analysed through western-blot, to observe the expression of acetylated α-tubulin and α-tubulin. **(b-d)** Densitometry of acetylated α-tubulin bands from western-blot analysis normalized to α-tubulin.

The positive results obtained through western-blot encouraged me to pursue the experiments with the immunocytochemistry assays in N2a cells. I seeded N2a cells in a glass-bottomed petri dish and in the next morning added the compounds in cell media, at a final concentration of 50µM. I analysed cells after 6 and 24 hours of exposure with the compounds, for the expression of acetylated α-tubulin and α-tubulin, the results and representative images of the immunofluorescence assay are represented in Figure 25.





c

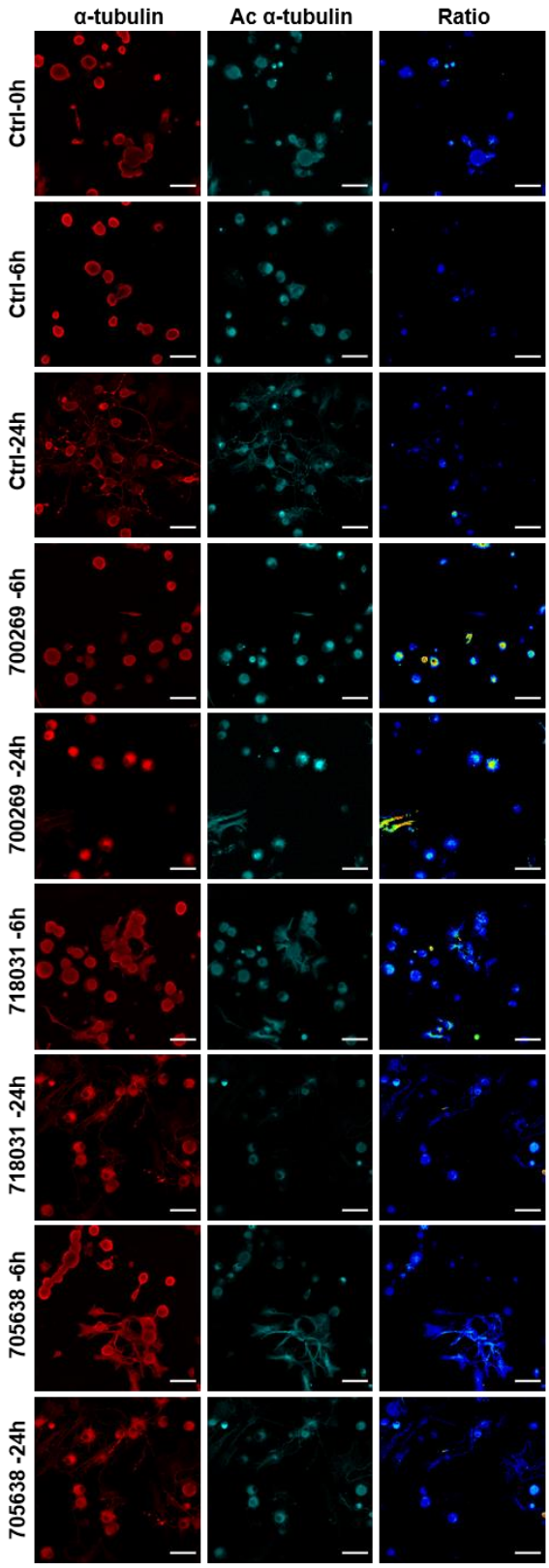
	0h	6h	24h
Control	0.21 ± 0.11 (n=420)	1.22 ± 0.67 (n=317)	1.19 ± 0.56 (n=486)
700269		0.64 ± 0.30 (n=201)	1.33 ± 0.68 (n=506)
718031		2.04 ± 0.44 (n=112)	1.73 ± 0.91 (n=646)
705638		0.91 ± 0.49 (n=198)	1.15 ± 0.63 (n=327)

Figure 25 – Immunocytochemistry of N2a cells incubated with 50µM of the shortlisted chemical compounds and analysed at different time points. (a) Cells were immunostained for α-tubulin (red), acetylated α-tubulin (cyan), ratios of the images of acetylated α-tubulin over α-tubulin are shown on the right. Scale bar 50µm. **(b)** Quantification of the fluorescence intensity of acetylated α-tubulin over α-tubulin of all imaged cells, ****p<0.001, **p<0.1, Kruskal-Wallis test. Replicate experiments not shown, each data point represents one cell. **(c)** Resume of quantification results in all conditions.

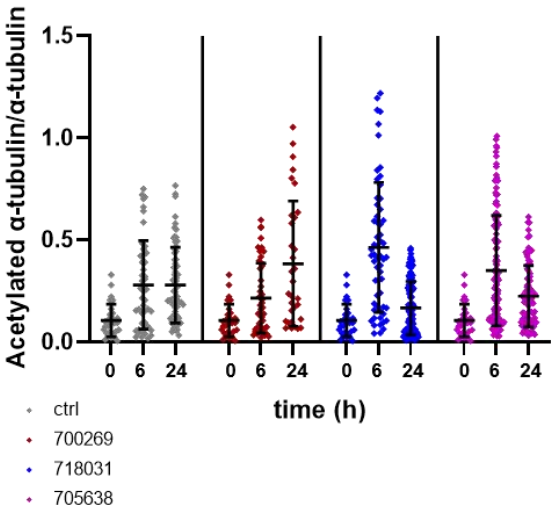
The analysis through immunofluorescence (Figure 25) demonstrated an increase in the amount of the ratios of acetylated α-tubulin over α-tubulin overtime at 6h (from 0.21±0.11, n=420 at time zero to 1.93±0.67, n=317 at 6 hours). This ratio was maintained at 24 hours (1.19±0.56, n=486). Regarding the compounds, 700269 was the most efficient preventing acetylation of α-tubulin at 6h incubation (0.64±0.30, n=201), followed by 705638 (0.91±0.49, n=198). At 24 hours, both compounds seemed to lose their inhibitory effect (700269 (1.33±0.68, n=506) and 705638 (1.15±0.63, n=327)). Surprisingly, cells incubated with compound 718031 showed an increase in the ratio of acetylated α-tubulin at 6h, compared to control (1.73±0.91, n=646), an effect that was lost at 24 hours (1.15±0.63, n=327).

I have also performed an analysis of the effect of compounds in primary cultures of DRG neurons (Figure 26). As observed in N2a cells, the ratio of acetylated α-tubulin increases over time from 0.20±0.22 (n=36) at time zero, to 0.35±0.22 (n=33) at 6 hours, to 0.50±0.78 (n=77) at 24 hours. At 6 hours, only compound 700269 seems to prevent this increase in acetylated α-tubulin (0.24±0.21 (n=51)). Both 718031 (0.46±0.31 (n=59)) and 0.45±0.41 (n=133) do not seem to have an effect at 6 hours. Nonetheless, at 24h hours compound 700269 seem to lose activity (0.49±0.47 (n=35), while 718031 (0.22±0.24 (n=59)) and 705638 (0.35±0.36 (n=102)) seem to cause a decrease in fluorescence intensity of acetylated α-tubulin over α-tubulin.

a



b



c

	0h	6h	24h
Control	0.20 ± 0.22 (n=36)	0.35 ± 0.33 (n=52)	0.50 ± 0.78 (n=77)
700269		0.24 ± 0.21 (n=51)	0.49 ± 0.47 (n=35)
718031		0.46 ± 0.31 (n=59)	0.22 ± 0.24 (n=129)
705638		0.45 ± 0.41 (n=133)	0.35 ± 0.36 (n=102)

Figure 26 - Immunocytochemistry of *ex-vivo* cultures of DRG neurons incubated with 50µM of the shortlisted chemical compounds and analysed at different time points. (a) Cells were immunostained for α-tubulin (red), acetylated α-tubulin (cyan), ratios of the images of acetylated α-tubulin over α-tubulin are shown on the right. Scale bar 50µm. **(b)** Quantification of the fluorescence intensity of acetylated α-tubulin over α-tubulin of all imaged cells. Replicated experiments not shown, each dot represents one cell. **(c)** Resume of quantification results in all conditions.

The incongruent results of protein expression analysis through western blot and immunocytochemistry in N2a cells and DRG neurons and the lack of reproducibility of the experiments (data not shown) motivated the Chemical Core Facility to run experiments addressing the chemical stability of the compounds tested. For this analysis, since compound 705638 did not perform as expected in any of the experiments, it was excluded from the screening, moreover the Chemical Core Facility used also compounds 700269 and 718031 from different batches. The analysis through UPCL demonstrated that compounds 700269 and 718031 were unstable at low pH. We reasoned that potentially, even though the chemicals could inhibit Atat1, their chemically instability would not be compatible with its use in biology, for example, if these compounds would enter the endocytic pathway, they would most likely be degraded once inside lysosomes, given the high acidity of these cellular structures.

For this reason, we halted the collaboration for accessing the chemical compounds and focused our attention on the genetic strategies for ablating Atat1 expression.

7. Discussion

In my dissertation studies, I investigated the efficacy of Atat1 repression in the peripheral nervous system, using three independent approaches. Firstly, I aimed to edit the genome of cells, using CRISPR-Cas9, to knock-out Atat1 gene. Secondly, I aimed to target Atat1 at post-transcriptional level, knocking-down Atat1 mRNA levels with RNAi. Lastly, I aimed to inhibit the enzyme Atat1, using synthetic putative inhibitors. In my first two approaches, I used rAAV platforms to deliver genetic material to cells.

Atat1 and its orthologues are essential proteins for mechanosensation in different organisms. In mice, ablation of Atat1 specifically in the peripheral nervous system is compatible with a normal development of animals (Morley et al., 2016). Of particular interest, rescue experiments in models of genetic ablation of Atat1 demonstrated that the loss of mechanosensation of in Atat1 deficient animals was due to the loss of acetylated α-tubulin and not for the loss of Atat1 expression (Morley et al., 2016). For these reasons, instead of using antibodies targeting the protein Atat1, given that I aimed ultimately to apply my hypothesis for the treatment of chronic pain, I analysed the expression of acetylated α-tubulin during the experiments.

The apparent safety of ablation of Atat1, makes it an appealing target for the treatment of exacerbated mechanosensation diseases, such as chronic pain (Mills et al., 2019). Currently, chronic pain affects more than 20% of the world population and treatment options rely on drugs, such as opioids, that can lead to addiction and a reduced life experience (Skolnick, 2018). Moreover, other therapeutic approaches have been shown to be ineffective to a substantial cohort of patients. There is therefore a great need to improve treatment options for chronic pain patients.

7.1 Targeting Atat1 through gene editing

The elucidation of the mechanism through which one can redirect the nuclease Cas9 to specific regions within a cell's genome (Jinek et al., 2012) and apply it to research was one of the most important hallmarks in science of the recent years. CRISPR-Cas9 democratized the possibility of achieving gene editing and shined light to novel therapeutic targets to many monogenic diseases. Here I used this technology to promote ablation of Atat1 gene in mouse cells.

Even though CRISPR-Cas9 technologies are easier to use comparing to the alternative gene editing technologies, not every possible gRNA sequence can promote indel events. Screening of potential gRNA sequences *in-vitro* in cell lines offer a bigger flexibility to troubleshoot constructs, because it is easy to manipulate and to have higher amounts of cells, compared to primary cultures. Moreover, cell lines are easy to transfect, this feature is particularly important, since primary cultures of neurons are difficult to transfect with traditional methods for gene delivery. From an initial pool of 5 potential gRNA candidates, only one of the sequences (gRNA1, Figure 9) lead to knock-out of Atat1 in N2a cells, with an efficiency of nearly 60%.

The packaging capacity constraints of rAAV (<4.5kb) forced the replacement of the pAAV vector initial used for the screening experiments, for another one that allowed a correct packaging of rAAV. This new plasmid, pAAV-Atat1-CRISPR, contained the promoter mini-CMV for driving the expression of SaCas9, while the first plasmid contained the promoter and enhancer CMV. Immunocytochemistry analysis of N2a cells showed that both plasmids were able to efficiently cause a reduction in the ratios of fluorescence intensity of acetylated α-tubulin over α-tubulin, nonetheless pX601-mCherry-Atat1-CRISPR (0.21±0.16, n=680) plasmid seemed to be more efficient than pAAV-Atat1-CRISPR (0.31±0.00, n=1094). Considering that the methods used in both experiments were the same and that in both plasmids, the gRNA sequence was constitutively expressed under the U6 promoter, the differences observed in the average ratios could be explained by differences in the strength of CMV and mini-CMV promoters in driving the expression of SaCas9. Notwithstanding, in regards to CRISPR

experiments, the amount of gRNA available is a more limiting factor, compared to the amount of Cas9 nuclease inside cells, and if I would extend the experiments for a longer period of time, these differences would be probably not observed.

Following validation of the gRNA sequence through immunocytochemistry and western blot analysis, I produced a recombinant adeno-associated virus (rAAV) with the serotype 2, containing a mutation (*Δ*HSPG-rAAV2), that prevented binding to cells' receptors and therefore impairing viral internalization and transduction. Retargeting of the viruses was achieved by modification of the surface of the capsid of viruses. N2a cells do not survive upon rAAV administration (Vora et al., 2018), which made it impossible to test the viruses in *in-vitro* preparations. Notwithstanding, testing the viruses in *ex-vivo* preparations was particularly challenging, because primary cultures of DRG neurons built a dense net of axons, making it impossible to visualise any individual structure and because Atat1-CRISPR virus did not contain a fluorescent reporter and visualisation through immunofluorescence assays was not possible to achieve. Fortunately, all these obstacles were surpassed with the use of *ex-vivo* organotypic cultures of spinal cord and DRG neurons, replacement of one of the antibodies used in immunofluorescence assays and with the co-infection of Atat1-CRISPR virus with mini-CMV-tdTomato virus. Results show a ratio of the fluorescence intensity of acetylated α-tubulin over βIII-tubulin of 0.44±0.17 (n=7) in Atat1-CRISPR and 0.97±0.06 (n=7) in mini-CMV-tdTomato.

While we still see a significant difference between both conditions, the amplitude of those differences are smaller than what was observed previously in the *in-vitro* screening. One of the reasons that might lead to this difference may be due to the fact that in cell lines there is more chromatin accessibility, because cells are undergoing cycles of cell division, which facilitates Cas9 contact with the target locus.

7.2 Targeting Atat1 through RNAi

RNAi based therapies have been under investigation for many years now, the ability of harnessing protein expression by targeting mRNA sequences to degradation has a particularly importance in the treatment of monogenic diseases caused by toxic products consequent of compromised gene expression (Bumcrot et al., 2006). Despite the vast potential of RNAi based therapies, delivery of RNAi has been an enormous challenge. The biggest caveats of RNAi technologies relate to poor stability of RNA molecules, toxicity, off-target effects, loss of shRNA expression over time or immunogenic responses (Crooke et al., 2018; van Haasteren et al., 2020).

Here I explored the potential of a stable delivery of RNAi technology as a shRNA incorporated into a pAAV vector. In my initial screening, I cloned separately three different RNAi sequences in a pAAV vector and delivered it to N2a cells using a lipid based method. The immunocytochemistry analysis demonstrated that the sequences that I tried were able to reduce the ratio of fluorescence intensities of acetylated α-tubulin over α-tubulin in N2a cells expressing the reporter eYFP. A subsequent analysis of soluble proteins of N2a cells transfected with the plasmids encoding shRNA sequences, showed that all plasmids were able to reduce the amount of acetylated α-tubulin, compared to control. Nonetheless, most likely because in the western blot analysis it was not possible to separate positively from negatively transfected cells, the differences observed were less marked (Figure 20). Combining both experiments, I decided to use Atat1-sh2 targeting exon 5 of Atat1 gene to pursue the experiments with rAAV viruses.

Ex-vivo primary cultures of DRG neurons did not provide a good preparation to visualise the effects of Atat1-sh in microtubules. This type of preparation is useful and adequate for screening of viral transduction, especially if the virus contains a fluorescent reporter. However, for my experiments, my readout rather than observing the expression of Atat1, I aimed to observe the effects of knocking-down Atat1 on acetylation of α-tubulin. Therefore, I used organotypic cultures of spinal cord and DRG neurons, to understand if the Atat1-sh was

able to have an effect in *ex-vivo* cultures. Results of immunofluorescence assays demonstrated that slices receiving Atat1-sh virus had a slightly lower ratio of the fluorescence intensity of acetylated α-tubulin over α-tubulin (0.49±0.15, n=4) in comparison to slices that received Ctrl-sh virus (0.83±0.39, n=5).

7.3 Targeting Atat1 *in-vivo*

The encouraging results observed in both CRISPR and RNAi strategies to decrease acetylated α-tubulin in sensory neurons lead to testing them in fully developed mice. To do that, viruses were administrated into the intrathecal space at the lumbar region of the spinal cord. This rout is widely used to deliver substances to DRG neurons and also to deliver drugs to patients (Vulchanova et al., 2010). Transgene expression of rAAV *in-vivo* initiates 2 to 3 weeks following treatment administration (Maffei et al., 2019). However, because in my experiments I was using an indirect measurement to observe the effects of the virus, I needed to consider that in order to observe a reduction in acetylated α-tubulin it is necessary to wait for the turnover of already translated Atat1 and the turnover of stable microtubules in DRG neurons. Therefore, I waited from 7 to 10 weeks before collecting tissues of animals injected with the viruses and performed immunohistochemistry in sections of lumbar DRG.

Unfortunately, the absence of signal for the fluorescent protein reporters of the viruses demonstrated that both CRISPR, RNAi and control viruses failed to be efficiently transduced to DRG neurons. This lack of viral transduction could be a consequence of the type of capsid used to make the virus that could impair its internalization to the targeted cells or even by a deficient capsid assembly, or inefficient packaging of the cargo. The reason why this was not evident in the *ex-vivo* assays could be explained by the fact that these preparations have the target cells much more accessible and that the ratio of delivered viral genomes to cells is much higher, compared to *in-vivo* models. In order to improve viral transduction, the constructs validated in the *in-vitro* and *ex-vivo* analyses could be specifically delivered to DRG neurons with another capsid, such as the capsid PHP.S, that is an improved version of the AAV9 serotype with a tropism for DRG neurons (Chan et al., 2017).

7.4 Targeting Atat1 with protein inhibitors

The screening of Atat1 inhibitors was a collaboration with the Chemical Core Facility and technology transfer office EMBLEM from EMBL. We started with 111 chemicals that were screened for solubility, cell toxicity and potential of reducing tubulin acetylation in mouse fibroblasts. From this initial pool, three compounds were shortlisted. I analysed their potential in decreasing acetylated α-tubulin in N2a cells through immunocytochemistry and western-blot at different time points (Figure 24). Furthermore, I have tested the compounds in primary cultures of DRG neurons (Figure 25). The conflicting results between replicate experiments motivated the assessment of chemical stability of the compounds, this analysis demonstrated that the compounds were too unstable to be used as we intended to. In order to use the compounds, we needed to identify which chemical groups of the putative inhibitors were interacting with Atat1 and search for chemical analogues to add to the screen. Moreover, following identification of core regions of the chemicals responsible for inhibiting Atat1, those molecules could be engineered to have an increased chemical stability.

7.5 Atat1 as a potential therapeutic target for different diseases

This project was based on previous findings that identified Atat1 and its orthologues are essential for mechanosensation in different organisms (Akella et al., 2010; Chalfie and Sulston, 1981; Morley et al., 2016; Yan et al., 2018). Particularly in mice, Atat1 depletion specifically in the peripheral nervous system leads to a reduced mechanosensitivity without any other effect identified in other sensory modalities (Morley et al., 2016). In my thesis, I tried to understand if it was possible to achieve this phenotype in fully developed mice with CRISPR and RNAi technologies delivered by rAAV and with putative chemical inhibitors of Atat1.

Microtubules act as tracks for intracellular trafficking and post-translational modifications have been implicated as regulators of this physiological process (Janke and Bulinski, 2011). Previous experiments on hippocampal neurons showed that interactions between motor proteins and post-translational modifications on microtubules, such as acetylation of microtubule tracks could guide intracellular transport to specific locations within cells (Reed et al., 2006).

In Huntington's disease, microtubule acetylation is reduced and vesicular transport is impaired. Experiments performed in models of Huntington's disease demonstrated that inhibition of α-tubulin desacetylase HDAC6 in cortical neurons leads to an increase in acetylated α-tubulin and intracellular transport which improves the physiopathology of this disease (Dompierre et al., 2007). Moreover, in Parkinson's disease, inhibition of the deacetylase Sirt-2 has shown to be neuroprotective (Outeiro et al., 2007), while HDAC6 inhibition has been proposed as a therapeutic target for the treatment of Alzheimer's disease (Govindarajan et al., 2013). Furthermore, in different models of cancer, α-tubulin acetylation has been associated with an increased capacity of cancer cell invasion (Boggs et al., 2015; Castro-Castro et al., 2012; Yoshimoto et al., 2021). These findings point out the importance of acetylated α-tubulin in different physiological processes. For instances, the treatment for neurodegenerative diseases, such as Huntington's, Parkinson's and Alzheimer's disease can be an upregulation of Atat1 or inhibition of HDAC6 or Sirt-2. However, in the context of cancer, inhibiting acetylation of α-tubulin can be a way of avoiding metastasis.

For these reasons, there is a great need in finding therapies that can specifically deliver the treatment for the target cell population.

8. Conclusions

Here I presented three different strategies targeting Atat1 at genomic (CRISPR), post-transcriptional (RNAi) and protein level (chemical screening).

Starting the genome editing strategy, from my work it is possible to conclude that the delivery of SaCas9 with gRNA as a single rAAV vector is an efficient way of achieving gene editing. Nonetheless, it is important to acknowledge that not all possible gRNA sequences adjacent to PAM motifs can successfully guide Cas9 to the target gene locus. From my work, it was possible to conclude that even in cases where the nuclease SaCas9 is expressed at low levels, if the gRNA sequence is driven by a strong promoter, one can still observe that knock-out of Atat1 gene leads to a decrease in acetylated α-tubulin in *in-vitro* mouse models. Delivery of Atat1-CRISPR to *ex-vivo* models of organotypic cultures of spinal cord and DRG neurons show a tendency of Atat1-CRISPR to cause a decrease in acetylated α-tubulin that needs further clarification.

Regarding the RNAi strategy, the analysis of the experiments demonstrated that having a fluorescent reporter in the construct carrying the shRNA sequence facilitates enormously detection of recipient cells of the RNAi constructs. Similarly to what was observed previously, delivery of Atat1-sh leads to a decrease of acetylated α-tubulin *in-vitro* and shows a tendency in *ex-vivo* models, that also requires a better characterization.

Delivery of genetic material to cells, has been one of the main challenges in translational research. rAAV vectors allow a stable delivery of genetic material, however there is a great need in improving how to specifically delivery methods. Here I used a modified version of rAAV2 viruses, aiming to improve cell tropism. Unfortunately, while this type of rAAV showed to be efficient in delivering genes to organotypic cultures of spinal cord and DRG, it failed to deliver it efficiently in *in-vivo* mouse models.

The chemical screen of putative inhibitors of Atat1 revealed that it may be possible to inhibit Atat1 in an *in-vitro* experimental model, however, there is still a great need in optimizing the structure of the compounds.

Overall, with my project, I provided a platform for *in-vitro* and *ex-vivo* experiments in which Atat1 expression is depleted. In these preparations, Atat1 depletion caused a decrease in the acetylated α-tubulin in microtubules. Further optimization of the viral vectors will allow the assessment of the consequences of depleting Atat1 expression in fully developed animals and potentially point out Atat1 expression in DRG neurons as a therapeutic target for the treatment of chronic pain. This therapy could be further translated to as a treatment for other pathologies, in which depletion of Atat1 is beneficial for health.

9. References

Abraira, V.E., and Ginty, D.D. (2013). The sensory neurons of touch. Neuron *79*, 618–639.

Akella, J.S., Wloga, D., Kim, J., Starostina, N.G., Lyons-Abbott, S., Morrissette, N.S., Dougan, S.T., Kipreos, E.T., and Gaertig, J. (2010). MEC-17 is an α-tubulin acetyltransferase. Nature *467*, 218–222.

Anders, C., Niewoehner, O., Duerst, A., and Jinek, M. (2014). Structural basis of PAM-dependent target DNA recognition by the Cas9 endonuclease. Nature *513*, 569–573.

Anderson, E.O., Schneider, E.R., and Bagriantsev, S.N. (2017). Piezo2 in Cutaneous and Proprioceptive Mechanotransduction in Vertebrates (Elsevier Ltd).

Andrews, C.D., Luo, Y., Sun, M., Yu, J., Goff, A.J., Glass, P.J., Padte, N.N., Huang, Y., and Ho, D.D. (2017). In Vivo Production of Monoclonal Antibodies by Gene Transfer via Electroporation Protects against Lethal Influenza and Ebola Infections. Mol. Ther. - Methods Clin. Dev. *7*, 74–82.

Assad, J.A., Shepherd, G.M.G., and Corey, D.P. (1991). Tip-link integrity and mechanical transduction in vertebrate hair cells. Neuron *7*, 985–994.

Aurnhammer, C., Haase, M., Muether, N., Hausl, M., Rauschhuber, C., Huber, I., Nitschko, H., Busch, U., Sing, A., Ehrhardt, A., et al. (2012). Universal Real-Time PCR for the Detection and Quantification of Adeno-Associated Virus Serotype 2-Derived Inverted Terminal Repeat Sequences. Hum. Gene Ther. Methods *23*, 18–28.

Barman, A., Deb, B., and Chakraborty, S. (2020). A glance at genome editing with CRISPR–Cas9 technology. Curr. Genet. *66*, 447–462.

Basbaum, A.I., Bautista, D.M., Scherrer, G., and Julius, D. (2009). Cellular and Molecular Mechanisms of Pain. Cell *139*, 267–284.

Beaulieu-Laroche, L., Christin, M., Donoghue, A., Agosti, F., Yousefpour, N., Petitjean, H., Davidova, A., Stanton, C., Khan, U., Dietz, C., et al. (2020). TACAN Is an Ion Channel Involved in Sensing Mechanical Pain. Cell *180*, 956-967.e17.

Boggs, A.E., Vitolo, M.I., Whipple, R.A., Charpentier, M.S., Goloubeva, O.G., Ioffe, O.B., Tuttle, K.C., Slovic, J., Lu, Y., Mills, G.B., et al. (2015). α-Tubulin acetylation elevated in metastatic and basal-like breast cancer cells promotes microtentacle formation, adhesion, and invasive migration. Cancer Res. *75*, 203–215.

Bott, C.J., and Winckler, B. (2020). Intermediate filaments in developing neurons: Beyond structure. Cytoskeleton 1–19.

Brinkman, E.K., Chen, T., Amendola, M., and Van Steensel, B. (2014). Easy quantitative assessment of genome editing by sequence trace decomposition. Nucleic Acids Res. *42*.

Brohawn, S.G. (2015). How ion channels sense mechanical force: Insights from mechanosensitive K2P channels TRAAK, TREK1, and TREK2. Ann. N. Y. Acad. Sci. *1352*, 20–32.

Brummelkamp, T.R., Bernards, R., and Agami, R. (2002). A system for stable expression of short interfering RNAs in mammalian cells. Science (80-.). *296*, 550–553.

Bumcrot, D., Manoharan, M., Koteliansky, V., and Sah, D.W.Y. (2006). RNAi therapeutics: A potential new class of pharmaceutical drugs. Nat. Chem. Biol. *2*, 711–719.

Büning, H., and Srivastava, A. (2019). Capsid Modifications for Targeting and Improving the Efficacy of AAV Vectors. Mol. Ther. - Methods Clin. Dev. *12*, 248–265.

Castro-Castro, A., Janke, C., Montagnac, G., Paul-Gilloteaux, P., and Chavrier, P. (2012). ATAT1/MEC-17 acetyltransferase and HDAC6 deacetylase control a balance of acetylation of alpha-tubulin and cortactin and regulate MT1-MMP trafficking and breast tumor cell invasion. Eur. J. Cell Biol. *91*, 950–960.

Cavanaugh, D.J., Lee, H., Lo, L., Shields, S.D., Zylka, M.J., Basbaum, A.I., and Anderson, D.J. (2009). Distinct subsets of unmyelinated primary sensory fibers mediate behavioral responses to noxious thermal and mechanical stimuli (Proceedings of the National Academy of Sciences of the United States of America (2009) 106, 22, (9075-9080) DOI: 10.1073/pnas.0. Proc. Natl. Acad. Sci. U. S. A. *106*, 11424.

Chalfie, M. (2009). Neurosensory mechanotransduction. Nat. Rev. Mol. Cell Biol. *10*, 44–52.

Chalfie, M., and Sulston, J. (1981). Developmental genetics of the mechanosensory neurons of Caenorhabditis elegans. Dev. Biol. *82*, 358–370.

Challis, R.C., Kumar, S.R., Chan, K.Y., Challis, C., Beadle, K., Jang, M.J., Kim, H.M., Rajendran, P.S., Tompkins, J.D., Shivkumar, K., et al. (2019). Systemic AAV vectors for widespread and targeted gene delivery in rodents. Nat. Protoc. *14*, 2597.

Chan, K.Y., Jang, M.J., Yoo, B.B., Greenbaum, A., Ravi, N., Wu, W., Sánchez-Guardado, L., Lois, C., Mazmanian, S.K., Deverman, B.E., et al. (2017). Engineered AAVs for efficient noninvasive gene delivery to the central and peripheral nervous systems. Nat. Neurosci. *20*, 1172–1179.

Choudhary, C., Kumar, C., Gnad, F., Nielsen, M.L., Rehman, M., Walther, T.C., Olsen, J. V., and Mann, M. (2009). Lysine acetylation targets protein complexes and co-regulates major cellular functions. Science (80-.). *325*, 834–840.

Collier, R. (2018). A short history of pain management. CMAJ *190*, E26–E27.

Coombes, C., Yamamoto, A., McClellan, M., Reid, T.A., Plooster, M., Luxton, G.W.G., Alper, J., Howard, J., and Gardner, M.K. (2016). Mechanism of microtubule lumen entry for the α-tubulin acetyltransferase enzyme αTAT1. Proc. Natl. Acad. Sci. U. S. A. *113*, E7176–E7184.

Cox, C.D., Bavi, N., and Martinac, B. (2018). Bacterial Mechanosensors. Annu. Rev. Physiol. *80*, 71–93.

Cox, C.D., Bavi, N., and Martinac, B. (2019). Biophysical Principles of Ion-Channel-Mediated Mechanosensory Transduction. Cell Rep. *29*, 1–12.

Crooke, S.T., Witztum, J.L., Bennett, C.F., and Baker, B.F. (2018). RNA-Targeted Therapeutics. Cell Metab. *27*, 714–739.

Cunningham, F., Achuthan, P., Akanni, W., Allen, J., Amode, M.R., Armean, I.M., Bennett, R., Bhai, J., Billis, K., Boddu, S., et al. (2019). Ensembl 2019. Nucleic Acids Res. *47*, D745–D751.

Dhandapani, R., Arokiaraj, C.M., Taberner, F.J., Pacifico, P., Raja, S., Nocchi, L., Portulano, C., Franciosa, F., Maffei, M., Hussain, A.F., et al. (2018). Control of mechanical pain hypersensitivity in mice through ligand-targeted photoablation of TrkB-positive sensory neurons. Nat. Commun. *9*.

Dias Florencio, G., Precigout, G., Beley, C., Buclez, P.O., Garcia, L., and Benchaouir, R. (2015). Simple downstream process based on detergent treatment improves yield and in vivo transduction efficacy of adeno-associated virus vectors. Mol. Ther. - Methods Clin. Dev. *2*, 15024.

Dompierre, J.P., Godin, J.D., Charrin, B.C., Cordelières, F.P., King, S.J., Humbert, S., and Saudou, F. (2007). Histone deacetylase 6 inhibition compensates for the transport deficit in Huntington's disease by increasing tubulin acetylation. J. Neurosci. *27*, 3571–3583.

Doudna, J.A. (2020). The promise and challenge of therapeutic genome editing. Nature *578*, 229–236.

Dowdy, S.F. (2017). Overcoming cellular barriers for RNA therapeutics. Nat. Biotechnol. *35*, 222–229.

Dunbar, C.E., High, K.A., Joung, J.K., Kohn, D.B., Ozawa, K., and Sadelain, M. (2018). Gene therapy comes of age. Science (80-.). *359*.

Echeverri, C.J., and Perrimon, N. (2006). High-throughput RNAi screening in cultured cells: A user's guide. Nat. Rev. Genet. *7*, 373–384.

Elbashir, S.M., Harborth, J., Lendeckel, W., Yalcin, A., Weber, K., and Tuschl, T. (2001). Duplexes of 21-nucleotide RNAs mediate RNA interference in cultured mammalian cells. *411*, 1–5.

Even, A., Morelli, G., Broix, L., Scaramuzzino, C., Turchetto, S., Gladwyn-Ng, I., Le Bail, R., Shilian, M., Freeman, S., Magiera, M.M., et al. (2019). ATAT1-enriched vesicles promote microtubule acetylation via axonal transport. Sci. Adv. *5*.

Fire, A., Xu, S., Montgomery, M.K., Kostas, S.A., Driver, S.E., and Mello, C.C. (1998). Potent and specific genetic interference by double-stranded RNA in Caenorhabditis elegans. Nature *391*, 806–811.

Fletcher, D.A., and Mullins, R.D. (2010). Cell mechanics and the cytoskeleton. Nature *463*, 485–492.

Fonfara, I., Le Rhun, A., Chylinski, K., Makarova, K.S., Lécrivain, A.L., Bzdrenga, J., Koonin, E. V., and Charpentier, E. (2014). Phylogeny of Cas9 determines functional exchangeability of dual-RNA and Cas9 among orthologous type II CRISPR-Cas systems. Nucleic Acids Res. *42*, 2577–2590.

Friedmann, T., and Roblin, R. (1972). Gene therapy for human genetic disease? Science (80-.). *175*, 949–955.

Friedmann, D.R., Aguilar, A., Fan, J., Nachury, M. V., and Marmorstein, R. (2012). Structure of the α-tubulin acetyltransferase, αTAT1, and implications for tubulin-specific acetylation. Proc. Natl. Acad. Sci. U. S. A. *109*, 19655–19660.

Fu, Z., and Shi, J. (2017). Differential expression of tubulin acetylase and deacetylase between the damaged central and peripheral branch of dorsal root ganglion neurons. Med. Sci. Monit. *23*, 3673–3678.

Gadadhar, S., Bodakuntla, S., Natarajan, K., and Janke, C. (2017). The tubulin code at a glance. J. Cell Sci. *130*, 1347–1353.

Garrison, S.R., Dietrich, A., and Stucky, C.L. (2012). TRPC1 contributes to light-touch sensation and mechanical responses in low-threshold cutaneous sensory neurons. J. Neurophysiol. *107*, 913–922.

Gaub, B.M., and Müller, D.J. (2017). Mechanical Stimulation of Piezo1 Receptors Depends on Extracellular Matrix Proteins and Directionality of Force. Nano Lett. *17*, 2064–2072.

Giacco, V., Panattoni, G., Medelin, M., Bonechi, E., Aldinucci, A., Ballerini, C., and Ballerini, L. (2019). Cytokine inflammatory threat, but not LPS one, shortens GABAergic synaptic currents in the mouse spinal cord organotypic cultures. J. Neuroinflammation *16*, 1–14.

Goodman, M.B., Ernstrom, G.G., Chelur, D.S., O'Hagan, R., Yao, C.A., and Chalfie, M. (2002). MEC-2 regulates C. elegans DEG/ENaC channels needed for mechanosensation. Nature *415*, 1039–1042.

Govindarajan, N., Rao, P., Burkhardt, S., Sananbenesi, F., Schlüter, O.M., Bradke, F., Lu, J., and Fischer, A. (2013). Reducing HDAC6 ameliorates cognitive deficits in a mouse model for Alzheimer's disease. EMBO Mol. Med. *5*, 52–63.

Grieger, J.C., Choi, V.W., and Samulski, R.J. (2006). Production and characterization of adeno-associated viral vectors. Nat. Protoc. *1*, 1412–1428.

Gu, S., Jin, L., Zhang, Y., Huang, Y., Zhang, F., Valdmanis, P.N., and Kay, M.A. (2012). The loop position of shRNAs and pre-miRNAs is critical for the accuracy of dicer processing in vivo. Cell *151*, 900–911.

van Haasteren, J., Li, J., Scheideler, O.J., Murthy, N., and Schaffer, D. V. (2020). The delivery challenge: fulfilling the promise of therapeutic genome editing. Nat. Biotechnol. *38*.

Handler, A., and Ginty, D.D. (2021). The mechanosensory neurons of touch and their mechanisms of activation. Nat. Rev. Neurosci. *0123456789*.

Herget, R., Lapatsina, L., Ngo, H., Poole, K., and Lewin, G.R. (2014). Tuning Piezo ion channels to detect molecular-scale movements relevant for fine touch. Nat. Commun. *5*, 1–14.

Hernández, G., Osnaya, V.G., and Pérez-Martínez, X. (2019). Conservation and Variability of the AUG Initiation Codon Context in Eukaryotes. Trends Biochem. Sci. *44*, 1009–1021.

Hill, R.Z., and Bautista, D.M. (2020). Getting in Touch with Mechanical Pain Mechanisms. Trends Neurosci. *43*, 311–325.

Hirakawa, M.P., Krishnakumar, R., Timlin, J.A., Carney, J.P., and Butler, K.S. (2020). Gene editing and CRISPR in the clinic: current and future perspectives. Biosci. Rep. *0*.

Hirokawa, N., Noda, Y., Tanaka, Y., and Niwa, S. (2009). Kinesin superfamily motor proteins and intracellular transport. Nat. Rev. Mol. Cell Biol. *10*, 682–696.

Hjerling-Leffler, J., AlQatari, M., Ernfors, P., and Koltzenburg, M. (2007). Emergence of functional sensory subtypes as defined by transient receptor potential channel expression. J. Neurosci. *27*, 2435–2443.

Hohmann, and Dehghani (2019). The Cytoskeleton—A Complex Interacting Meshwork. Cells *8*, 362.

Howes, S.C., Alushin, G.M., Shida, T., Nachury, M. V., and Nogales, E. (2014). Effects of tubulin acetylation and tubulin acetyltransferase binding on microtubule structure. Mol. Biol. Cell *25*, 257–266.

Hu, J., and Lewin, G.R. (2006). Mechanosensitive currents in the neurites of cultured mouse sensory neurones. J. Physiol. *577*, 815–828.

Hu, J., Chiang, L.Y., Koch, M., and Lewin, G.R. (2010). Evidence for a protein tether involved in somatic touch. EMBO J. *29*, 855–867.

Hubbert, C., Guardiola, A., Shao, R., Kawaguchi, Y., Ito, A., Nixon, A., Yoshida, M., Wang, X.F., and Yao, T.P. (2002). HDAC6 is a microtubule-associated deacetylase. Nature *417*, 455–458.

Hughes, D.I., and Todd, A.J. (2020). Central Nervous System Targets: Inhibitory Interneurons in the Spinal Cord. Neurotherapeutics *17*, 874–885.

Hutvagner, G., and Simard, M.J. (2008). Argonaute proteins: Key players in RNA silencing. Nat. Rev. Mol. Cell Biol. *9*, 22–32.

Janke, C., and Bulinski, J.C. (2011). Post-translational regulation of the microtubule

cytoskeleton: Mechanisms and functions. Nat. Rev. Mol. Cell Biol. *12*, 773–786.

Janke, C., and Magiera, M.M. (2020). The tubulin code and its role in controlling microtubule properties and functions. Nat. Rev. Mol. Cell Biol.

Jin, P., Bulkley, D., Guo, Y., Zhang, W., Guo, Z., Huynh, W., Wu, S., Meltzer, S., Cheng, T., Jan, L.Y., et al. (2017). Electron cryo-microscopy structure of the mechanotransduction channel NOMPC. Nature *547*, 118–122.

Jinek, M., Chylinski, K., Fonfara, I., Hauer, M., Doudna, J.A., and Charpentier, E. (2012). A Programmable Dual-RNA – Guided DNA Endonuclease in Adaptive Bacterial Immunity. *337*, 816–822.

Jinek, M., Jiang, F., Taylor, D.W., Sternberg, S.H., Kaya, E., Ma, E., Anders, C., Hauer, M., Zhou, K., Lin, S., et al. (2014). Structures of Cas9 endonucleases reveal RNA-mediated conformational activation. Science (80-.). *343*.

Johari, Y.B., Mercer, A.C., Liu, Y., Brown, A.J., and James, D.C. (2021). Design of synthetic promoters for controlled expression of therapeutic genes in retinal pigment epithelial cells. Biotechnol. Bioeng. *118*, 2001–2015.

Julius, D. (2013). TRP Channels and Pain.

Jun-ichi, M., Satoshi, T., Kimi, A., Fumi, T., Akira, T., Kiyoshi, T., and Ken-ichi, Y. (1989). Expression vector system based on the chicken β-actin promoter directs efficient production of interleukin-5. Gene *79*, 269–277.

Kalebic, N., Sorrentino, S., Perlas, E., Bolasco, G., Martinez, C., and Heppenstall, P.A. (2013a). αTAT1 is the major α-tubulin acetyltransferase in mice. Nat. Commun. *4*.

Kalebic, N., Martinez, C., Perlas, E., Hublitz, P., Bilbao-Cortes, D., Fiedorczuk, K., Andolfo, A., and Heppenstall, P.A. (2013b). Tubulin Acetyltransferase αTAT1 Destabilizes Microtubules Independently of Its Acetylation Activity. Mol. Cell. Biol. *33*, 1114–1123.

Kefauver, J.M., Ward, A.B., and Patapoutian, A. (2020). Discoveries in structure and physiology of mechanically activated ion channels. Nature *587*, 567–576.

Kim, G.W., Li, L., Gorbani, M., You, L., and Yang, X.J. (2013). Mice lacking α-tubulin acetyltransferase 1 are viable but display α-tubulin acetylation deficiency and dentate gyrus distortion. J. Biol. Chem. *288*, 20334–20350.

Kim, H.K., Min, S., Song, M., Jung, S., Choi, J.W., Kim, Y., Lee, S., Yoon, S., and Kim, H. (2018). Deep learning improves prediction of CRISPR-Cpf1 guide RNA activity. Nat. Biotechnol. *36*, 239–241.

Kleeman, B., Olsson, A., Newkold, T., Kofron, M., DeLay, M., Hildeman, D., and Grimes, H.L. (2018). A guide to choosing fluorescent protein combinations for flow cytometric analysis based on spectral overlap. Cytom. Part A *93*, 556–562.

Kleinstiver, B.P., Prew, M.S., Tsai, S.Q., Topkar, V. V., Nguyen, N.T., Zheng, Z., Gonzales,

A.P.W., Li, Z., Peterson, R.T., Yeh, J.R.J., et al. (2015). Engineered CRISPR-Cas9 nucleases with altered PAM specificities. Nature *523*, 481–485.

Krames, E.S. (2014). The role of the dorsal root ganglion in the development of neuropathic pain. Pain Med. (United States) *15*, 1669–1685.

L'Hernaul, S.W., and Rosenbaum, J.L. (1985). Chlamydomonas α-Tubulin Is Posttranslationally Modified by Acetylation on the ε-Amino Group of a Lysine. Biochemistry *24*, 473–478.

Lechner, S.G., and Lewin, G.R. (2013). Hairy sensation. Physiology *28*, 142–150.

LeDizet, M., and Piperno, G. (1987). Identification of an acetylation site of Chlamydomonas alpha-tubulin. Proc. Natl. Acad. Sci. U. S. A. *84*, 5720–5724.

Lee, E.J., Guenther, C.M., and Suh, J. (2018). Adeno-associated virus (AAV) vectors: Rational design strategies for capsid engineering. Curr. Opin. Biomed. Eng. *7*, 58–63.

Lett, A.R.F., Sukharev, S.I., Blount, P., Martinac, B., Blattnert, F.R., and Kung, C. (1994). A large-conductance mechanosensitive channel in E. coli encoded by mscL alone. Nature *368*, 265–268.

Lewin, G.R., and Moshourab, R. (2004). Mechanosensation and pain. J. Neurobiol. *61*, 30–44.

Li, C., and Samulski, R.J. (2020). Engineering adeno-associated virus vectors for gene therapy. Nat. Rev. Genet.

Li, L., Rutlin, M., Abraira, V.E., Cassidy, C., Kus, L., Gong, S., Jankowski, M.P., Luo, W., Heintz, N., Koerber, H.R., et al. (2011). The functional organization of cutaneous low-threshold mechanosensory neurons. Cell *147*, 1615–1627.

Li, L., Jayabal, S., Ghorbani, M., Legault, L.M., McGraw, S., Watt, A.J., and Yang, X.J. (2019). ATAT1 regulates forebrain development and stress-induced tubulin hyperacetylation. Cell. Mol. Life Sci. *76*, 3621–3640.

Liu, Z., Chen, O., Wall, J.B.J., Zheng, M., Zhou, Y., Wang, L., Ruth Vaseghi, H., Qian, L., and Liu, J. (2017). Systematic comparison of 2A peptides for cloning multi-genes in a polycistronic vector. Sci. Rep. *7*, 1–9.

Loeb, J.E., Cordier, W.S., Harris, M.E., Weitzman, M.D., and Hope, T.J. (1999). Enhanced Expression of Transgenes from Adeno-Associated Virus Vectors with the Woodchuck Hepatitis Virus Posttranscriptional Regulatory Element: Implications for Gene Therapy. Hum. Gene Ther. *10*, 2295–2305.

Lu, J., Wu, T., Zhang, B., Liu, S., Song, W., Qiao, J., and Ruan, H. (2021). Types of nuclear localization signals and mechanisms of protein import into the nucleus. Cell Commun. Signal. *19*, 1–10.

Ly, N., Elkhatib, N., Bresteau, E., Piétrement, O., Khaled, M., Magiera, M.M., Janke, C.,

Le Cam, E., Rutenberg, A.D., and Montagnac, G. (2016). αtAT1 controls longitudinal spreading of acetylation marks from open microtubules extremities. Sci. Rep. *6*, 1–10.

Maffei, M., Morelli, C., Graham, E., Patriarca, S., Donzelli, L., Doleschall, B., de Castro Reis, F., Nocchi, L., Chadick, C.H., Reymond, L., et al. (2019). A ligand-based system for receptor-specific delivery of proteins. Sci. Rep. *9*, 1–14.

Mali, P., Yang, L., Esvelt, K.M., Aach, J., Guell, M., DiCarlo, J.E., Norville, J.E., and Church, G.M. (2013). RNA-guided human genome engineering via Cas9. Science (80-.). *339*, 823–826.

Maroto, R., Raso, A., Wood, T.G., Kurosky, A., Martinac, B., and Hamill, O.P. (2005). TRPC1 forms the stretch-activated cation channel in vertebrate cells. Nat. Cell Biol. *7*, 179–185.

McGlone, F., Wessberg, J., and Olausson, H. (2014). Discriminative and Affective Touch: Sensing and Feeling. Neuron *82*, 737–755.

Mietzsch, M., Broecker, F., Reinhardt, A., Seeberger, P.H., Heilbronn, R., and Imperiale, M.J. (2014). Differential Adeno-Associated Virus Serotype-Specific Interaction Patterns with Synthetic Heparins and Other Glycans. J. Virol. *88*, 2991–3003.

Mills, S.E.E., Nicolson, K.P., and Smith, B.H. (2019). Chronic pain: a review of its epidemiology and associated factors in population-based studies. Br. J. Anaesth. *123*, e273–e283.

Mitchison, T., and Kirschner, M. (1984). Dynamic instability of microtubule growth. Nature *312*, 237–242.

Moineau, S., Barrangou, R., Boyaval, P., Deveau, H., Romero, D.A., Horvath, P., Richards, M., and Fremaux, C. (2007). CRISPR Provides Acquired Resistance Against Viruses in Prokaryotes. Science (80-.). *315*, 1709–1712.

Mojica, F.J.M., Díez-Villaseñor, C., García-Martínez, J., and Almendros, C. (2009). Short motif sequences determine the targets of the prokaryotic CRISPR defence system. Microbiology *155*, 733–740.

Morley, S.J., Qi, Y., Iovino, L., Andolfi, L., Guo, D., Kalebic, N., Castaldi, L., Tischer, C., Portulano, C., Bolasco, G., et al. (2016). Acetylated tubulin is essential for touch sensation in mice. Elife *5*, 25.

Motulsky, H.J., and Brown, R.E. (2006). Detecting outliers when fitting data with nonlinear regression - A new method based on robust nonlinear regression and the false discovery rate. BMC Bioinformatics *7*, 1–20.

Najm, F.J., Strand, C., Donovan, K.F., Hegde, M., Sanson, K.R., Vaimberg, E.W., Sullender, M.E., Hartenian, E., Kalani, Z., Fusi, N., et al. (2018). Orthologous CRISPR-Cas9 enzymes for combinatorial genetic screens. Nat. Biotechnol. *36*, 179–189.

Niu, Y., Tao, X., Vaisey, G., Olinares, P.D.B., Alwaseem, H., Chait, B.T., and MacKinnon, R.

(2021). Analysis of the mechanosensor channel functionality of TACAN. Elife *10*, 2021.06.11.448078.

North, B.J., Marshall, B.L., Borra, M.T., Denu, J.M., Verdin, E., and Francisco, S. (2003). The Human Sir2 Ortholog, SIRT2, is an NAD+ -Dependent Tubulin Deacetylase. Mol. Cell *11*, 437–444.

Outeiro, T.F., Kontopoulos, E., Altmann, S.M., Kufareva, I., Strathearn, K.E., Amore, A.M., Volk, C.B., Maxwell, M.M., Rochet, J.C., McLean, P.J., et al. (2007). Sirtuin 2 inhibitors rescue α-synuclein-mediated toxicity in models of Parkinson's disease. Science (80-.). *317*, 516–519.

Paule, M.R., and White, R.J. (2000). Transcription by RNA polymerases I and III. Nucleic Acids Res. *28*, 1283–1298.

Pegoraro, A.F., Janmey, P., and Weitz, D.A. (2017). Mechanical properties of the cytoskeleton and cells. Cold Spring Harb. Perspect. Biol. *9*.

Pezet, S., and McMahon, S.B. (2006). Neurotrophins: Mediators and Modulators of Pain. Annu. Rev. Neurosci. *29*, 507–538.

Portran, D., Schaedel, L., Xu, Z., Théry, M., and Nachury, M. V. (2017). Tubulin acetylation protects long-lived microtubules against mechanical ageing. Nat. Cell Biol. *19*, 391–398.

Qi, Y., Andolfi, L., Frattini, F., Mayer, F., Lazzarino, M., and Hu, J. (2015). Membrane stiffening by STOML3 facilitates mechanosensation in sensory neurons. Nat. Commun. *6*, 1–13.

Qin, J.Y., Zhang, L., Clift, K.L., Hulur, I., Xiang, A.P., Ren, B., and Lahn, B.T. (2010). Systematic Comparison of Constitutive Promoters and the Doxycycline-Inducible Promoter. *5*, 3–6.

Ran, F.A., Hsu, P.D., Wright, J., Agarwala, V., Scott, D.A., and Zhang, F. (2013). Genome engineering using the CRISPR-Cas9 system. Nat. Protoc. *8*, 2281–2308.

Ranade, S.S., Woo, S.H., Dubin, A.E., Moshourab, R.A., Wetzel, C., Petrus, M., Mathur, J., Bégay, V., Coste, B., Mainquist, J., et al. (2014). Piezo2 is the major transducer of mechanical forces for touch sensation in mice. Nature *516*, 121–125.

Ranade, S.S., Syeda, R., and Patapoutian, A. (2015). Mechanically Activated Ion Channels. Neuron *87*, 1162–1179.

Raoux, M., Rodat-Despoix, L., Azorin, N., Giamarchi, A., Jizhe, H., Maingret, F., Crest, M., Coste, B., and Delmas, P. (2007). Mechanosensor channels in mammalian somatosensory neurons. Sensors *7*, 1667–1682.

Reed, N.A., Cai, D., Blasius, T.L., Jih, G.T., Meyhofer, E., Gaertig, J., and Verhey, K.J. (2006). Microtubule Acetylation Promotes Kinesin-1 Binding and Transport. Curr. Biol. *16*, 2166–2172.

Ren, X., Halder, P., Seal, R.P., Goulding, M.D., Gatto, G., Bourane, S., Ren, X., Costanzo,

S. Di, Fenton, P.K., and Halder, P. (2021). Article A Functional Topographic Map for Spinal Sensorimotor Reflexes Article A Functional Topographic Map for Spinal Sensorimotor Reflexes. Neuron 1–14.

Riyad, J.M., and Weber, T. (2021). Intracellular trafficking of adeno-associated virus (AAV) vectors: challenges and future directions. Gene Ther.

Salas, A., López, J., Reyes, R., Évora, C., de Oca, F.M., Báez, D., Delgado, A., and Almeida, T.A. (2020). Organotypic culture as a research and preclinical model to study uterine leiomyomas. Sci. Rep. *10*, 1–12.

Sharma, N., Flaherty, K., Lezgiyeva, K., Wagner, D.E., Klein, A.M., and Ginty, D.D. (2020). The emergence of transcriptional identity in somatosensory neurons. Nature *577*, 392–398.

Shida, T., Cueva, J.G., Xu, Z., Goodman, M.B., and Nachury, M. V. (2010). The major α-tubulin K40 acetyltransferase αTAT1 promotes rapid ciliogenesis and efficient mechanosensation. Proc. Natl. Acad. Sci. U. S. A. *107*, 21517–21522.

Shin, J., Adams, D., Paukert, M., Siba, M., Sidi, S., Levin, M., Gillespie, P.G., and Gru, S. (2005). Xenopus TRPN1 (NOMPC) localizes to microtubule-based cilia in epithelial cells , including inner-ear hair cells. *1*, 1–6.

Sidi, S., Friedrich, R.W., and Nicolson, T. (2003). NompC TRP channel required for vertebrate sensory hair cell mechanotransduction. Science (80-.). *301*, 96–99.

Siolas, D., Lerner, C., Burchard, J., Ge, W., Linsley, P.S., Paddison, P.J., Hannon, G.J., and Cleary, M.A. (2005). Synthetic shRNAs as potent RNAi triggers. Nat. Biotechnol. *23*, 227–231.

Skolnick, P. (2018). The Opioid Epidemic: Crisis and Solutions. Annu. Rev. Pharmacol. Toxicol. *58*, 143–159.

Sonntag, F., Schmidt, K., and Kleinschmidt, J.A. (2010). A viral assembly factor promotes AAV2 capsid formation in the nucleolus. Proc. Natl. Acad. Sci. U. S. A. *107*, 10220–10225.

Soppina, V., Herbstman, J.F., Skiniotis, G., and Verhey, K.J. (2012). Luminal Localization of α-tubulin K40 Acetylation by Cryo-EM Analysis of Fab-Labeled Microtubules. PLoS One *7*, 1–9.

Srivastava, A. (2016). Adeno-Associated Virus: The Naturally Occurring Virus Versus the Recombinant Vector. Hum. Gene Ther. *27*, 1–6.

Stinski, M.F., and Isomura, H. (2008). Role of the cytomegalovirus major immediate early enhancer in acute infection and reactivation from latency. Med. Microbiol. Immunol. *197*, 223–231.

Story, G.M., Peier, A.M., Reeve, A.J., Eid, S.R., Mosbacher, J., Hricik, T.R., Earley, T.J., Hergarden, A.C., Andersson, D.A., Hwang, S.W., et al. (2003). ANKTM1, a TRP-like channel expressed in nociceptive neurons, is activated by cold temperatures. Cell *112*, 819–829.

Svitkina, T. (2018). The actin cytoskeleton and actin-based motility. Cold Spring Harb.

Perspect. Biol. *10*, 1–21.

Szyk, A., Deaconescu, A.M., Spector, J., Goodman, B., Valenstein, M.L., Ziolkowska, N.E., Kormendi, V., Grigorieff, N., and Roll-Mecak, A. (2014). Molecular basis for age-dependent microtubule acetylation by tubulin acetyltransferase. Cell *157*, 1405–1415.

Talavera, K., Startek, J.B., Alvarez-Collazo, J., Boonen, B., Alpizar, Y.A., Sanchez, A., Naert, R., and Nilius, B. (2020). Mammalian transient receptor potential TRPA1 channels: From structure to disease. Physiol. Rev. *100*, 803.

Thompson, M.J., and Baenziger, J.E. (2020). Ion channels as lipid sensors: from structures to mechanisms. Nat. Chem. Biol. *16*, 1331–1342.

Todd, A.J. (2010). Neuronal circuitry for pain processing in the dorsal horn. Nat. Rev. Neurosci. *11*, 823–836.

Topalidou, I., Keller, C., Kalebic, N., Nguyen, K.C.Q., Somhegyi, H., Politi, K.A., Heppenstall, P., Hall, D.H., and Chalfie, M. (2012). Genetically separable functions of the MEC-17 tubulin acetyltransferase affect microtubule organization. Curr. Biol. *22*, 1057–1065.

Vora, S., Cheng, J., Xiao, R., VanDusen, N.J., Quintino, L., Pu, W.T., Vandenberghe, L.H., Chavez, A., and Church, G. (2018). Rational design of a compact CRISPR-Cas9 activator for AAV-mediated delivery. BioRxiv *9*, 298620.

Vulchanova, L., Schuster, D.J., Belur, L.R., Riedl, M.S., Podetz-Pedersen, K.M., Kitto, K.F., Wilcox, G.L., McIvor, R.S., and Fairbanks, C.A. (2010). Differential adeno-associated virus mediated gene transfer to sensory neurons following intrathecal delivery by direct lumbar puncture. Mol. Pain *6*, 1–9.

Wang, D., Tai, P.W.L., and Gao, G. (2019). Adeno-associated virus vector as a platform for gene therapy delivery. Nat. Rev. Drug Discov. *18*, 358–378.

Wang, H., La Russa, M., and Qi, L.S. (2016). CRISPR/Cas9 in Genome Editing and beyond. Annu. Rev. Biochem. *85*, 227–264.

Waxman, S.G., and Zamponi, G.W. (2014). Regulating excitability of peripheral afferents: Emerging ion channel targets. Nat. Neurosci. *17*, 153–163.

Wetzel, C., Hu, J., Riethmacher, D., Benckendorff, A., Harder, L., Eilers, A., Moshourab, R., Kozlenkov, A., Labuz, D., Caspani, O., et al. (2007). A stomatin-domain protein essential for touch sensation in the mouse. Nature *445*, 206–209.

Wiedenheft, B., Sternberg, S.H., and Doudna, J.A. (2012). RNA-guided genetic silencing systems in bacteria and archaea. Nature *482*, 331–338.

Wilkinson, R.A., Martin, C., Nemudryi, A.A., and Wiedenheft, B. (2019). CRISPR RNA-guided autonomous delivery of Cas9. Nat. Struct. Mol. Biol. *26*, 14–24.

Woolf, C.J., and Ma, Q. (2007). Nociceptors-Noxious Stimulus Detectors. Neuron *55*, 353–364.

Xiang, X., Li, C., Chen, X., Dou, H., Li, Y., Zhang, X., and Luo, Y. (2019). CRISPR/Cas9-Mediated Gene Tagging: A Step-by-Step Protocol. In CRISPR Gene Editing: Methods and Protocols, Y. Luo, ed. (New York, NY: Springer New York), pp. 255–269.

Xu, Z., Schaedel, L., Portran, D., Aguilar, A., Gaillard, J., Peter Marinkovich, M., Théry, M., and Nachury, M. V. (2017). Microtubules acquire resistance from mechanical breakage through intralumenal acetylation. Science (80-.). *356*, 328–332.

Yan, C., Wang, F., Peng, Y., Williams, C.R., Jenkins, B., Wildonger, J., Kim, H.J., Perr, J.B., Vaughan, J.C., Kern, M.E., et al. (2018). Microtubule Acetylation Is Required for Mechanosensation in Drosophila. Cell Rep. *25*, 1051-1065.e6.

Ye, L., Wang, J., Tan, Y., Beyer, A.I., Xie, F., Muench, M.O., and Kan, Y.W. (2016). Genome editing using CRISPR-Cas9 to create the HPFH genotype in HSPCs: An approach for treating sickle cell disease and β-thalassemia. Proc. Natl. Acad. Sci. U. S. A. *113*, 10661–10665.

Yi, R., Qin, Y., Macara, I.G., and Cullen, B.R. (2003). Exportin-5 mediates the nuclear export of pre-microRNAs and short hairpin RNAs. Genes Dev. *17*, 3011–3016.

Yoshimoto, S., Morita, H., Okamura, K., Hiraki, A., and Hashimoto, S. (2021). αTAT1-induced tubulin acetylation promotes ameloblastoma migration and invasion. Lab. Investig.

Yu, H., Su, Y., Shin, J., Zhong, C., Guo, J.U., Weng, Y.L., Gao, F., Geschwind, D.H., Coppola, G., Ming, G.L., et al. (2015). Tet3 regulates synaptic transmission and homeostatic plasticity via DNA oxidation and repair. Nat. Neurosci. *18*, 836–843.

Zhang, W., Cheng, L.E., Kittelmann, M., Li, J., Petkovic, M., Cheng, T., Jin, P., Guo, Z., Göpfert, M.C., Jan, L.Y., et al. (2015). Ankyrin Repeats Convey Force to Gate the NOMPC Mechanotransduction Channel. Cell *162*, 1391–1403.

Zhao, N., Kamijo, K., Fox, P.D., Oda, H., Morisaki, T., Sato, Y., Kimura, H., and Stasevich, T.J. (2019). A genetically encoded probe for imaging nascent and mature HA-tagged proteins in vivo. Nat. Commun. *10*.

Zincarelli, C., Soltys, S., Rengo, G., and Rabinowitz, J.E. (2008). Analysis of AAV serotypes 1-9 mediated gene expression and tropism in mice after systemic injection. Mol. Ther. *16*, 1073–1080.

Zylka, M.J., Rice, F.L., and Anderson, D.J. (2005). Topographically distinct epidermal nociceptive circuits revealed by axonal tracers targeted to Mrgprd. Neuron *45*, 17–25.